Department of AERONAUTICS and ASTRONAUTICS
STANFORD UNIVERSITY

OPTIMIZATION OF STRUCTURES UNDERGOING HARMONIC OR STOCHASTIC EXCITATION

by

Erwin H. Johnson

June 1975

This research was partially supported by

NASA NGL 05-020-243

OPTIMIZATION OF STRUCTURES UNDERGOING HARMONIC OR STOCHASTIC EXCITATION

A DISSERTATION

SUBMITTED TO THE DEPARTMENT OF AERONAUTICS AND ASTRONAUTICS

AND THE COMMITTEE ON GRADUATE STUDIES

OF STANFORD UNIVERSITY

IN PARTIAL FULFILLMENT OF THE REQUIREMENTS

FOR THE DEGREE OF

DOCTOR OF PHILOSOPHY

By

Erwin Harry Johnson

May 1975

I certify that I have read this thesis and that in my opinion it is fully adequate, in scope and quality, as a dissertation for the degree of Doctor of Philosophy.

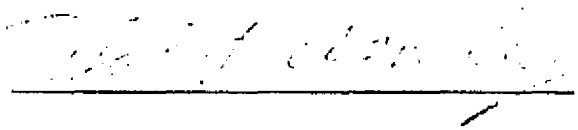

I certify that I have read this thesis and that in my opinion it is fully adequate, in scope and quality, as a dissertation for the degree of Doctor of Philosophy.

Samuel C. McIntosh, Jr.

I certify that I have read this thesis and that in my opinion it is fully adequate, in scope and quality, as a dissertation for the degree of Doctor of Philosophy.

P. C. Chu

Approved for the University Committee on Graduate Studies:

Dean of Graduate Studies

ABSTRACT

This study investigates the optimal design of simple structures subjected to dynamic loads, with constraints on the structures' responses. Previous studies have mainly dealt with static loads, and their methodology has been extended here to time dependent cases. The contributions of this work are in the formulation and satisfaction of the complicated dynamic constraints and in the insights gained into the nature of these problems.

Three separate analyses search for the optimal design of: (1) one-dimensional structures excited by harmonically oscillating loads, (2) similar structures excited by white noise and (3) a wing in the presence of continuous atmospheric turbulence. The first problem has constraints on the maximum allowable stress while the last two place bounds on the probability of failure of the structure. In all of these problems, approximations are made in order to replace the time parameter with a frequency parameter. For the first, this involves the simple assumption that the steady state response is the area of interest. In the remaining cases, power spectral techniques are employed to find the root mean square values of the responses. The primary means of search for the optimal solutions is through the use of computer algorithms that combine finite element methods with optimization techniques based on mathematical programming.

A general conclusion is that the inertial loads for these dynamic problems can result in optimal structures that are radically different from those obtained for structures loaded statically by forces of comparable magnitude. In the case of the harmonically loaded structure, it is found that the design space can be disjoint. This makes the task of finding the global optimum difficult for even the simplest of problems.

An interesting feature of the optimal designs for cantilevered structures with a white noise excitation is that there is a tendency for some mass to be concentrated near the tip. The inertial forces from this mass tend to relieve the inboard stress.

The wing in a turbulent gust environment demonstrates a possible practical application of the methods developed in the study. The model used contains a fuselage and nacelle and permits rigid body plunging as well as transverse bending. It is felt that the preliminary techniques developed are of practical value towards the design of aircraft that have fatigue life as an important design factor.

ACKNOWLEDGMENTS

The author wishes to express his appreciation to Dr. Samuel C. McIntosh, Jr. who, in the capacity of thesis adviser, aided in the original definition and development of the thesis. Professor Holt Ashley assumed the adviser duties, and his enthusiasm and physical understanding helped bring this work to completion. Valuable assistance was obtained from fellow students Paulo Rizzi and Sully Segenreich and from Dr. Garrett N. Vanderplaats of the NASA Ames Research Center. Suzanne Bennett expertly typed the final manuscript while under a tight time schedule.

The Fannie and John Hertz Foundation provided generous fellowship aid during the last two years of the author's doctoral studies. Additional funds for computer expenses were partially supplied by NASA under Contract NASA NGL 05-020-243.

TABLE OF CONTENTS

LIST OF ILLUSTRATIONS

LIST OF TABLES

NOMENCLATURE

$[A]$	Aerodynamic matrix
a_i	Modal participation factor
b	Beam width
$b(y)$	Wing semichord
b_{ref}	Reference semichord
$C(k)$	Theodorsen's function
$c(y)$	Wing chord length
d	Beam depth
DR	Damage rate
E	Young's modulus
$E(\ )$	Expected value
G	Shear modulus
g_i	Equality or inequality constraint
$\{G\}$	Vector of gust loads
$\{GG\}$	Generalized gust loads
$[GA]$	Generalized aerodynamic forces
H	Hamiltonian

$[H]$	Matrix in variable metric algorithm
I_α	Mass polar moment of inertia
I	Area moment of inertia
$\Im m(z)$	Imaginary part
J	cost function or functional
J	Area polar moment of inertia
$J_0(\ ) \& J_1(\ )$	Bessel functions of the first kind
$[K]$	Stiffness matrix
$[\mathcal{K}]$	Generalized stiffness matrix
k	Reduced frequency $(= \omega b_{ref}/U)$
L	Structural span length
ℓ	Element length
L_F	Fatigue life
L_S	Strength life
L_T	Turbulence scale
$[M]$	Mass matrix
$[\mathcal{M}]$	Generalized mass matrix
m_0	Structural mass/thickness
mn	Number of modes
n	Number of elements

nc	Number of constraints
P	Transverse load
$\{p_i\}$	I^{th} mode shape
$p_x(x)$	Probability density function of x
r	Penalty function parameter
R	Rod radius
$\Re e(z)$	Real part of z
S	Stress
s	Nondimensional length
t	Time
t_i	Thickness design variable
$\overline{T}$	Amplitude of a torsional load
U	Free stream velocity
U_S	Ultimate stress
u_i	Transformed design variable
w	Transverse displacement
w_g	Vertical gust velocity
x_i	State variable
X_{ab}	Covariance of a and b
z	Complex number

α	One-dimensional search parameter
α	Structural damping parameter
$\Gamma(\ )$	Gamma function
Γ	Nondimensional frequency
$\Delta(\ )$	Incremental value
ϵ	Transition point for the extended penalty function
θ	Rotational displacement
λ_i	Adjoint variable of the states
λ	Nondimensional frequency
λ_e	Nondimensional excitation frequency
μ	Adjoint variable of the constraints
ρ_a	Atmospheric density
ρ_s	Structural density
σ_{xx}	Root mean square value of x
Φ	Augmented cost function
$\Phi_{xx}(\omega)$	Power spectrum of x
Ω	Spatial frequency ($= \omega/U$)
ω	Frequency
ω_e	Excitation frequency
ω_i	Modal frequency

$\nabla( )$	Gradient operator
$( )'$	Differentiation
$( )^T$	Transpose
$(\bar{\ })$	Complex conjugate
{ }	Column vector
[ ]	Matrix

Note: Additional nomenclature is explicitly defined in the text

CHAPTER I

INTRODUCTION

A. PROBLEM MOTIVATION

The goal of the field of structural optimization can be succinctly described as one of finding the structure of least weight that satisfies certain specified constraints. The combination of more efficient algorithms with modern computers has expanded the capabilities of this field rapidly and to the extent that techniques have been developed that routinely optimize practical, statically loaded structures. Similar results for dynamically loaded structures have lagged behind due to the complications introduced by inertial loads and the time parameter. This thesis attempts a partial remedy of this situation by investigating a series of dynamic response problems in order to find the least weight structure that can withstand the dynamic loads.

The design of many engineering structures is influenced by the dynamic loads that act on the structure so that the search for optimal structures is a legitimate exercise. Landing impacts, gust excitation, rotating machinery and acoustic noise create loads on aeronautical vehicles that are dynamic in nature and that are of primary importance in the design of aircraft substructures. Similarly, for astronautical vehicles, rocket exhausts and atmospheric turbulence

are important design loads. These aerospace applications were the ones that were kept in mind while the methods of analysis used in this thesis were developed. However, other disciplines could benefit from the methods presented here. Specifically, for architectural structures, earthquakes and winds create loads that are dynamic in nature, and these loads are playing an increasingly important role in building design. Further examples could be drawn from naval architecture and from mechanical design.

Many of the examples mentioned above include loads that are stochastic, or random, in nature. Coupled with the fact that a large proportion of in-service failure of metal structures are due to fatigue, this provides a powerful motivation for studying the optimal design of structures under stochastic loading conditions.

While no claim is made as to the direct applicability of the techniques developed in this work to practical problems in engineering design, techniques are developed and results achieved that could be a useful starting point for the more practical problems. The usefulness is enhanced by the use of constraints in the examples worked that are of practical interest in actual designs. For instance, constraints are placed on the maximum stress in the structure or on the fatigue life in the case of random loads.

Due to the paucity of studies dealing with the optimization of dynamically loaded structures, it is felt that this work makes significant contributions to the basic understanding of these types of problems. The inertial loads present in these problems can have an

important effect on the loads a structure is required to withstand. The results obtained show that the optimal structure can be radically different from one obtained based on static strength considerations.

B. RELATED WORK

This section presents a survey of studies that have been done that relate to the present one, pointing out their characteristics and how they compare with the present study. The thesis uses elements from a number of disciplines, but the unique portion of this work is the use of structural optimization and it is in this area that the survey will concern itself. Even in this specialized field, it would be impractical to give a comprehensive survey; instead, only the most relevant works are described. A more general view of the structural optimization field can be obtained from a survey article by Sheu and Prager (Ref. 1) while a text by Fox (Ref. 2) serves as an excellent introduction to the computational aspects of optimal design. Two recent conferences (Ref. 3 and Ref. 4) provide "state of the art" descriptions of various portions of the field.

Structural optimization with constraints on the dynamic behavior is a more specific area that includes the present study. A survey by Pierson (Ref. 5) on this subject divided it further into two subdivisions: (1) problems with eigenvalue constraints, and (2) problems with constraints on the response. The present investigation clearly falls into the latter category, but problems of the first kind played an important role in the development of the methodology used in this

report. In particular, references 6 through 10 are works that place constraints on the natural frequency or the flutter speed of the systems to be optimized and that provided a basis from which to attack the response problem. In fact, as Pierson pointed out, one of the dynamic response problems solved by Icerman (Ref. 11) has results identical to a problem with a natural frequency constraint that was first solved by Turner (Ref. 9).

It is to be understood that the five references cited above for the eigenvalue constraint studies are in no way inclusive of the contributions made to these problems. An attempt is made below to include all the significant studies that have been conducted with constraints on dynamic response quantities. These papers are a small, but rapidly increasing, part of the literature.

The relative youth of the field presents difficulties when one tries to classify the types of problems that have been studied. The ideal procedure would be to describe the problem that was studied, the method of solution and a discussion of results. Unfortunately, and unlike the more developed field of optimization with static loads, each paper treats a unique problem, usually in a unique way and, of course, obtains a unique result. Therefore, only the features of the studies that are relevant to the present work will be stressed in what follows.

The youthfulness of the field is indicated by the fact that the earliest papers of this type known to the author were published in 1968. This work, published by Brach in two papers (Ref. 12 and Ref. 13),

found approximate optimal solutions for some one-dimensional structures loaded by impulsive or step forces. The problem formulation for these studies was in terms of finding the structure of fixed weight that minimized a specified deflection. This is a transformation of the formulation used in this work: finding the structure of least weight with a constraint on the size of the maximum deflection.

Fox and Kapoor (Ref. 14) published another "early" work that developed a mathematical programming algorithm for finding the optimal design of truss-frame structures subjected to a half-cycle sine pulse. The response was estimated by using shock spectral techniques that gave conservative upper bound limits on the deflection and stress. A previous work by Fox and Kapoor (Ref. 15) made the important contribution of developing a simple technique for finding the derivatives of the eigenvalues and eigenvectors with respect to the system parameters.

Levy and Wolf (Ref. 16 and Ref. 17) provide a means of finding the fully stressed design for one-dimensional structures under dynamic loading. A fully stressed design is one where all structural elements exactly satisfy the stress constraints imposed on them. The motivation for their study comes from the fact that for determinate, statically loaded structures with constraints on the stress, the fully stressed design is optimal. For the impulsive loading conditions and the finite element representations used, the solutions shown in these references are found to be optimal. However, fully stressed designs are usually not optimal in cases where more general dynamic loads are considered.

A series of related papers by Venkayya, et al. (Ref. 18 and Ref. 19) describes an optimality criterion that is used to find approximate optimal solutions for various types of dynamic loading. The criterion was developed specifically for problems with constraints on the natural frequency, so that it is exact for that case. When more general dynamic conditions are considered, the results obtained have to be considered as preliminary, qualitative designs.

A specific area of practical interest that can benefit from the methods of optimization with dynamic constraints is that of the optimal design of structures to withstand earthquake loads. The 5th World Conference on Earthquake Engineering held in Rome in June, 1973 included four short papers on this topic. One of these, by Solnes and Holst (Ref. 20), replaced the dynamic load by an equivalent static load, so that it is not a dynamic response problem, strictly speaking. However, inertial effects are artificially included in the statically equivalent load. Another paper from the conference, by Nigam and Narayanan (Ref. 21), considered the excitation to be either a specified acceleration or a probabilistic acceleration with a given power spectrum. The techniques employed in the paper and in another paper by Nigam (Ref. 22) to deal with the probabilistic nature of the excitation come closest to the techniques employed in Chapters IV and V of the present work to treat similar loadings. Another work of optimization for earthquake type of loads is given by Kato, et al. (Ref. 23). The loads in this case are approximated by shock spectra in a manner similar to that of Ref. 14. The diversity of models and

techniques used to study the optimization problem for civil engineering structures indicates that it is a fertile ground for further research and systemization.

A study that is more general in scope, but that has application to the earthquake problem, is contained in a recent report by Cassis (Ref. 24). In this case, the load is modelled as a half-cycle sine pulse and the response is obtained by performing a time integration of the equations of motion. The constraints considered include integrals of the time history of the response. This is one of the few papers dealing with dynamic response that retain the time parameter in an explicit form. It is also the first report known to the author that includes mention of the fact that the feasible design space can be disjoint for certain types of dynamic excitations. This feature of such problems is one of the more exciting. The disjoint design space receives extensive treatment in Chapter III of this report.

Chapter III deals with the optimization of structures excited by harmonically varying loads. In one sense, this is the simplest of the dynamic response problems since the time parameter can be removed by assuming that the steady state response is the only response of interest. By the use of energy methods, Icerman (Ref. 11) was able to develop an optimality criterion for one-dimensional structures excited by a point load with an equality constraint on the displacement directly under the load. In order to develop the optimality criterion, it was necessary to add the further constraint that the excitation frequency be less than the first natural frequency of the structure. Plaut

(Ref. 25) made a similar investigation but allowed the loading to be more general. While several examples were analyzed, and their optimality criteria obtained, no explicit solutions were shown in this second study. Mroz (Ref. 26) conducted a mathematically more rigorous study, which replaced the displacement constraints by one on the dynamic compliance of the structure. This is defined as the integral, over the entire structure, of the product of the magnitude of the load times the magnitude of the displacement under it. Despite the successes reported in these studies, the author knows of no effort that was made to expand on the results. An obvious, although difficult, extension would be to find an energy method that allowed the sinusoidal excitation to be applied at a frequency greater than the structures' first natural frequency.

Finally, a series of papers that deal with static loads should be mentioned because of their relevance to the problem investigated in Chapters IV and V. They include some relatively early papers that sought optimal structures with constraints on their reliability (Ref. 27 and Ref. 28). Moses and Kinser (Ref. 29) extended these results and used mathematical programming to find the optima. Araslanov (Ref. 29) developed an optimality criterion that is applicable to simple beam structures loaded statically by forces whose properties are known only probabilistically. To do this, he defined the optimal structure to be the one where all cross sections have the same specified probability of failure. These problems are the counterpart of the present study in that they assume that the structure and the load distributions

are described in some probabilistic manner but the loads are assumed independent of time. In the present work, the structural properties are assumed to be given and the loads are constant in the space coordinate but vary in a probabilistic fashion with time. Perhaps an enterprising investigator will integrate these two problems.

C. SCOPE OF WORK

The preceding literature survey omitted a few papers that were considered redundant or of little importance. It is quite likely that other papers were inadvertently overlooked. However, the survey attempted to demonstrate the full scope of the field of structural optimization with dynamic excitation and to indicate that this scope is still quite narrow. In addition, few of the papers cited were published, or, if published, were known to the author when this research began. For these reasons, the work reported on here does not build on the results of previous investigations to any major extent but rather attacks new problems. Of course, the tools needed for the analyses are gathered from existing disciplines, such as structural optimization, structural dynamics, aeroelasticity and probability.

The core of the thesis is contained in three chapters that deal with three distinct optimization problems. In addition, a separate chapter describes the optimization algorithm used for the majority of the examples studied and an appendix details the finite element models that feed into each of the three problems.

The first problem is that of the structural optimization of one-dimensional structures excited by harmonically oscillating loads. This is similar to the cases dealt with in references 11, 25, and 26, but a different approach is used that provides added insight into the problem. In particular, the constraint that the first natural frequency of the optimal structure be greater than the excitation frequency, which was an integral part of developing the optimality criterion of the previous studies, is removed. Another change is that the equality constraints on the displacements or the dynamic compliance are replaced by inequality constraints on the allowable stress within the structure. It is felt that these innovations provide for solutions of greater physical interest. Another facet of the present formulation is that the feasible region is disjoint. This provides an interesting theoretical result and one that may be of physical usefulness as well. The major drawback of this formulation is that it is no longer possible to find an optimality criterion based on energy methods. This forces the investigator to deal with each problem on an ad hoc basis. One way of combatting this deficiency is the construction of analytical solutions to the optimization problems by the use of concepts from optimal control. This is a technique that met with some success when applied to problems with constraints only on the natural frequencies (Ref. 9). It is introduced, with limited success, in the present investigation because it holds the promise of providing solutions that analytically detail the effects of the various parameters.

Chapter IV deals with the second problem, which is the structural optimization of one-dimensional structures excited by white noise uniformly distributed along the span. A technical note by Nigam (Ref. 22) aided in developing the means for dealing with this type of problem, although the specific structures and constraints of Chapter IV differ substantially from those used by Nigam. Since the excitation is expressed in probabilistic terms, the constraints also have to be evaluated using probability theory. Much of the chapter is therefore devoted to defining the failure criteria used to evaluate a structure's lifetime. The methods ultimately used were obtained from Chapter 9 of a text by Lin (Ref. 31) and include both fatigue failure and first excursion failure. Further analysis in Chapter IV is devoted to outlining how the response quantities and their derivatives, which are needed in the optimization procedure, are obtained through the use of superposition of natural modes. Finally, some numerical results are given and comments are made on points of interest.

The methods of the earlier chapters are applied in Chapter V to a more practical problem, that of finding the optimal design for a wing excited by continuous atmospheric turbulence. The turbulence was represented by a power spectrum so that methods similar to those used in Chapter IV could be used to obtain the lifetime of the structure. A complicating factor is the translation of the atmospheric turbulence to the loads a wing experiences. A text by Bisplinghoff, et al. (Ref. 32, Chap. 5), provided the theory that permitted this. This

text also supplied the example (Ref. 32, Example 10.6) that was optimized, a tapered unswept wing that includes a nacelle and a fuselage and allows rigid body plunging in addition to wing bending.

Finally, the last chapter summarizes the results obtained from the research and indicates areas that merit further study.

CHAPTER II

OPTIMIZATION TECHNIQUES

This chapter provides a description of the optimization methods that were used for the majority of the examples studied in this work. It does not attempt to describe alternative methods or to compare them with the methods used here. As mentioned in the introductory chapter, references 2, 3, and 4 collectively provide a good survey of the current state of various methods.

Briefly stated, the methods used here involve coupling an interior penalty function technique with a variable metric algorithm. These methods have been described elsewhere; in particular, Fox's text (Ref. 2) provides an excellent general presentation. Therefore, the present chapter gives only a brief outline of the method with emphasis on modifications developed during the use of the techniques.

The first section defines terms that are common to optimization studies and are needed when the actual procedures are described in the following sections. A final section offers some observations on the algorithm based on experience gained from exercising it for the problems of the thesis.

A. CONCEPTS OF OPTIMIZATION

The general process of optimization entails searching for the design that minimizes some specified function while satisfying all

the limitations applied to the design or its response. This section briefly outlines the concepts that put this general concept into quantifiable terms. Since finite elements are used for the majority of examples presented in this thesis, the development is presented in terms applicable to a finite element analysis.

The first term to be defined is the objective or cost function. This is the function (or functional) to be minimized and is designated by J. For the problems of this thesis, the cost function is always simply the sum of the design variables.

The design variable is the second concept to be defined. This is an element of the system that may be changed in the process of seeking an optimum. The present study is concerned with one-dimensional thin walled structures whose design variables are the thicknesses of individual elements. The design variables are elements of a design vector that is notationally represented by $\{t\}$. A related concept is that of the design space, which is simply the space of all physically possible design variables.

Limitations on the design are termed constraints, and it is to the formulation and satisfaction of these constraints that the bulk of the effort of this work is directed. The constraints are designated by the requirement that

$$g_i \geq 0 \quad , \quad (i = 1, 2, \ldots, \text{no. of constraints}) \quad , \qquad (2.1)$$

where g_i is a function (explicit or implicit) of the design variables and the time and space coordinates.

The simple two-dimensional example shown in Fig. 2.1 depicts these concepts plus some additional terms. This figure illustrates the problem of minimizing the cost function $J = t_1^2 + t_2^2$ subject to the constraints:

$$g_1 = t_1 - 1 \geq 0 \quad ,$$

$$g_2 = t_2 - 0.5 \geq 0 \quad ,$$

$$g_3 = t_1 t_2 - 1 \geq 0 \quad .$$

The circular arcs are lines along which J is constant. The design vector is $\{t_1, t_2\}^T$ and the design space is given by all real values of t_1 and t_2. This design space is divided into two regions by the constraint conditions: the "feasible" and the "infeasible" region. The shaded, infeasible region is where the constraints are not satisfied, while the unshaded portion is the feasible region from which the optimal design must be found. While the optimal value of $t_1 = t_2 = 1.0$ can almost be found by inspection (or by methods of ordinary calculus) in this case, it should be obvious that problems involving a large number of design variables and more complicated constraints require considerable effort and ingenuity in the search for the optimum.

A further concept that can be demonstrated with this two-dimensional example is that of the active and the inactive constraint. At

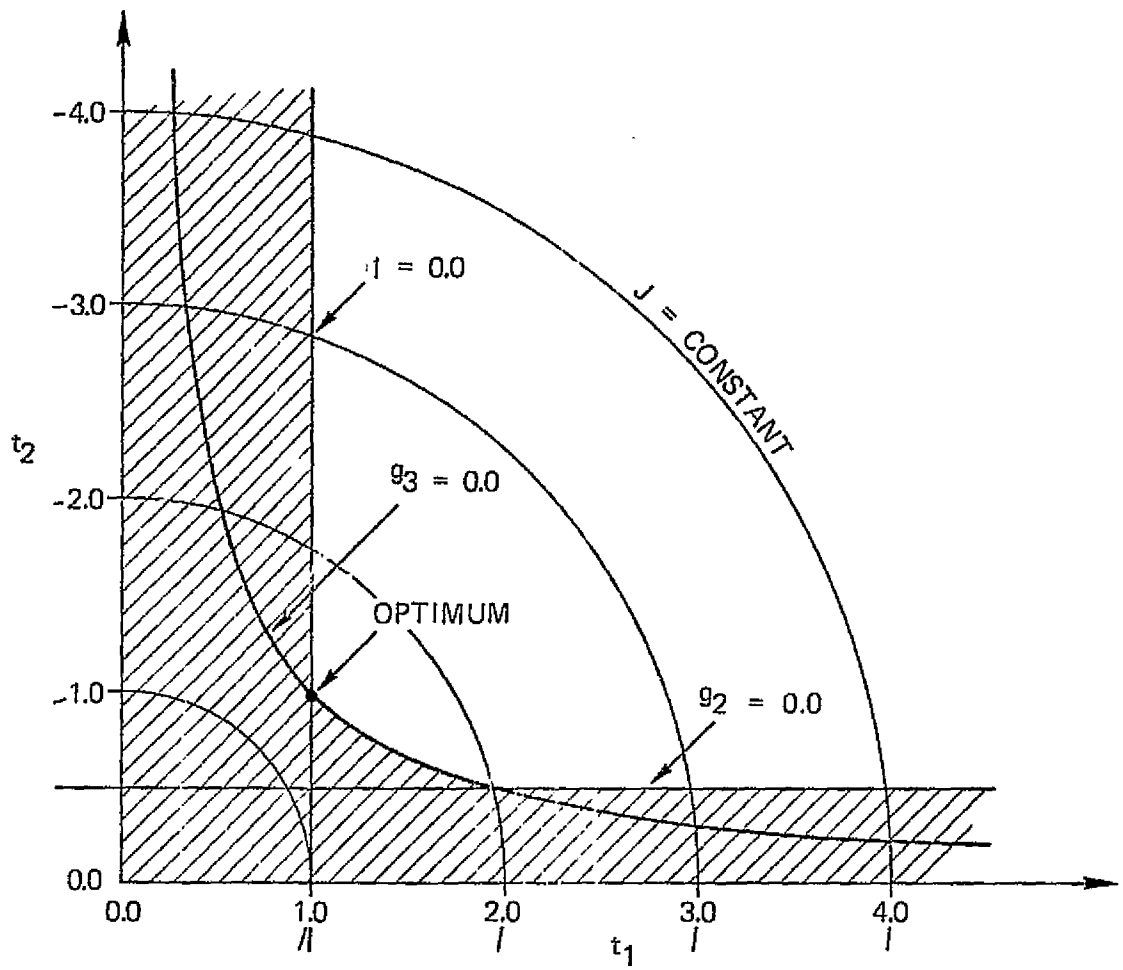

FIG. 2.1--Concepts of Optimization.

the optimum it is seen that constraints g_1 and g_3 are satisfied as equality constraints (i.e., $g_1 = g_3 = 0.0$). These are therefore designated active constraints. Constraint g_2 is also satisfied, but the optimum does not lie on this constraint so that it is designated inactive.

B. THE INTERIOR PENALTY FUNCTION

When inequality constraints are imposed on the design, penalty function methods can be used to include the constraint in the objective function. This strategem converts the problem to one that can utilize the powerful methods used to solve the unconstrained minimization problem. Reference 2 contains a good description of these methods, and this presentation therefore focuses on the details of the particular penalty function used here.

An interior penalty function is one that forces the trial design always to be in the feasible region. The specific function used in this work was of the form:

$$\Phi = J - r \sum_{i=1}^{nc} \ell n\ (g_i) \quad . \tag{2.2}$$

The modified objective function, Φ , is seen to become arbitrarily large as the design vector approaches the constraint $g_i = 0$. As mentioned, this has the effect of forcing the trial design to be in the feasible region. Note that the form used here requires that the constraint be in the range $0 \leq g_i \leq 1$. This is accomplished by

redefining a given constraint so that it fits within these limits (e.g., the constraint $g_1 = t_1 - 1.0$ of Fig. 2.1 can be cast into the equivalent form $g_1 = 1.0 - 1.0/t_1$. The r used in equation (2.2) is a specified scalar. The procedure followed is to minimize Φ for a chosen value of r and then to reduce r by some factor and repeat the optimization. In the limit as $r \to 0$, the optimal result for the modified problem is seen to be arbitrarily close to the optimum of the unmodified problem.

The extended interior penalty function method is a variation that was applied in reference 24 to a similar penalty function method. Figure 2.2 depicts an optimization problem that aids in explaining this refinement. In this diagram the function $J = ax$ is being minimized subject to the constraint that $x \geq b$ (or $g = 1 - (b/x) \geq 0$). While the modified cost function $\Phi = ax - r \ln (1.0 - b/x)$ blows up as x approaches b , the extended penalty function remains finite. This is done by using the formulation:

$$\Phi = J - r \sum_{i=1}^{nc} G_i(g_i) \quad , \tag{2.3}$$

where:

$$G_i(g_i) = \begin{cases} \ln (g_i) & g_i \geq \epsilon \\ \ln \epsilon + \dfrac{g_i - \epsilon}{\epsilon} & g_i < \epsilon \end{cases} .$$

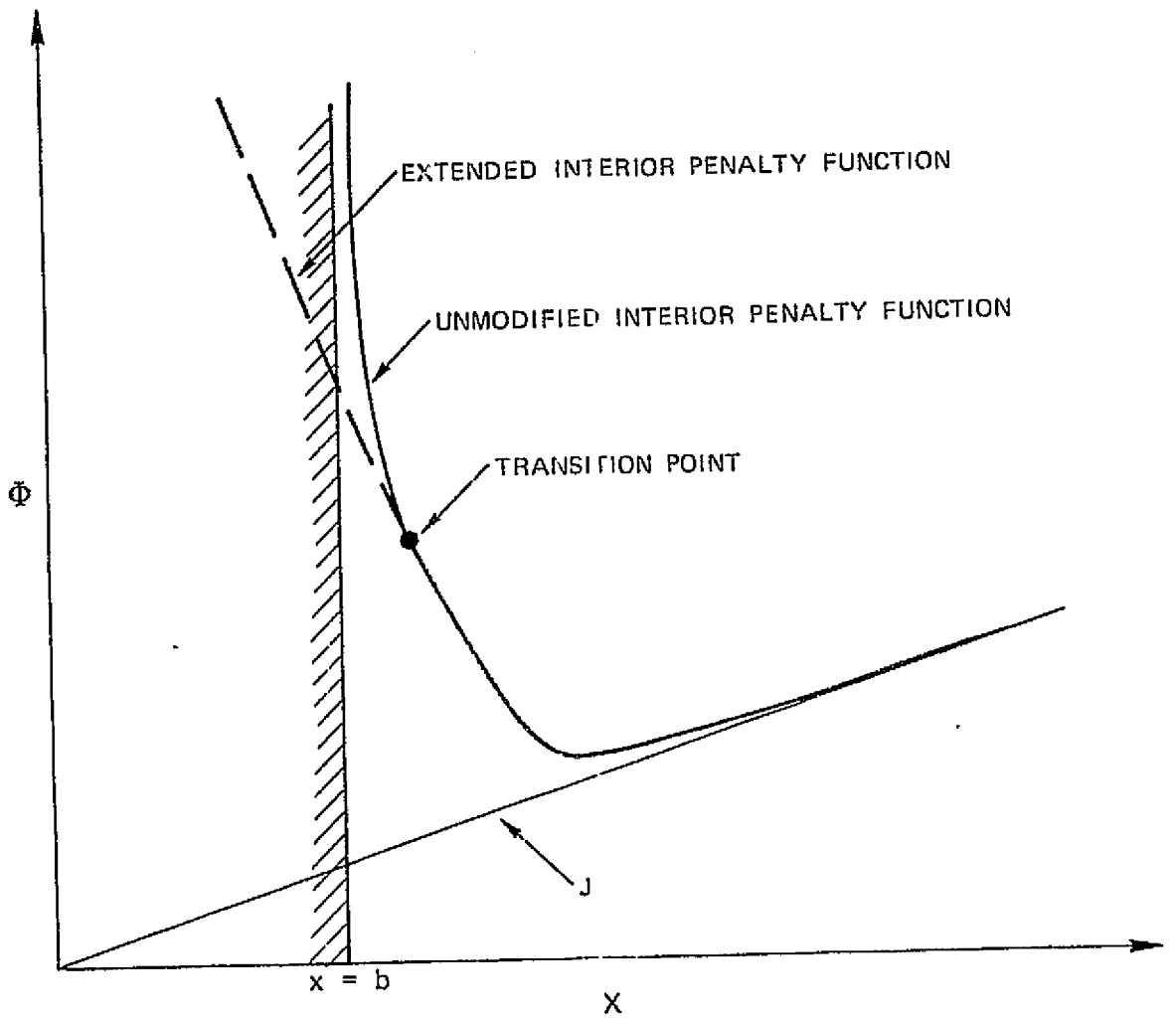

FIG. 2.2--Extended Interior Penalty Function.

The new expression is a Taylor series expansion of $\ell n\ (g_i)$ about the point $\ell n\ (g_i) = \epsilon$. The reason for this esoteric construction is that the optimization process can now deal with designs in the infeasible region. Analysis of designs that are infeasible may sometimes be inadvertently performed either during the one-dimensional minimization described in the next section or by starting from an initial design that is infeasible.

The value used for ϵ was selected by recourse to an argument similar to one used by Cassis (Ref. 24) for a different penalty function. For the present penalty function, this gives $\epsilon = \exp\ (-\ r/\Phi)$. More comments on this choice for ϵ are made at the end of this chapter.

C. THE VARIABLE METRIC METHOD

This section describes the particular mathematical programming algorithm used for the numerical optimizations of the thesis. When this study was in its early stages, a steepest descent algorithm was tried. The latter technique simply computes the gradient of the objective function with respect to the design vector at the design point. A new design is then found by taking an improving step in the direction of the gradient ("down the hill"). It is well known that the steepest descent method has very poor convergence properties but it was felt that it would suffice for the simple problems to be dealt with. For designs with more than three elements, this proved not to be the case.

Following an investigation of various alternative algorithms, the variable metric method (also referred to as the Davidon-Fletcher-Powell method, after its developers) was settled upon. Reference 2 contains an excellent description of this method, and what follows is essentially a summary of that description. The variable metric method can be motivated by looking at a Taylor series expansion, about design $\{t_0\}$, of an objective function:

$$\begin{aligned} \Phi(t) &= \Phi(t_0) + \{\nabla\Phi(t_0)\}^T \{\Delta t\} \\ &+ \frac{1}{2} \{\Delta t\}^T [\nabla^2\Phi(t_0)] \{\Delta t\} \\ &+ \text{higher order terms} \quad , \end{aligned} \tag{2.4}$$

where:

$$\underset{n \times 1}{\{\Delta t\}} = \{t - t_0\}$$

$$\underset{n \times 1}{\{\nabla\Phi(t_0)\}} = \left\{ \frac{\partial\Phi}{\partial t_i} \right\}_{\{t\} = \{t_0\}}$$

$$\underset{n \times n}{[\nabla^2\Phi(t_0)]} = \left[\frac{\partial^2\Phi}{\partial t_i \partial t_j} \right]_{\{t\} = \{t_0\}} .$$

At the optimum $\{\nabla\Phi\} \equiv \{0\}$, so that, to terms of second order, near the optimum

$$\{\nabla\Phi(t)\} = \{\nabla\Phi(t_0)\} + [\nabla^2\Phi(t_0)]\{\Delta t\} = \{0\} \quad . \tag{2.5}$$

Starting from $\{t_0\}$, the indicated correction step is:

$$\{\Delta t\} = -[\nabla^2\Phi(t_0)]^{-1}\{\nabla\Phi(t_0)\} \quad . \tag{2.6}$$

If this were the actual procedure used to find the new design, it would be a second-order method. In practice, the $[\nabla^2\Phi]$ matrix is often difficult to obtain. This is particularly true for problems dealt with here since the constraints used are very complex.

The variable metric method was developed to circumvent this problem by finding an approximation to the $[\nabla^2\Phi]^{-1}$ matrix. The method is outlined below and is followed by a brief justification of the algorithm.

Directly from Ref. 2:

(1) Start with some initial design vector $\{t\}_0$ and an initial positive definite matrix $[H]_0$ (typically the identity matrix). Set $\{S\}_0 \equiv -[H]_0\{\nabla\Phi(t_0)\}$.

(2) Find $\{\Delta t\} = \alpha_q\{S\}_q$, picking α_q so as to minimize $\Phi(t_{q-1} + \alpha_q S_q)$. The q subscript refers to the iteration number.

(3) Compute:

$$[H]_{q+1} = [H]_q + [A]_q + [B]_q \quad , \tag{2.7}$$

where, designating

$$\{V\}_q \equiv \{\nabla\Phi(t_{q+1}) - \nabla\Phi(t_q)\} \quad ,$$

$$\{A\}_q \equiv [\alpha_q \{S\}_q \{S\}_q^T]/(\{S\}_q^T \{V\}_q)$$

$$\{B\}_q \equiv - [\{[H]_q \{V\}_q\}\{[H]_q \{V\}_q\}^T]/(\{V\}_q^T [H]_q \{V\}_q) \quad .$$

(4) Then set $\{S\}_{q+1} = - [H]_{q+1} \{\nabla\Phi(t_{q+1})\}$ and return to (2) until convergence is achieved.

This rather complicated procedure can be heuristically justified by the fact that, for a quadratic objective function with n design variables, the procedure yields $[H]_n = [\nabla^2\Phi]^{-1}$.

That is, if Φ is of the form:

$$\Phi = \{t\}^T [M]\{t\} + [N]\{t\} + C$$

$$\text{Then:} \quad [H]_n = [M]^{-1} \quad . \tag{2.8}$$

A proof of this statement can be found in Ref. 33. While the problems dealt with here are not quadratic in the design vector, the assumption is made that, close to the optimum, the objective can be approximated by a quadratic.

1. Interpolation

A remaining task is the elaboration of the rather innocent statement contained in step two of the algorithm: "picking α_q so as to minimize $\Phi(t_q + \alpha_q s_q)$ ". This entails performing a one-dimensional minimization at each iteration, and it proved to be the most difficult and time consuming aspect of the optimization. The procedure finally settled on to perform this 1-D search was a rather complex form of cubic interpolation that will be summarized here.

The goal is to find the value α^* that minimizes the scalar function $\Phi(t + \alpha s)$. Assume that the objective function can be approximated by a cubic equation in α

$$\Phi = a + b\alpha + c\alpha^2 + d\alpha^3 \quad . \tag{2.9}$$

If this approximation were exact, the minimum could be readily found by setting the derivative of Φ with respect to α equal to zero and then solving for α :

$$\frac{\partial \Phi}{\partial \alpha} = b + 2c\alpha + 3d\alpha^2 = 0 \quad , \tag{2.10}$$

$$\therefore \quad \alpha^* = \left(-c \pm \sqrt{c^2 - 3db} \right) / 3d \quad .$$

The choice of sign is resolved by using the additional constraint that, at the minimum, the second derivative of the function is positive:

$$\frac{\partial^2 \Phi}{\partial \alpha^2} = 2c + 6d\alpha \geq 0 \quad . \tag{2.11}$$

Substituting the solution for α^* from equation (2.10) into (2.11) gives:

$$2c + \frac{6d}{3d}\left(-c \pm \sqrt{c^2 - 3db}\right)$$

$$= \pm 2\sqrt{c^2 - 3db} > 0 \quad . \tag{2.12}$$

Clearly, the positive sign must be chosen.

To complete the analysis, the values of the coefficients (a , b , c and d) must be obtained. The original design is the value of the objective function at $\alpha = 0$. The slope of the objective in the α direction at $\alpha = 0$ is given by $\{\nabla\Phi(t_0)\}^T\{S\}$. Immediately then, $a = \Phi(t_0)$ and $b = \{\nabla\Phi(t_0)\}^T\{S\}$. The remaining coefficients are determined by evaluating Φ at two different values of α . In order to assure convergence, these values were picked so that the minimum was bracketed by the three function evaluations.

Once α^* is obtained using the above procedure, a test is made to see if it indeed is at the minimum value of $\Phi(t + \alpha S)$. The test used was to compute $|\{\nabla\Phi(t + \alpha^* S)\}^T\{S\}|/(|\{\nabla\Phi(t + \alpha^* S)\}^T||\{S\}| \equiv CI$.

If α^* is exactly at the minimum, CI is zero. The criterion used was that if CI was less than some specified δ then the optimization would proceed. If not, then an additional interpolation must be made utilizing the new values of $\Phi(t + \alpha^* S)$ and $\{\nabla\Phi(t+\alpha^* S)\}^T\{S\}$ until the criterion is satisfied.

2. Minimum Thickness Constraints

Under certain design conditions, it is possible, in the absence of constraints on their size, that design variables may go to zero and even take on negative values. Since these design variables correspond to element thicknesses, it is physically and computationally undesirable for this to happen. Various methods have been constructed to deal with this problem, and this section describes a novel method used in Chapter III of this work. It is a method that worked quite well and is not well known in the structural optimization field.

The technique used is a transformation employed by Pierson (Ref. 10) for a continuous design variable. Modified to accept a discrete design vector, this transformation has the form:

$$\{t\} = \{t_{min}\} + \frac{1}{2}\{u^2\} \quad . \tag{2.12}$$

The t_{min} is a constant minimum thickness constraint while u is considered the new design variable. The beauty of this transformation is the $\{t\}$ remains positive even if $\{u\}$ inadvertently has some negative components.

A minor difficulty arises when derivatives are needed with respect to the new design vector $\{u\}$. The indicated procedure is to use the chain rule by first taking the derivative with respect to $\{t\}$ and then use

$$\left\{\frac{\partial \Phi}{\partial u}\right\} = \left\{\frac{\partial \Phi}{\partial t}\ \frac{\partial t}{\partial u}\right\} = \left\{u\ \frac{\partial \Phi}{\partial t}\right\} \quad . \tag{2.13}$$

D. COMMENTS

Despite the analytical underpinnings described above, optimization techniques remain very much an art. It is felt that some personal observation from one who began this work with a limited knowledge of optimization techniques might prove of value to others who are in a similar situation.

First, a disclaimer must be made to the effect that the use of the variable metric method coupled with an interior penalty function should not be considered a recommendation of either technique as the best method for solving a general problem. Each problem must be approached on an individual basis, with a consideration of the requirements and capabilities of each technique. The strong points of the method are that it is a sophisticated gradient method that proceeds to the optimum in a deliberate fashion. Other techniques, utilizing feasible directions (Ref. 34) or optimality criteria (Ref. 3), are more efficient for certain applications and may even be better suited

for the problems worked here. A further general comment is that computer centers are now likely to contain optimization routines in their libraries. The first step for anyone embarking on an optimization problem should then be to determine if these readily available routines are adequate or can be adapted for their needs.

Given these general comments, specific perceptions gained while exercising the programs are offered below.

The use of the $- \ell n\ (g_i)$ as a penalty function is an innovation with respect to structural optimization problems as far as the author knows. The more common interior penalty function is one of the form $1/g_i$. The log function seems to provide a smooth function with an easily calculated derivative. It would be interesting to hear of others' experience with different functions.

The values chosen for the penalty parameter r of equation (2.2) have to be selected in an arbitrary manner. For this thesis, values of r ranging from 10 to 10^{-5} were used. The reduction $r_{i+1} = r_i/10$ was always used until the minimum r was reached.

Texts on this method advocate iterating on each value of r until an optimum is reached before reducing it. This seems to be an unnecessarily strict requirement and an alternative was used that reduced r after it appeared that little improvement would be made at the present value. This was done by specifying that if $\Phi_q/\Phi_{q-1} \geq 1.0/(1.0 + 10\ r)$, then r should be reduced by ten and the new optimization problem initiated. If not, iteration continued until the criterion was met. This

approach has the added benefit that the criterion is satisfied quickly for large values of r and becomes increasingly more stringent as r is reduced. For the final value of r, a convergence criterion was employed. The criterion used was obtained from Ref. 2 and entailed checking if

$$|\{\nabla\Phi\}^T [H] \{\nabla\Phi\}|/\Phi < 0.02 \quad .$$

If the inequality was satisfied, the problem was considered solved; if not, the iteration continued.

The use of the extended interior penalty function described in Section II.B proved to be of marginal value. The main reason for this is that the values of ϵ were so small that the objective functions calculated using the extended penalty function were almost always too large to be of value in the interpolation procedure. This in turn was due to the way in which ϵ is calculated. In order to assure that the transition point (i.e., ϵ) is between the minimum point and the infeasible region it was found necessary to use $\epsilon = \exp(-r/\Phi)$. Without going into detail, it is recommended that, if the extended penalty function is to be used, further efforts be made to obtain a better transition point when using the log penalty function, or that the $1/g_i$ penalty function be used coupled with a transition point calculated by Cassis (Ref. 24): $\epsilon = r/\phi$.

A number of other "tricks" were employed in the optimization and particularly in the one-dimensional search. However, it seems of

little value to detail them here. The main thing to be kept in mind is the nature of the optimization process and the mechanics involved. Some of the calculations of the next three chapters may appear excessive unless it is remembered why the optimization algorithm makes them necessary.

CHAPTER III

HARMONIC EXCITATION

A. INTRODUCTION

Among the simplest dynamic response problems to formulate and solve are those of one-dimensional structures excited by harmonically oscillating loads. If only the steady state response is of interest, the time parameter can be removed from the equations of motion by assuming that the structure responds at the frequency of excitation. It was supposed, therefore, that this type of problem would be a logical beginning to a study of structural optimization in the presence of dynamic loading. The results of this chapter indicate that this supposition is essentially correct but there there are unanticipated difficulties related to the fact that the feasible region is disjoint. In order to demonstrate this difficulty, some extremely simple examples are presented in the following paragraphs.

Consider a uniform cantilevered rod excited by a uniformly distributed sinusoidal torque. The differential equation and related boundary conditions for this system are (Ref. 32, Chap. 3)

$$\frac{\partial}{\partial x}\left(GJ\frac{\partial\theta}{\partial x}\right) - I_\alpha \frac{\partial^2\theta}{\partial t^2} = -\bar{T}\, e^{i\omega_e t} \quad , \qquad (3.1)$$

and

$$\theta\big|_{x=0} = 0 \quad \text{and} \quad GJ \left.\frac{\partial\theta}{\partial x}\right|_{x=L} = 0 \quad .$$

Here, ω_e is the excitation frequency. The amplitude of the steady state solution of Eq. (3.1) is

$$\bar{\theta}(x) = \frac{\bar{T}}{GJ\lambda}\left[\cos\sqrt{\lambda}x - 1 + \tan\sqrt{\lambda}L \sin\sqrt{\lambda}x\right] \quad , \quad (3.2)$$

where

$$\lambda = \frac{I_\alpha \omega_e^2}{GJ} \quad .$$

A graphical representation of $\theta(L)$ is presented in Figure 3.1. The points to be made are that the magnitude of the deflection does not increase monotonically with the magnitude of the excitation frequency and that, given a specified deflection, there is not a unique value of the excitation frequency that results in that deflection. In fact, there are an infinite number of such excitation frequencies. This should provide an inkling of the problems to be encountered with a harmonic excitation. To make it more explicit, a further example is presented below that involves a structural optimization problem with only two design variables.

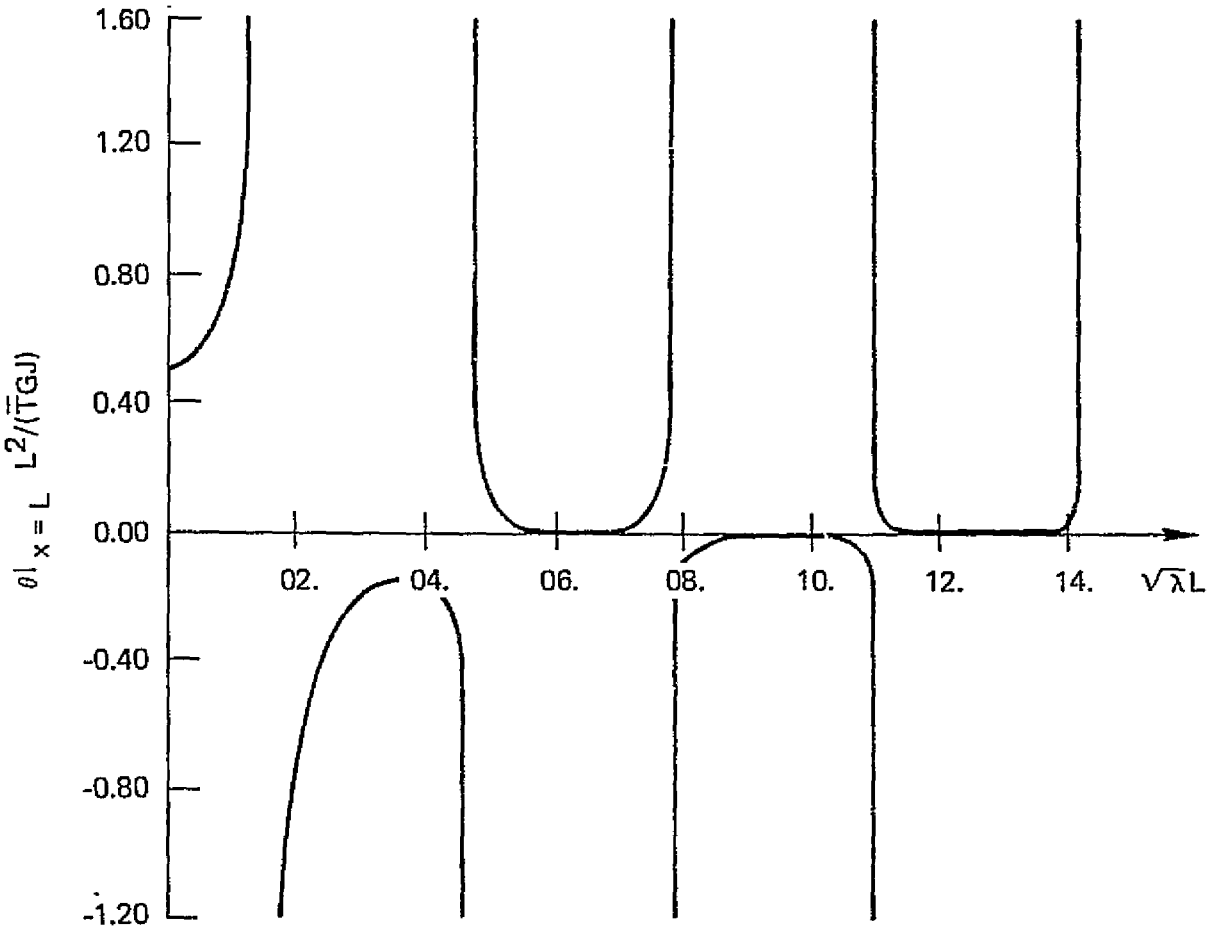

FIG. 3.1--Response of the Tip of a Uniform Rod Excited by a Uniformly Distributed Harmonic Load as a Function of the Frequency of Excitation.

B. TWO DESIGN VARIABLE EXAMPLE

This section seeks the optimal design of a thin walled cantilevered rod excited uniformly in torsion by a harmonically varying load. If this system is modelled by two finite elements of equal length, equations from Section A.1 can be specialized to the $n = 2$ case to give the steady state equation of motion:

$$\left(- \frac{\omega_e^2 I_{\rho 0} L^2}{24 G J_0} \begin{bmatrix} 2(t_1 + t_2) & t_2 \\ t_2 & 2t_2 \end{bmatrix} + \begin{bmatrix} t_1 + t_2 & - t_2 \\ - t_2 & t_2 \end{bmatrix} \right) \begin{Bmatrix} \theta_1 \\ \theta_2 \end{Bmatrix} = \frac{\bar{T} L^2}{8 G J_0} \begin{Bmatrix} 2 \\ 1 \end{Bmatrix} \quad . \tag{3.3}$$

The constraints considered are that the magnitude of the stress be no greater than some specified value. From the Appendix, the stress can be expressed as:

$$\{S\} = \frac{2GR}{L} \begin{bmatrix} 1 & 0 \\ - 1 & 1 \end{bmatrix} \begin{Bmatrix} \theta_1 \\ \theta_2 \end{Bmatrix} \quad .$$

The motivation for representing the structure by two design variables is that it is possible to depict the results graphically, thereby gaining a qualitative description of what would be encountered with a more realistic representation containing many elements. In this particular case, an added benefit is that it is relatively easy to compute

the stress amplitudes explicitly:

$$\frac{S_1}{S_{max}} = \frac{2GR}{L}\theta_1 = \frac{3T_n\, t_2(1 - \lambda_e)}{DET} \quad , \qquad (3.4)$$

$$\frac{S_2}{S_{max}} = \frac{2GR}{L}(\theta_2 - \theta_1) = \frac{T_n(3\lambda_e t_2 + t_1(1 - 2\lambda_e)}{DET} \quad ,$$

where:

$$\lambda_e = \frac{\omega_e^2 I_{\infty} L^2}{24 G J_0} \quad ,$$

$$T_n = \bar{T}LR/(4J_0\, S_{max}) \quad ,$$

$$DET = t_2\{t_1(1 - 2\lambda_e)^2 - t_2(6\lambda_e - 3\lambda_e^2)\} \quad .$$

The constraints for this problem are that the absolute values of S_i/S_{max} must be less than unity. In the notation of Chapter II, these are written as $g_i = 1 - (S_i/S_{max})^2 \geq 0$.

Figures 3.2 and 3.3 show the feasible and infeasible regions for values of λ_e ranging from zero to three and for T_n equal to 0.085.

For the $\lambda_e = 0$ case (static loading), presented in Fig. 3.2(a), the constraints are seen to be two straight lines. The cost function is simply $J = t_1 + t_2$ so that the optimum is at the intersection of these two lines. Figure 3.2(b) shows the design space for $\lambda_e = 1/24$

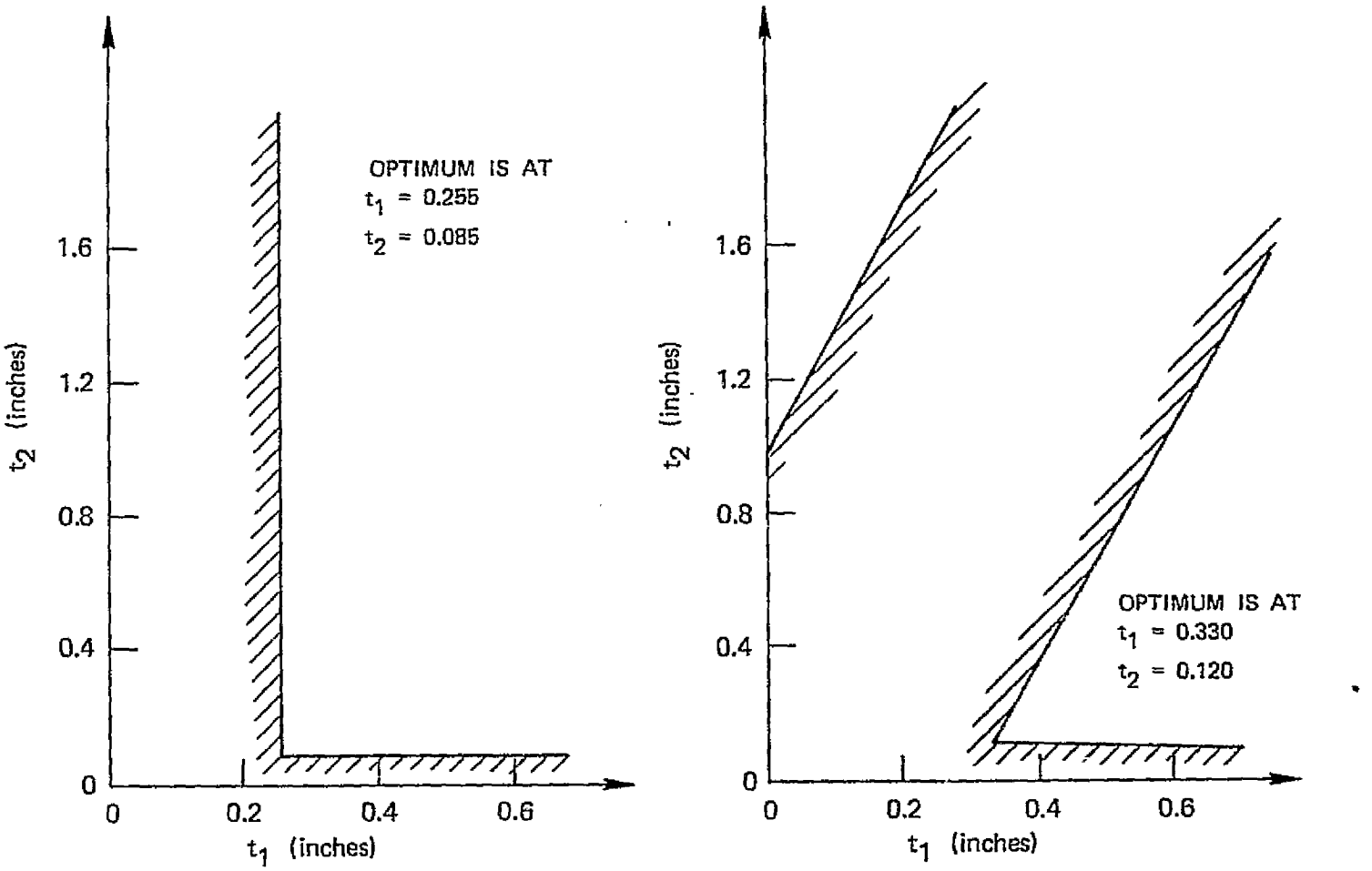

(a) $\lambda_e = 0.0$ (b) $\lambda_e = 1/24$

FIG. 3.2--Design Space for a Cantilevered Rod Excited in Torsion at Nondimensional Frequency λ_e.

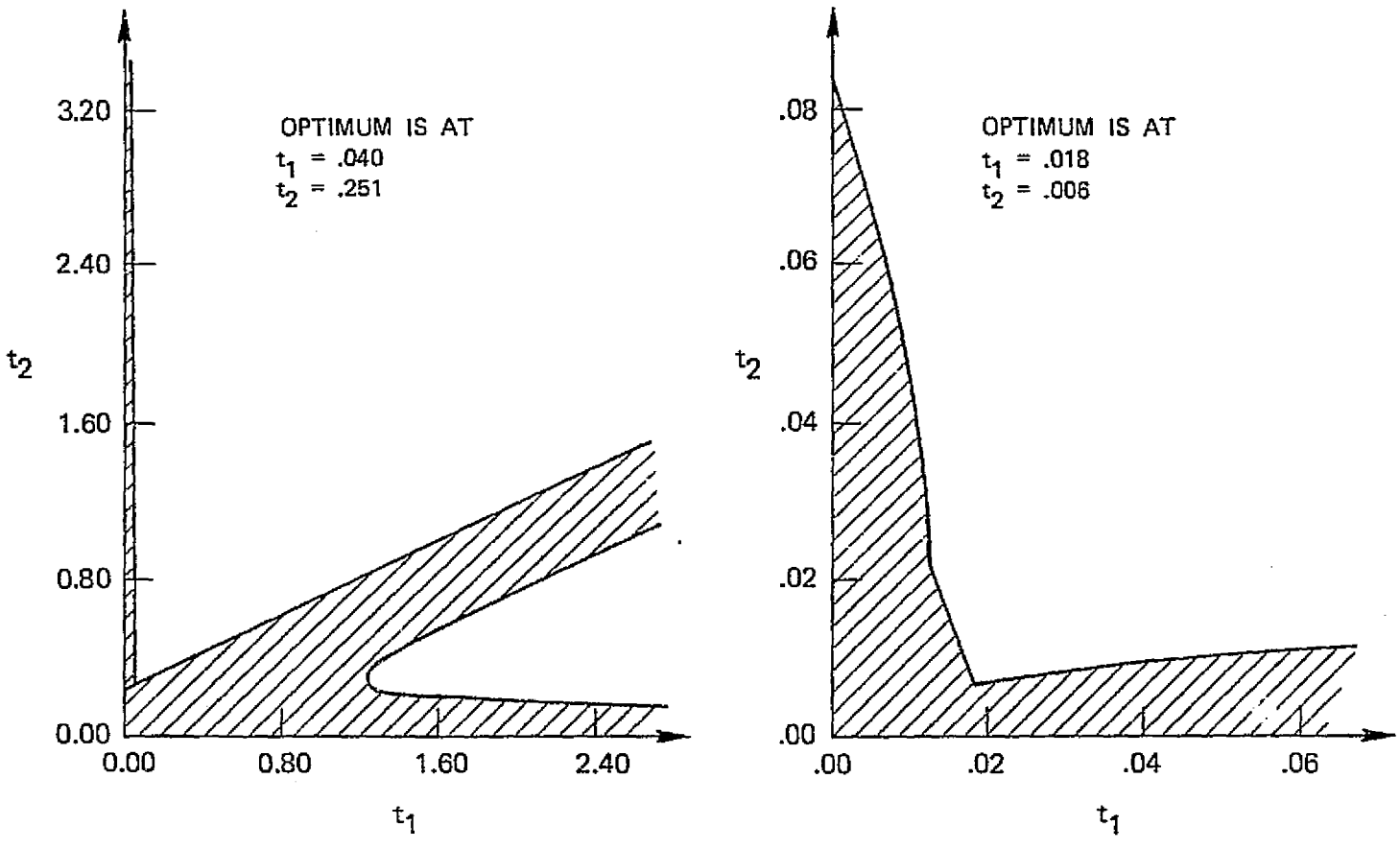

(a) $\lambda_e = 1/6$ (b) $\lambda_e = 3$

FIG. 3.3--Design Space for a Cantilevered Rod Excited in Torsion at Nondimensional Frequency λ_e.

and it is seen that there are two separate feasible regions. This is the difficulty that is illustrated by this example and is discussed further below.

Figure 3.3(a) shows the results for $\lambda_e = 1/6$. The constraint at $t_1 = 0.04$ is a minimum thickness constraint that is included to eliminate the $t_1 = 0.0$ solutions that satisfy the stress constraints but are physically unrealistic. It is seen that the least weight solution is in the upper region at $t_1 = 0.04$ and $t_2 = 0.25$. Finally, Fig. 3.3(b) shows that for the $\lambda_e = 3$ case there is again only one feasible region.

The explanation for this curious behavior is to be found by studying the eigenvalues of the system. Let λ_1 and λ_2 denote the non-dimensional values of the first and second eigenvalues. In Fig. 3.3(a), the designs with λ_1 equal to the excitation frequency are all on a straight line emanating from the origin with an equation given by $t_1 = 2.06\ t_2$. This line proceeds directly through the middle of the infeasible region, dividing the design space into two distinct regions. Clearly designs that have $\lambda_e = \lambda_1$ are infeasible because this represents a resonance condition with an unbounded response. The region $t_1 > 2.06\ t_2$ contains designs where $\lambda_1 > \lambda_e$ while the region $t_1 < 2.06\ t_2$ contains designs where $\lambda_1 < \lambda_e$. Each of these regions has its own optimum, as is demonstrated by the figure.

Segenreich and Rizzi (Ref. 35) have shown that the eigenvalues of cantilevered rods modelled in the fashion described in the Appendix

have prescribed limits. For the specific case of two design variables of interest here, these limits are given by:

$$0 \leq \lambda_1 \leq 0.5 \quad ,$$

$$0.5 \leq \lambda_2 \leq 2.0 \quad . \tag{3.5}$$

As a function of the excitation frequency, there are, therefore, either one or two distinct feasible regions. These regions are given by:

Excitation Frequency	No. of Regions	Eigenvalue Relationships
$\lambda_e = 0$	1	$\lambda_2 > \lambda_1 > \lambda_e$
$0 < \lambda_e \leq 0.5$	2	1.) $0 < \lambda_e < \lambda_1 < \lambda_2$ 2.) $0 \leq \lambda_1 < \lambda_e < \lambda_2$
$0.5 < \lambda_e < 2.0$	2	1.) $\lambda_1 < \lambda_e < \lambda_2$ 2.) $\lambda_1 < \lambda_2 < \lambda_e$
$\lambda_e > 2.0$	1	$\lambda_e > \lambda_2 > \lambda_1$

The $\lambda_e > 2.0$ case explains why Fig. 3.3(b) contains only one feasible region; the excitation frequency is greater than any possible eigenvalue of the system.

It should be clear why this disjoint property of the feasible region presents a difficult obstacle in the search for a global optimum. While it is possible to analyze the two design variable case graphically in a thorough fashion, this is not practical for designs with a greater number of elements. Figure 3.1 was presented to motivate the hypothesis that for the continuous case there are an infinite number of local optima corresponding to the infinite number of distinct regions where $\lambda_i < \lambda_e < \lambda_{i+1}$, $i = 1,2,\ldots,\infty$.

For problems with an arbitrary number of elements, some method such as that described in Chapter II has to be utilized to search for an optimum. But such methods have the drawback that the search takes place inside one feasible region. Therefore, for a given problem, the global optimum is found by selecting the minimum of all the distinct local minima. Cassis (Ref. 24) encountered disjoint feasible design spaces while studying a different dynamic response problem and found it preferable to search for the optimum in the infeasible region by using an exterior penalty function method. His thought was that the solution would be more likely to proceed to the global optimum. But this technique provides no advantage here since an exterior penalty function technique still proceeds "downhill" and would not, therefore, cross over the infinitely high "ridge" where the excitation frequency equals an eigenfrequency in order to descend into the "valley" of the global optimum. More comments are offered on this problem in Section D.

It might be supposed that the disjoint nature of the feasible region is due to the omission of structural damping; in a sense, this is true. The addition of damping gets rid of the infinitely high ridges, since a damped structure excited at its resonant frequency has a finite response. A brief study that included damping was made, and a result from the study is presented in Fig. 3.4. The figure superimposes the $\lambda_e = 1/6$ case of Fig. 3.3(a) and the results from an identical problem except that the shear modulus was multiplied by $(1 + i\alpha)$, where α is a small structural damping factor. This is a technique frequently used to take account of the fact that structures have damping present in them (Ref. 36, Chap. 12). The value of α used to obtain the results shown was 0.1 — an unrealistically high value, but one that depicts the damping effect clearly. It is seen that the damping reduces the infeasible region and prevents it from extending to infinity. The disjoint character of the design space has been eliminated, but two minima are still retained as pockets of the unified design space. The basic problem of finding the global optimum still remains. Note that the optimal solutions for the damped case do not differ greatly from the undamped case. Damping was not included in the analyses presented in the remainder of this chapter since it was felt that the benefits gained from added practicality or realism do not offset the complications introduced by complex variables.

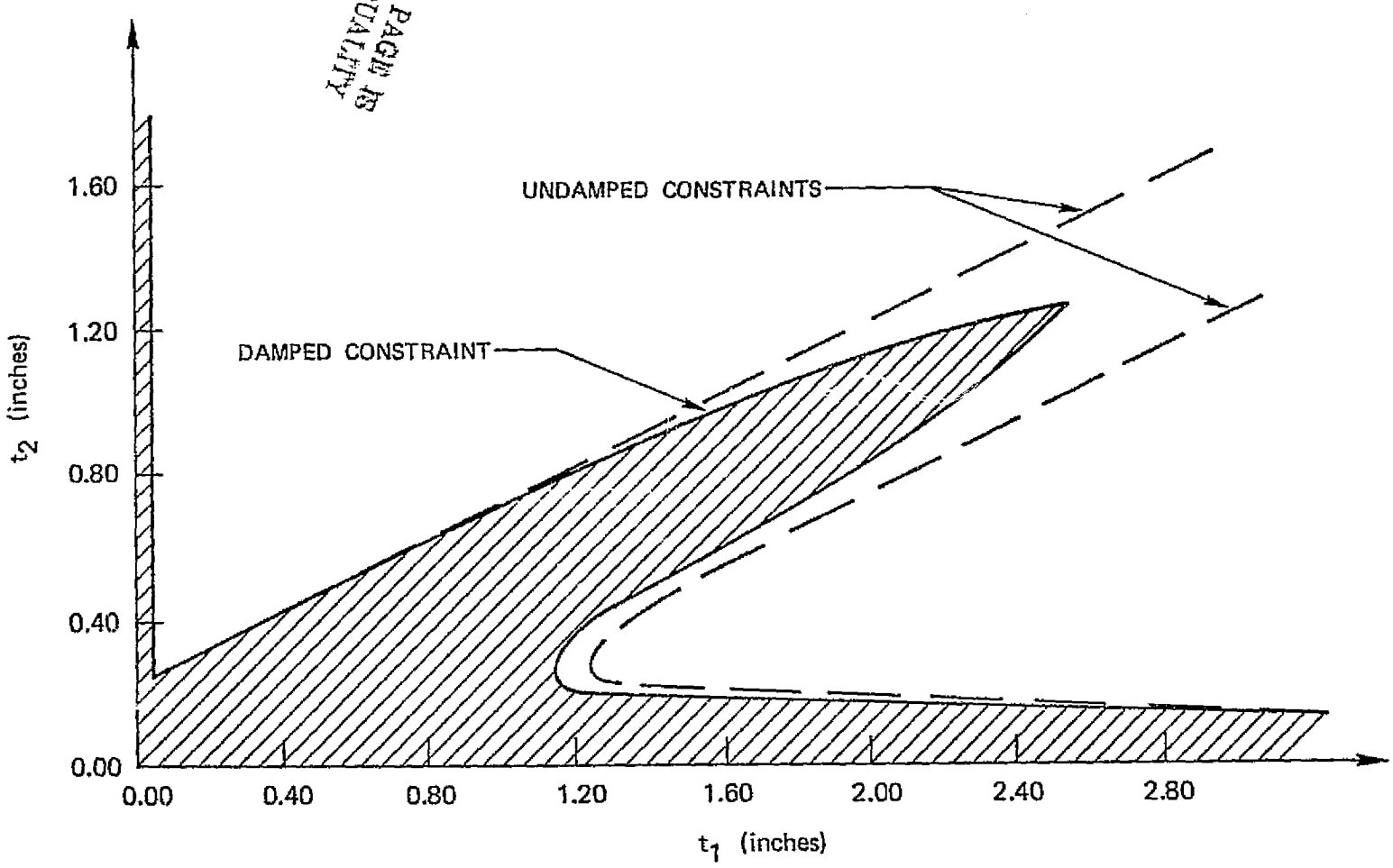

FIG. 3.4--Comparison of Two-Dimensional Design Spaces for Damped and Undamped Solutions, $\lambda_e = 1/6$.

C. FUNCTION SPACE SOLUTIONS

Before proceeding to the finite element solutions, another procedure that is applicable to these sorts of problems is presented: that of solving optimization problems by dealing with the differential equations directly. The motivation for this section comes from the success others achieved while applying optimal control techniques to structural optimization problems. In particular, Weisshaar (Ref. 7) and Armand and Vitte (Ref. 8) were able to find optimal thickness distributions for a number of problems that had constraints on the system eigenvalues.

This section develops the criteria for an optimal solution for a harmonically loaded structure and solves some special cases.

Only one-dimensional structures are used in this study; therefore, the equations can be put into the first order form generally used in control theory:

$$\{x\}' = [F(t,s)]\{x\} + \{P\} \quad . \tag{3.6}$$

With boundary conditions at $s = 0$ and $s = 1$. The terms used are defined as:

$\{x\} = \{x(s)\}$ = $n \times 1$ vector of state variables

$t = t(s)$ = thickness distribution, the control variable of the problem

and

$\{P\}$ = $n \times 1$ vector of the load amplitude

$( )'$ = denotes a derivative with respect to s

s = the nondimensional coordinate and independent variable.

The analysis given below is an application of the methods described by Bryson and Ho (Ref. 37). Only the barest outline of the procedure is presented here.

The problem statement used in this thesis is that of minimizing the weight subject to constraints on the response. Mathematically, minimize

$$J = \int_0^1 t\,ds \quad . \tag{3.7}$$

Subject to

$$\{g(x,s,t)\} \geq 0 \quad ,$$

$$q \times 1 \text{ vector} \quad . \tag{3.8}$$

The Hamiltonian is constructed by using standard procedures of Ref. 37

$$H = t + \{\lambda\}^T ([F]\{x\} + \{P\}) + \{\mu\}^T \{g\} \quad , \tag{3.9}$$

where

$\{\lambda\}$ = $n \times 1$ vector of adjoint states ,

$\{\mu\}$ = $q \times 1$ adjoint vector for the constraints .

The value of μ_i is zero when $g_i \neq 0$ and is ≥ 0 when $g_i = 0$.

The Euler-Lagrange equations are:

$$\{\lambda\}' = -\left\{\frac{\partial H}{\partial x}\right\} = -\{\lambda\}^T [F] - \{\mu\}^T \left\{\frac{\partial g}{\partial x}\right\} \quad . \quad (3.10)$$

And the "control equation" is:

$$\frac{\partial H}{\partial t} = 0 = 1 + \{\lambda\}^T \left[\frac{\partial F}{\partial t}\right] \{x\} + \{\mu\}^T \left\{\frac{\partial g}{\partial t}\right\} \quad . \quad (3.11)$$

The transversality condition provides the required boundary conditions:

$$\{\lambda\}^T \{\delta x\}\Big|_0^1 = 0 \quad . \quad (3.12)$$

It is felt that the method is best dealt with here by example. Hopefully, these examples also clarify the technique.

1. Example: Cantilevered Beam With a Static Load

A cantilevered beam acted upon by a uniform static load has a differential equation and associated boundary conditions given by

$$\frac{d^2}{dx^2}\left(EI\,\frac{d^2w}{dx^2}\right) = P \quad , \tag{3.13}$$

$$w|_{x=0} = \left.\frac{dw}{dx}\right|_{x=0} = \left.EI\,\frac{d^2w}{dx^2}\right|_{x=L} = \left.\frac{d}{dx}\left(EI\,\frac{d^2w}{dx^2}\right)\right|_{x=L} = 0 \quad .$$

Using notation and assumptions given in Ref. 7, the first order form of this system is

$$\begin{Bmatrix} x_1 \\ x_2 \\ x_3 \\ x_4 \end{Bmatrix}' = \begin{bmatrix} 0 & 1 & 0 & 0 \\ 0 & 0 & \frac{1}{t} & 0 \\ 0 & 0 & 0 & 1 \\ 0 & 0 & 0 & 0 \end{bmatrix} \begin{Bmatrix} x_1 \\ x_2 \\ x_3 \\ x_4 \end{Bmatrix} + \bar{P} \begin{Bmatrix} 0 \\ 0 \\ 0 \\ 1 \end{Bmatrix}$$

$$x_1(0) = x_2(0) = x_3(1) = x_4(1) = 0 \quad , \tag{3.14}$$

where

$$x_1 = w/L \quad ,$$

and

$$x_2 = \frac{1}{L}\frac{dw}{dx} \quad ,$$

$$x_3 = \frac{t}{L^2}\frac{d^2w}{dx^2} \quad ,$$

$$x_4 = \frac{1}{L^3}\frac{d}{dx}\left(t\frac{d^2w}{dx^2}\right) \quad ,$$

$$\bar{P} = \frac{PL^3}{EI_0} \quad .$$

The optimization problem is specified as that of finding the thickness distribution that minimizes the total weight while satisfying the constraint that the magnitude of the stress along the span of the beam is less than some specified S_{max} . By use of the familiar formula $S = (Ed/2)(d^2w/dx^2)$, this constraint can be put into the form:

$$g_1 = 1 - a|x_3|/t \quad , \qquad (3.15)$$

where $a = EdL^2/2S_{max}$.

Equation (3.9) is then:

$$H = t + \lambda_1 x_2 + \frac{\lambda_2 x_3}{t} + \lambda_3 x_4 + \lambda_4 \bar{P} + \mu\left(1 - \frac{a|x_3|}{t}\right) \quad . \qquad (3.16)$$

Equations (3.10) and (3.11) are evaluated to give:

$$\begin{Bmatrix} \lambda_1 \\ \lambda_2 \\ \lambda_3 \\ \lambda_4 \end{Bmatrix}' = \begin{bmatrix} 0 & 0 & 0 & 0 \\ -1 & 0 & 0 & 0 \\ 0 & -1/t & 0 & 0 \\ 0 & 0 & -1 & 0 \end{bmatrix} \begin{Bmatrix} \lambda_1 \\ \lambda_2 \\ \lambda_3 \\ \lambda_4 \end{Bmatrix} - \frac{a\mu}{t} \begin{Bmatrix} 0 \\ 0 \\ \text{sgn } (x_3) \\ 0 \end{Bmatrix}, \quad (3.17)$$

$$\frac{\partial H}{\partial t} = 0 = 1 - \frac{\lambda_2 x_3}{t^2} + \frac{\mu a|x_3|}{t^2} = 1 - \frac{\lambda_2 x_3}{t^2} + \frac{\mu}{t} \quad . \quad (3.18)$$

The last substitution is made because if $\mu \neq 0$, $[a(x_3)/t] = 1$.

The notation sgn ( ) designates that only the algebraic sign of the quantity is used.

The boundary conditions on the adjoint variables are

$$\lambda_1(1) = \lambda_2(1) = \lambda_3(0) = \lambda_4(0) = 0 \quad .$$

The first order equations and the boundary conditions give immediately

$$\begin{aligned} x_4 &= \bar{P}(s - 1) \quad , \\ x_3 &= \bar{P}(s^2 - 2s + 1)/2 \quad , \\ \lambda_1 &= 0 \quad , \\ \lambda_2 &= 0 \quad . \end{aligned} \quad (3.19)$$

These results can be placed in Eq. (3.15) to give:

$$1 + \frac{\mu}{t} = 0 \Rightarrow t = -\mu \quad . \tag{3.20}$$

Since μ is zero only when $a|x_3|/t$ is less than unity, it is clear that $t \geq \frac{a\bar{P}}{2}(1. - 2s + s^2)$. Equation (3.20) states that if μ is zero, then $t = 0$ and the inequality on t is violated except at $s = 1$. Therefore, μ cannot equal zero, requiring $a|x_3|/t = 1.0$ across the span. Stated another way, this says that the optimal solution is the one that creates a fully stressed structure. This is a well known result for problems of this type with a static loading.

The entire solution can now be written down as:

$$t = -\mu = a\bar{P}(1 - 2s + s^2)/2$$

$$x_2 = s/a \qquad \lambda_3 = as$$

$$x_1 = s^2/2a \qquad \lambda_4 = as^2/2 \quad . \tag{3.21}$$

The ease with which this analytical solution was obtained makes it appear that solutions with a harmonically oscillating load might also be tractable. The formulation for the same problem as above except that the excitation is harmonic with frequency ω_e can be written in terms of the static problem by adding several terms. The subscript $(\,)_{st}$ in the following equations refers to the static case

and Γ_e is a nondimensional frequency equal to $\omega_e \sqrt{m_0 L^3/EI_0}$. With this notation, the changes in Eqs. (3.14)-(3.18) for the harmonically excited structure are:

$$\dot{x}_4 = \Gamma_e^2 t x_1 + \bar{P} \quad ,$$

$$H = H_{st} + \lambda_4 \Gamma_e^2 t x_1 \quad ,$$

$$\dot{\lambda}_1 = -\Gamma_e^2 t \lambda_4 \quad ,$$

$$\frac{\partial H}{\partial t} = \frac{\partial H_{st}}{\partial t} + \lambda_4 \Gamma_e^2 x_1 = 0 \quad . \qquad (3.22)$$

These additions prevent determining that the optimal structure is fully stressed. Without this, it has been found impossible to treat these equations analytically. Numerical techniques that solve the two point boundary value problem and the associated control equation have been applied with little success. The main difficulty is in dealing with the stress constraint. The character of the solution changes at the value of s where the constraint changes from being inactive to being active. This requires patching together arcs as explained in Ref. 37, Chap. 3. If numerical techniques are to be used, it seems preferable to convert the problem to an unconstrained one by using the penalty function method as described in Section II.B.

If this is done, Eq. (3.7) becomes

$$J = \int_0^1 [t - r \ln (g)] \, ds \quad ,$$

and the difficulty in patching arcs is avoided, albeit the formulation becomes slightly more complex.

2. Example: Torsional Rod Excited by a Harmonically Varying End Load

Consider a torsional rod that is being excited at its tip by a harmonically oscillating load with frequency ω_e and constant amplitude $\overline{T}$. Pose the problem of finding the thickness distribution that minimizes the weight of the structure subject to the constraint that the tip rotational amplitude is equal to a specified value D . This problem was first solved by Icerman using energy considerations and with the additional constraint that the first natural frequency of the structure be greater than the excitation frequency. It is similar to a problem studied by Ashley and McIntosh (Ref. 6) and by Turner (Ref. 9) who found the minimum weight structure for a cantilevered torsional rod with a fixed tip mass and an equality constraint on the first natural frequency.

With the familiar assumptions that $GJ = GJ_0 t$ and $I_\alpha = I_{\alpha 0} t$, the differential equations can be put into the form (Ref. 8):

$$\begin{Bmatrix} x_1 \\ x_2 \end{Bmatrix}' = \begin{bmatrix} 0 & 1/t \\ -\Gamma^2 t & 0 \end{bmatrix} \begin{Bmatrix} x_1 \\ x_2 \end{Bmatrix} \quad . \qquad (3.23)$$

And the associated boundary conditions are

$$x_1(0) = 0 \quad ,$$
$$x_1(1) = D \quad ,$$
$$x_2(1) = \bar{T} \quad ,$$

where

$$\Gamma^2 \equiv \frac{\omega_e^2 I_{\alpha\alpha} L^2}{GJ_0} \quad .$$

Note that the equality constraint and the excitation are contained in the boundary conditions. The inertial loads appear in the $-\Gamma^2 t$ term.

The Hamiltonian of Eq. (3.9) has the form:

$$H = t + \frac{\lambda_1 x_2}{t} - \lambda_2 \Gamma^2 t x_1 \quad . \tag{3.24}$$

Equations (3.10) and (3.11) give the relations

$$\begin{Bmatrix} \lambda_1 \\ \lambda_2 \end{Bmatrix}' = \begin{bmatrix} 0 & \Gamma^2 t \\ -1/t & 0 \end{bmatrix} \begin{Bmatrix} \lambda_1 \\ \lambda_2 \end{Bmatrix} \quad , \tag{3.25}$$

$$\frac{\partial H}{\partial t} = 0 = 1 - \frac{\lambda_1 x_2}{t^2} - \lambda_2 \Gamma^2 x_1 \quad , \tag{3.26}$$

and the boundary condition $\lambda_2(0) = 0$.

A solution is found by noting that λ_2 and x_1 are equivalent in that they have the same differential equations and similar boundary conditions:

$$(t\lambda_2')' + \Gamma^2 t\lambda_2 = 0 \qquad \lambda_2(0) = 0 \ , \quad t\lambda_2'(1) = c_1 \ ,$$

$$(tx_1')' + \Gamma^2 tx_1 = 0 \qquad x_1(0) = 0 \ , \quad tx_1'(1) = \bar{T} \ .$$

Since the differential equations are linear, this requires that

$$\lambda_2 = - c_1 x_1 / \bar{T} \ , \tag{3.27}$$

where c_1 is an unspecified constant.

Similarly, it can be shown that

$$\lambda_1 = c_1 x_2 / \bar{T} \ . \tag{3.27a}$$

Substituting these relations into Eq. (3.26) gives

$$1 - \frac{x_2^2 c_1}{t^2 \bar{T}} + \frac{\Gamma^2 c_1 x_1^2}{\bar{T}} = 0 \ . \tag{3.28}$$

Since $x_2 = tx_1'$, this can be written as

$$(x_1')^2 = B^2 + \Gamma^2 x_1^2 \ , \tag{3.29}$$

where $B^2 = \bar{T}/c_1$.

Murphy (Ref. 38) lists three solutions to this differential equation, but they are essentially equivalent and can be expressed in the general form

$$x_1 = \pm \frac{B}{\Gamma} \sinh (C \pm \Gamma s) \quad . \tag{3.30}$$

Here C is the undetermined constant of the differential equation. Applying the boundary conditions on x_1 gives

$$x_1 = D \sinh \Gamma s / \sinh \Gamma \quad . \tag{3.31}$$

Note that this determines that $c_1 = \bar{T}/B^2 = \bar{T} \sinh^2 \Gamma/(D\Gamma)^2$.

Placing this value for x_1 in the original differential equation gives

$$t'\Gamma D \frac{\cosh \Gamma s}{\sinh \Gamma} + 2\Gamma^2 t \frac{\sinh \Gamma s}{\sinh \Gamma} \Longrightarrow \frac{dt}{t} = -2\Gamma \tanh \Gamma s \, ds \quad . \tag{3.32}$$

Integrating both sides:

$$\ell n \, t = -2 \, \ell n \cosh \Gamma s + c_2 \quad ,$$

or

$$t = c_2/\cosh^2 \Gamma s \quad . \tag{3.33}$$

The relation $tx_1'(1) = \overline{T}$ provides a value for c_2 and hence for the optimal thickness distribution:

$$c_2 = \frac{\overline{T}}{\Gamma D} \cosh \Gamma \sinh \Gamma \quad ,$$

and

$$t = \frac{\overline{T}}{\Gamma D} \frac{\cosh \Gamma \sinh \Gamma}{\cosh^2 \Gamma s} \quad . \tag{3.34}$$

This is the result found by Icerman while including the constraint that the first natural frequency must be greater than the excitation frequency. This constraint was not explicitly included in the present formulation, but it is clear that the constraint is satisfied since the solution is identical to Icerman's.

The question of whether additional solutions exist that do not satisfy the frequency constraint, and, if so, what they are, took up a large part of the time spent on the thesis. The answer to the question of existence is clearly "yes" and can be demonstrated by looking at the behavior of the solution as Γ becomes large. The total weight of the structure is proportional to:

$$J = \int_0^1 t ds = \overline{T} \sinh^2 \Gamma / \Gamma^2 D \quad . \tag{3.35}$$

J increases monotonically and without limit as Γ increases. The curves of Fig. 3.1 show that a uniform rod can also satisfy the

$x_1(1) = D$ constraint at any number of excitation frequencies. Clearly then, the uniform rod at some frequency satisfies the constraint and has less weight than the "optimal" solution. This indicates that the solution of Eqs. (3.31)-(3.34) is not a global solution for all frequencies.

Once this fact is established, the unanswered question is: "What are the other optimal solutions?" At first, it was thought that additional solutions could be found for Eq. (3.29). After a long fruitless search for other solutions, it was determined that the problem was ill-posed, in a special sense.

The adjective ill-posed has generally been reserved for formulations that possess no solutions or no physically meaningful ones. A structural optimization example of such a problem is that of finding the minimum weight thickness distribution for a cantilevered rod with the constraint that the first natural frequency of the optimum rod have the same natural frequency as the uniform rod. If the rod is modelled in the same way as was done at the beginning of this section, it is relatively easy to show (Ref. 8) that this problem statement is satisfied by a uniform rod of vanishingly small thickness, a physically uninteresting solution.

Since Eq. (3.34) gives one solution to the problem at hand, it cannot be considered to be ill-posed in a strict sense. However, by modelling the rod with three equal length segments, each with constant thickness, it is possible to find analytical solutions that satisfy

all the boundary conditions and constraints and that have a vanishingly small thickness distribution. The diagram below gives a qualitative comparison of the mode deflection shape given by Eq. (3.31) and the mode shape that this physically unrealistic thickness distribution would have.

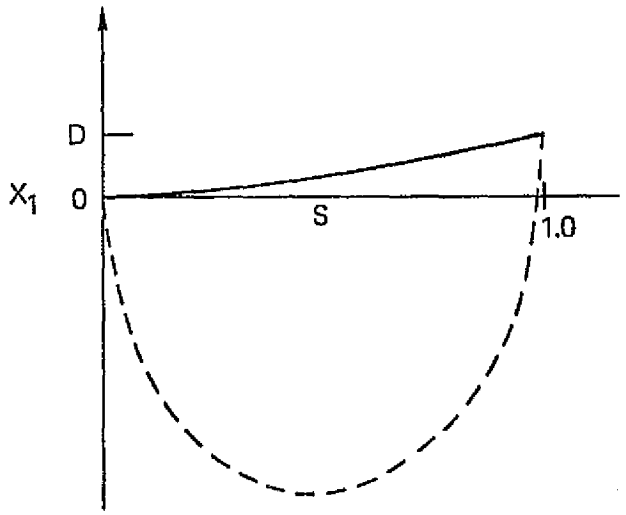

As the thickness goes to zero for the second solution, the displacement is unbounded, except for finite values at the root and tip.

A physically meaningful problem statement must, therefore, have additional constraints on the response or involve changes in the system equations themselves. Possible modifications include:

(1) Imposing a minimum allowable thickness constraint.

(2) Additions of non-structural mass along the rod.

(3) More constraints on the response quantities (e.g., inequality constraints on the stress or the displacement).

The first two modifications were successfully applied to the optimization problems with natural frequency constraints but have been unsuccessful for the forced case developed above. It is felt that, even with a minimum thickness constraint or a non-structural mass addition, an optimal structure with the frequency of excitation greater than a structural natural frequency has discontinuities in thickness. Specifically, it appears likely that the optimal structures have concentrated masses; i.e., thickness distributions that include terms of the form $t_c\delta(s - s_c)$, where δ is the dirac delta. The motivation for this speculation comes from solutions obtained using finite element models and piecewise constant continuous models. More comments on this are offered at the end of the chapter.

Inequality constraints, such as those mentioned above, can be included in the manner described in the original formulation. Unfortunately, the added complexity has made the problems so far insoluble by analytical means. As mentioned, there is no reason why the equations could not be solved by numerical means. However, once the decision is made to go to the computer, the most efficient means of attacking these problems is by the use of finite elements. The next sections detail how this can be done.

Before proceeding to this analysis, it should be stressed that finding additional function space solutions remains as a suitable goal. Variations on the example above are the only analytical solutions for harmonically excited structures, as far as is known. Additional analytic

solutions would aid tremendously in uncovering the special features of this type of problem.

D. FINITE ELEMENT SOLUTIONS

The frustration encountered while dealing with the function space formulation led to efforts utilizing finite elements. In any realistic problem, the use of finite elements is practically a necessity; but the generality and elegance of function space solutions makes them the first choice for preliminary investigations.

Examples are given below that extend the two element case of Section III.B to similar structures modelled by up to ten finite elements. Further examples deal with a cantilevered beam structure modelled by various numbers of elements.

The constraints used for these examples are inequality constraints on the stress. The Appendix indicates how the stress can be determined as a function of the displacements. With this formulation, the augmented cost function has the form:

$$\Phi = \sum_{i=1}^{n} t_i - r \sum_{i=1}^{n} \ell n \left[1 - (S_i/S_{max})^2\right] \quad . \qquad (3.36)$$

Note that the constraint $|S_i| \leq S_{max}$ is handled by squaring the stress values, thereby obviating the need for absolute value brackets.

The thickness is transformed by a technique motivated and described in Section II.C:

$$t_j = t_{min} + \frac{1}{2} u_j^2 \quad . \tag{2.11}$$

The u_j are considered the design variables. Derivatives of the cost unction with respect to u_j are given by

$$\frac{\partial \Phi}{\partial u_j} = u_j \left\{ 1 + \frac{r}{(S_{max})^2} \sum_{i=1}^{n} \frac{S_i \, \partial S_i / \partial t_j}{[1 - (S_i/S_{max})^2]} \right\} \quad . \tag{3.37}$$

The specific examples given below develop the values for $\partial S_i / \partial t_j$.

1. Example: Cantilevered Rod

This section deals with a cantilevered rod excited by a uniformly distributed load in torsion. Figure A.1 aids in depicting the nature of the problem. The steady state equation of motion for the problem is given by:

$$(- \omega_e^2 [M] + [K])\{\theta\} = \{P\} \quad . \tag{3.38}$$

The stresses in the elements are developed in the Appendix:

$$S_1 = \frac{GRn}{L} \theta_1 \quad , \tag{Cont'd}$$

and

$$S_i = \frac{GRn}{L} [\theta_i - \theta_{i-1}] \qquad i = 2,3,\ldots,n \quad . \qquad (A.9)$$

By taking the derivative of Eq. (3.38) with respect to t_j , an expression for the $\{\partial\theta/\partial t_j\}$ vector is obtained:

$$(-\omega_e^2 [M] + [K]) \left\{\frac{\partial\theta}{\partial t_j}\right\} = -\left(-\omega_e^2 \frac{\partial[M]}{\partial t_j} + \frac{\partial[K]}{\partial t_j}\right) \{\theta\} \quad . (3.39)$$

Note that $\{\theta\}$ and $\{\partial\theta/\partial t_j\}$ in Eqs. (3.38) and (3.39) have the same coefficient matrix. This fact can be exploited by using a subroutine that solves $[A]\{x\} = \{b\}$ by decomposing the $[A]$ matrix (Ref. 39). Since the $[A]$ matrix remains unchanged, it has to be decomposed only once to solve for the $n + 1$ systems of n simultaneous equations to find the separate vectors $\{\theta\}$ and $\{\partial\theta/\partial t_j\}$, $j = 1,2,\ldots,n$.

With $\{\partial\theta/\partial t_j\}$ determined, the stress derivative is found directly:

$$\frac{\partial S_i}{\partial t_j} = \frac{GRn}{L} \frac{\partial\theta_1}{\partial t_j} \quad ,$$

$$\frac{\partial S_i}{\partial t_j} = \frac{GRn}{L} \left[\frac{\partial\theta_i}{\partial t_j} - \frac{\partial\theta_{i-1}}{\partial t_j}\right] \quad . \qquad (3.40)$$

All the tools necessary for a solution using the techniques of Chapter II are now assembled. The numerical values used in the computer program were

$$G = 3.75 \times 10^6 \text{ psi} \qquad J_0 = 2\pi R^3 = 1352 \text{ in}^3$$

$$S_{max} = 5.5 \times 10^4 \text{ psi} \qquad \rho_s = 0.1 \text{ lbm/in}^3$$

$$R = 6 \text{ inches} \qquad I_{\alpha 0} = J_0 = 4.2 \text{ slugs}$$

$$L = 120 \text{ inches} \qquad p_x = 35{,}200 \text{ in-lbs/in}$$

$$t_{min} = 0.02 \text{ inches}$$

A check on the algorithm was made by first solving the $\omega_e = 0$ case. By using the methods of Section III.C, an exact answer can be found for the optimal solution for this statically loaded case. With the values of the structural parameters given above, this solution can be written as

$$t = \frac{p_x RL}{S_{max} J_0} (1 - s) = 0.34 (1 - s) \quad . \qquad (3.41)$$

Figure 3.5(a) shows a comparison of the optimal solution obtained using ten finite elements with the exact analytical solution. The agreement is seen to be excellent.

Figure 3.5(b) shows a ten element solution for $\bar{\omega}_e^2 \equiv \omega_e^2 I_{\alpha 0} L^2 / n^2 G J_0 = 1.0$. It is seen that the effect of the excitation is to make the

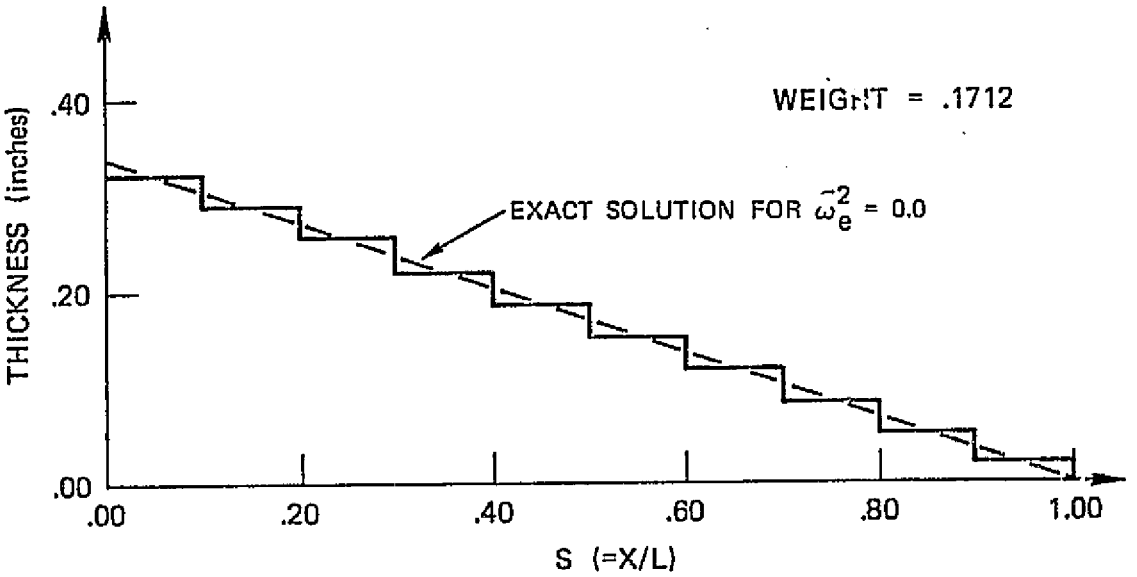

(a) $\bar{\omega}_e^2 = 0.0$

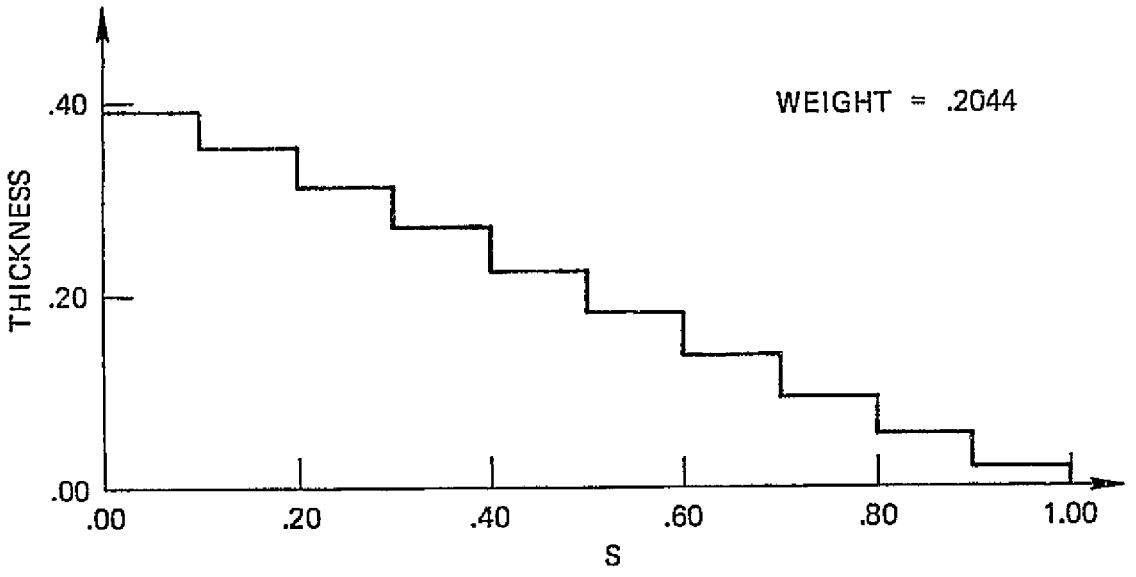

(b) $\bar{\omega}_e^2 = 1.0$

FIG. 3.5--Optimal Thickness Distribution for a Cantilevered Rod Using Ten Finite Elements.

thickness greater all along the span, compared to the static case. This is because the inertial loads act in phase with the excitation, necessitating a stronger structure.

Finally, Fig. 3.6 shows two solutions for the case $\bar{\omega}_e^2 = 4.0$. The solution of Fig. 3.6(b) is an example where the fundamental frequency is less than the excitation frequency and is designated the second solution. This second solution is lighter than the first solution by a factor of 1.36 to 3.93.

Table 3.1 compares the rotational displacements and the constraint values for these two solutions. The two deflection shapes are seen to have similar magnitudes but the second solution is 180^o out of phase from the excitation. This allows the inertial load to partially cancel the effects of the excitation, with the result that much less structure is required to satisfy the constraints. These constraints are presented in the form $g_i = [1.0 - (S_i/S_{max})^2]$ in Table 3.1. With the convergence criterion used for the particular example, a value of g_i that is less than 0.1 can be considered an active constraint. The root element of the second solution is at its minimum thickness and the constraint is clearly not tight for this element.

The constraints results for the first solution suggest an interesting question: "Is the first mode solution fully stressed?" The results presented here are ambiguous with the minimum thickness constraint clouding the issue further. One might suppose that it would be possible to hypothesize that the optimal solution is fully stressed

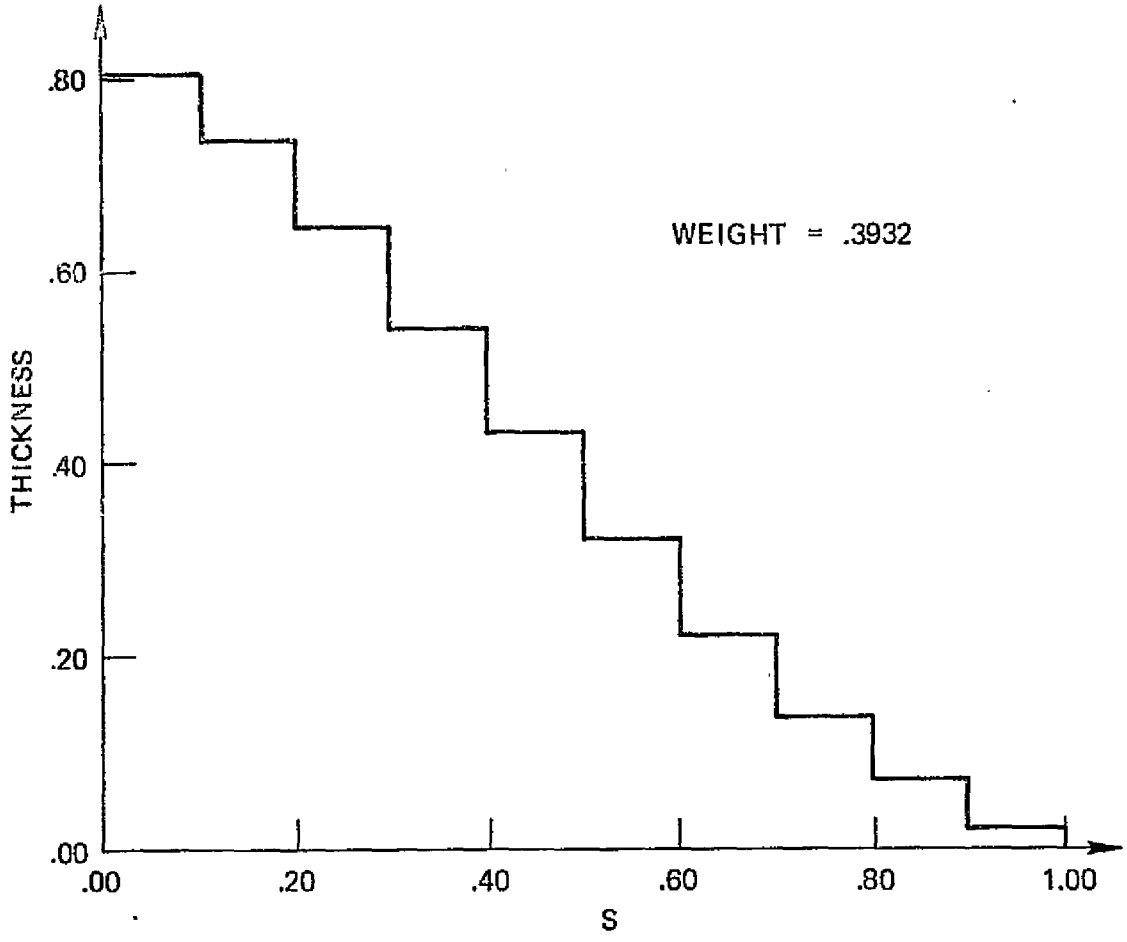

(a) Structure's First Natural Frequency Greater Than ω_e .

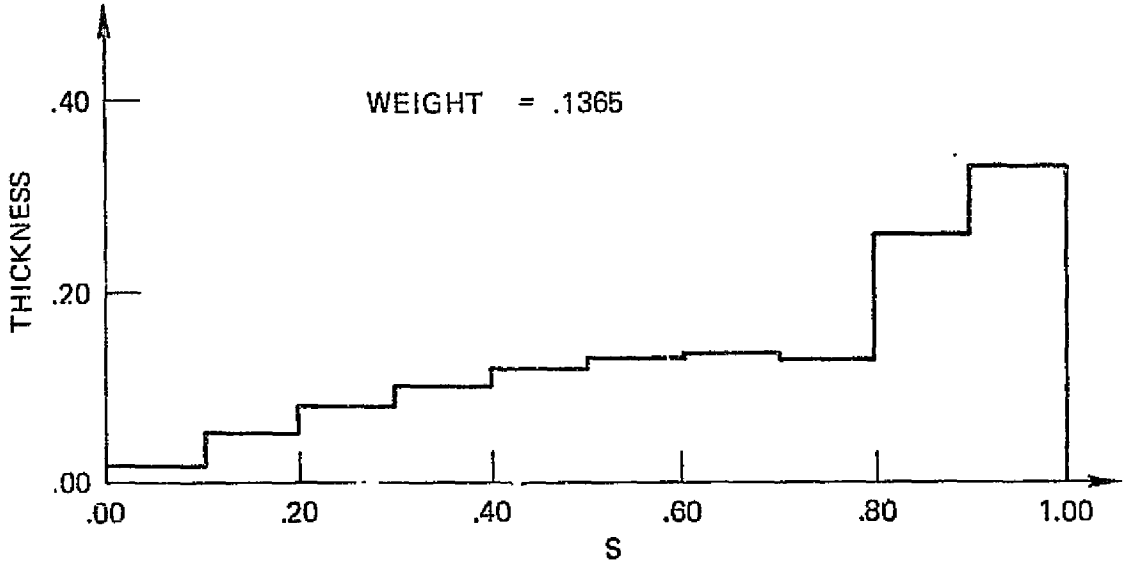

(b) Structure's First Natural Frequency Less Than ω_e .

FIG. 3.6--Two Solutions for the Optimal Thickness Distribution of a Cantilevered Rod Excited at $\bar{\omega}_e^2 = 4.0$.

Element	Displacement		Constraint (g_i)	
	First Solution	Second Solution	First Solution	Second Solution
1	0.029	- 0.027	0.024	0.150
2	0.058	- 0.056	0.012	0.030
3	0.088	- 0.085	0.010	0.016
4	0.117	- 0.115	0.006	0.008
5	0.146	- 0.144	0.006	0.002
6	0.176	- 0.173	0.006	0.014
7	0.205	- 0.202	0.004	0.041
8	0.234	- 0.231	0.006	0.018
9	0.264	- 0.242	0.006	0.851
10	0.293	- 0.246	0.006	0.987

TABLE 3.1--Properties of the Two Thickness Distributions of Figure 3.6.

and use the function space methods on Section III.C to test the hypothesis. However, even for this simple problem, the analytical complications make a closed form result impossible. A much simpler means

of testing the hypothesis is available, however. This is the two design variable example of Section III.B. Figure 3.3(a) shows an example where the first solution is not fully stressed. For this figure, the local optimum with the thickness values $\{t\} = \{1.27 , 0.35\}$ has a constraint vector given by $\{0.24 , 0.00\}$; i.e., the first element is not at the maximum allowable stress while the second is.

It should be admitted that the above demonstration is not a rigorous proof that the optimal continuous structure is not fully stressed and that the question merits further study.

2. Example: Cantilevered Beam

The second calculation examines the structural optimization of a beam excited transversely by a harmonically oscillating load. As in the previous example, a stress constraint is imposed, and it is first necessary to derive an expression for the derivative of the stress with respect to the design variables.

The Appendix shows that the stress at the center of the element can be expressed as:

$$S_1 = \frac{Edn}{2L} w_2 \quad ,$$

$$S_i = \frac{Edn}{2L} (w_{2i} - w_{2i-2}) \qquad i = 2,3,\ldots,n \quad . \qquad (A.18)$$

Physically, this equation says that the stress is proportional to the change in the end slopes of the elements. The analysis of Eqs. (3.38)-(3.40) can be repeated almost directly to give:

$$\left(-\omega_e^2\,[M] + [K]\right)\left\{\frac{\partial w}{\partial t_j}\right\} = -\left(-\omega_e^2\,\frac{\partial [M]}{\partial t_j} + \frac{\partial [K]}{\partial t_j}\right)\{w} \quad , \quad (3.42)$$

$$\frac{\partial S_1}{\partial t_j} = \frac{Edn}{2L}\,\frac{\partial w_2}{\partial t_j} \quad ,$$

$$\frac{\partial S_i}{\partial t_j} = \frac{Edn}{2L}\left(\frac{\partial w_{2i}}{\partial t_j} - \frac{\partial w_{2i-2}}{\partial t_j}\right) \quad , \quad (3.43)$$

$$(i = 2,3,\ldots,n) \quad .$$

The parameters chosen for the optimization program were

E	$= 10.5 \times 10^6$ psi	ρ_s	$= 0.1$ lbm/in^3
L	= length = 120 inches	p_x	= 100 lbs/in
d	= depth = 4 inches	t_{min}	= 0.02 inches
b	= width = 12 inches	S_{max}	= 30,000 psi

Solutions were found using five elements for excitation frequencies ranging from 42.5 rad/sec to 300 rad/sec. Figure 3.7 shows first type of solutions for ω_e = 42.5 rad/sec and 140 rad/sec . The line

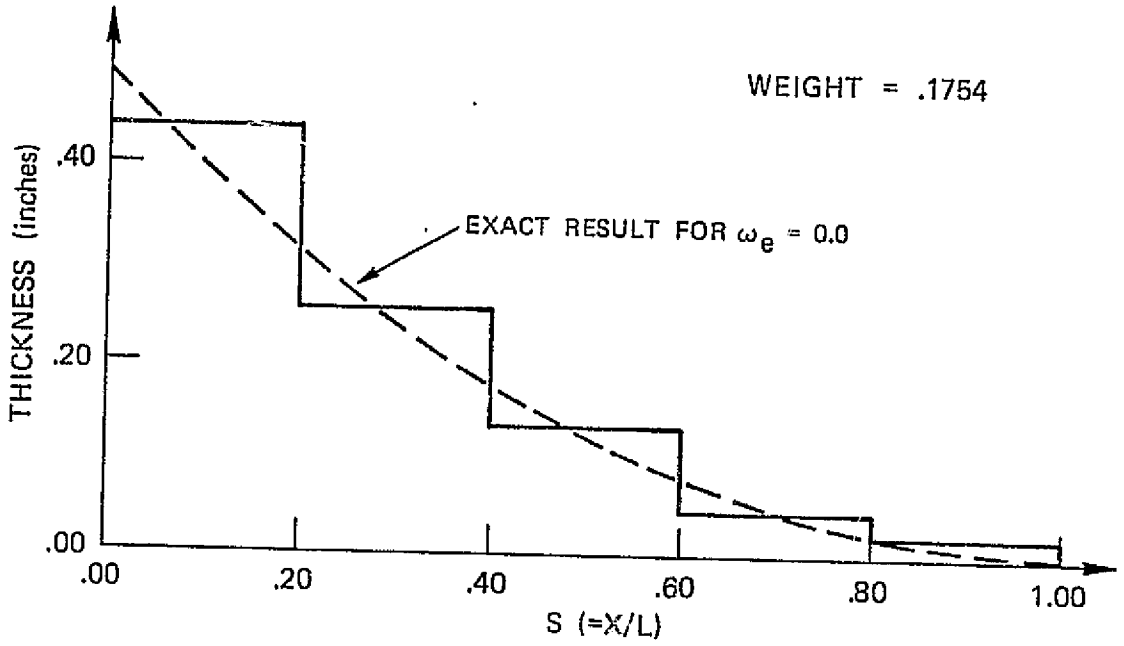

(a) ω_e = 42.5 rad/sec

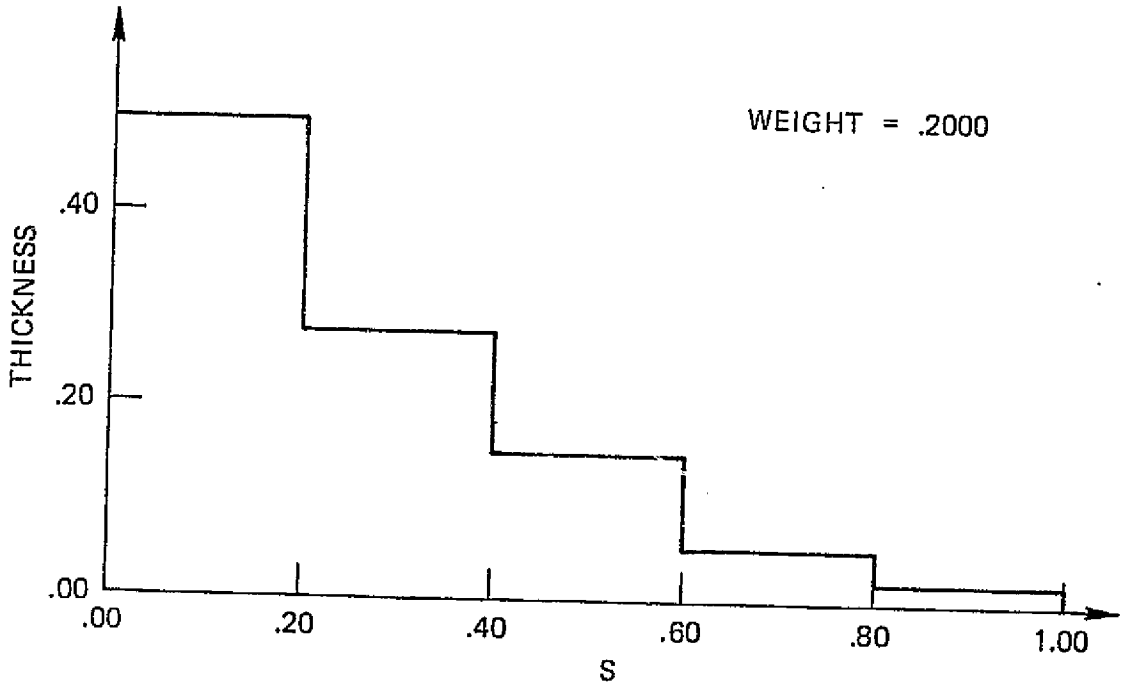

(b) ω_e = 100 rad/sec

FIG. 3.7--Optimal Thickness Distribution for a Cantilevered Beam Using Five Finite Elements.

superimposed on Fig. 3.7(a) is the exact solution for the statically loaded structure given by Eq. (3.21). For the parameters given above, the exact solution is $t = 0.5\ (1.0 - 2s + s^2)$. Even with the harmonic excitation, there is close correspondence between the two solutions.

Figure 3.8 shows two solutions for $\omega_e = 80$ rad/sec . The second solution is slightly lighter for this case. Another second type of solution is shown in Fig. 3.9(a), while Fig. 3.9(b) plots the weight of the two solutions as a function of frequency. It is seen that the first solution is the lighter for values of the excitation frequency less than 75 rad/sec and that the second solution becomes significantly lighter for higher excitation values.

E. CONCLUDING COMMENTS

Cassis (Ref. 24) reported on the existence of disjoint feasible design spaces in connection with problems dealing with truss structures excited by half-wave sine pulses. It is felt that the problems investigated in this chapter add a great deal to the understanding of this phenomenon, primarily because the simplicity of the formulation permits a minute examination of the behavior of the structure. The main conclusion from this investigation is that the natural frequencies play a central role in creating the many feasible regions. Structures respond vigorously when excited near a natural frequency, accordingly, the optimal designs try to stay away from these resonant conditions.

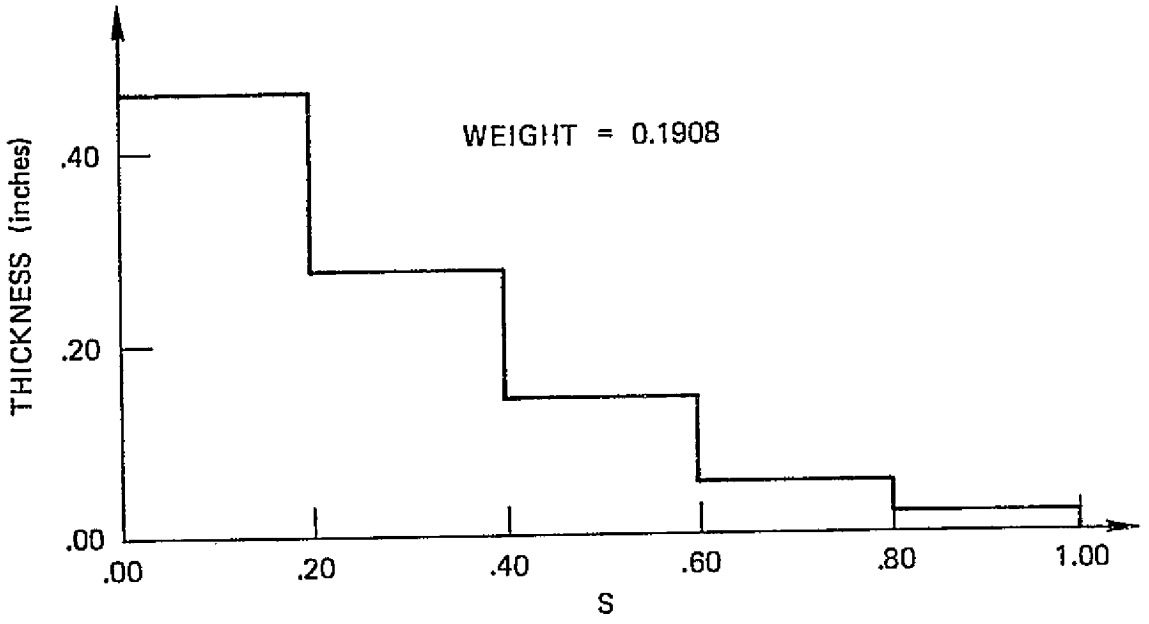

(a) Structure's First Natural Frequency Greater Than ω_e .

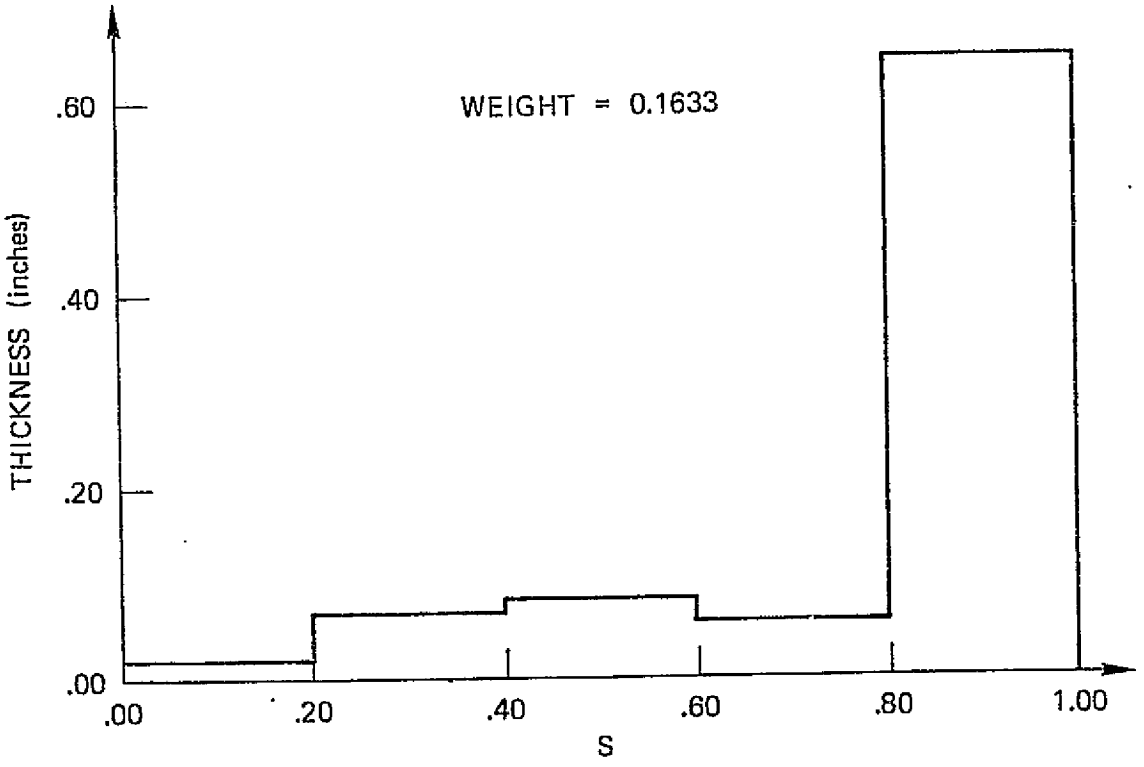

(b) Structure's First Natural Frequency Less Than ω_e .

FIG. 3.8--Two Solutions for the Optimal Thickness Distribution of a Cantilevered Beam Excited at ω_e = 80 rad/sec .

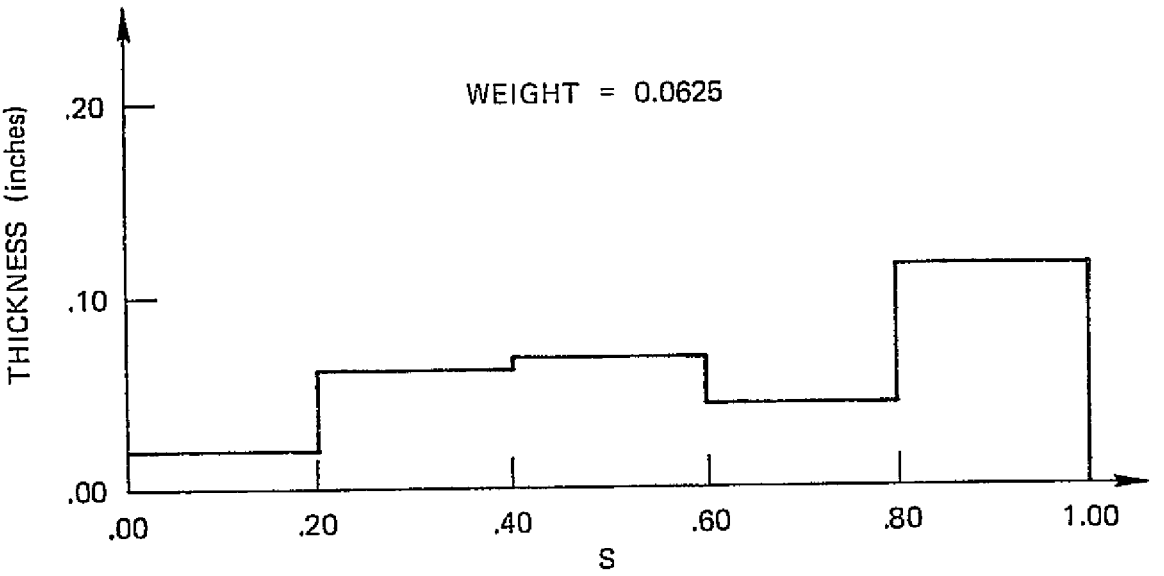

FIG. 3.9(a)--Optimal Thickness Distribution for a Cantilevered Beam Excited at 170 rad/sec (ω_e > Structure's First Natural Frequency).

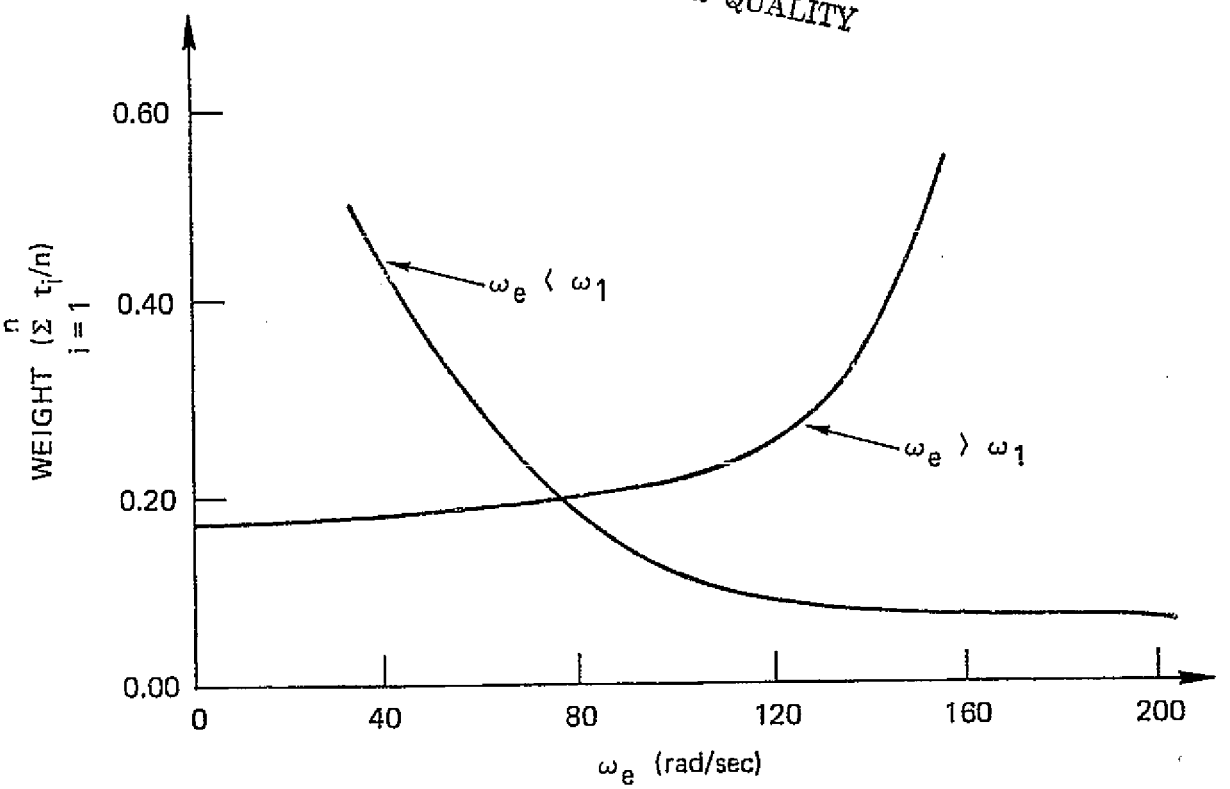

FIG. 3.9(b)--Comparison of the Weights of Local Optima as a Function of Excitation Frequency (ω_1 = the Structure's First Natural Frequency).

The construction of analytical solutions by the methods of Section III.C would further aid in the understanding of these types of problems because they show the role that various parameters of the problem (such as load, frequency and the constraints) play for a range of values rather than the specific values of a particular numerical solution. It is currently felt that much of the difficulty in attaining these analytical solutions is due to the fact that they often contain concentrated masses. At the present time, this is just a hypothesis that is partially based on the results shown in Figs. 3.5(b), 3.8(b) and 3.9(a). In these figures, it is seen that the elements at the tip are significantly larger than the other elements. Based on further studies that used more elements, it appears that in the limit as $n \to \infty$ the final element is discontinuous from the rest of the structure and, in fact, represents a concentrated mass. This is an area of current research and efforts to prove (or disprove) the hypothesis have so far been unsuccessful. It is mentioned here to indicate the quirks these problems can have and to hopefully aid in further research in this area.

CHAPTER IV

WHITE NOISE LOADING

A. INTRODUCTION

This chapter moves from the area of the previous chapter, where the structure was excited at a single frequency, to cases where the structure is excited at all frequencies. In particular, this chapter deals with excitations that possess a Gaussian probability density function and a power spectrum that has a constant value for all frequencies. The present analysis considers loads that are random in time only. It is possible to conceive of structures that are loaded randomly in space as well and of structures whose properties are described in a probabilistic fashion, but these complications are not considered here. The motivation for this type of formulation comes from the atmospheric turbulence example of the next chapter. The turbulence wavelengths are frequently so large that any variation in the turbulence magnitude across the span of the wing can be considered negligible compared with the time variation due to the aircraft's rapid penetration of the gust field.

The flat power spectrum mentioned above is a useful analytical concept and is frequently referred to as a "white noise" spectrum. Since the excitation is described in probabilistic terms, it is

necessary to use probabilistic estimates for the response quantities as well. The most useful of these, the mean square values of responses, are obtained by integrating the power spectrum of the response over the entire range of frequencies:

$$\sigma^2_{RR} = \int_{-\infty}^{\infty} \Phi_{RR}(\omega)\, d\omega \quad . \tag{4.1}$$

It has been shown (Ref. 40) that the quantities that are of interest here, the displacements and the stresses, have finite mean square values even though the excitation has a finite value over an infinite range of frequencies. This fact is very important since it allows the development of analyses using the attractively simple white noise model. It is, of course, necessary to include structural damping in the model in order to obtain a finite response.

It is not possible to have a disjoint feasible design space for this problem. The disjoint properties of the examples in the previous chapter arose because of the relationships between the excitation frequency and the natural frequencies of the structure. Since the white noise excites the structure at all frequencies, it is no longer possible to have these relationships and, in fact, the design space appears to be very well behaved for these problems. The next two sections develop the constraint criteria used for the study and the analysis needed to evaluate the constraints. These methods are then applied to beam and rod models, and optimizations are performed.

B. FAILURE CRITERIA

A difficulty intrinsic to the analysis of structures excited by random loads is that explicit values of the response quantities cannot be obtained. Instead, mean values or expected values are computed using principles from probability. A further complication is that it is often unclear what meaning these estimates have relative to the safe design of a structure. The aim of this section is to describe and evaluate methods that can be used to estimate the life of a structure subjected to random loads.

Cyclic loading, characteristic of white noise excitation, can cause a structure to fail even when the magnitude of the applied stress is well below the theoretical yield stress of the material used. These fatigue failures, which are a common source of failure in actual structures, are quite difficult to predict even empirically. This is an area of intensive active research that is generally designated fracture mechanics. Current efforts divide the fatigue process into three separate areas: (1) crack initiation, (2) crack propagation, and (3) strength degradation and failure. A recent summary of this type of analysis is given by Yang and Trapp (Ref. 41). These analyses require the definition of parameters relating to load time histories, crack size, material properties and other factors, in addition to involving lengthy calculations. While the reliability estimates obtained through the use of these methods should be quite good, it is felt that the complexity of the calculations involved makes them

ill-suited for the present preliminary analysis. Instead, assumptions were made that allowed relatively simple calculations and that required the definition of a minimum number of parameters. These assumptions were obtained from Lin (Ref. 31) with supporting material from Powell (Ref. 43).

With stochastic excitations, there are two logical failure criteria, corresponding to two separate modes of failure, that could be used in the optimization procedure. The first type is failure due to the stress exceeding some specified upper limit. This is commonly referred to as first passage or first excursion failure. The other type of failure mode treats the damage to the structure as a cumulative process resulting from the fluctuations in the load. When the accumulated damage becomes equal to some specified value, the structure is assumed to have failed. (It should be mentioned that while this analysis treats these types of failure separately, the more recent fracture mechanics studies combine these two modes by postulating that the random loading causes damage through crack initiation and growth which results in the reduction of the failure stress so that the final failure is of the first type.)

The reader's familiarity with certain concepts of probability theory is assumed in the following discussion. Papoulis (Ref. 44) was found to be a useful text for reviewing this theory and should aid in the understanding of the pertinent results described below.

1. First Excursion Failure

In order to determine an estimate of the time to the arrival of the first stress greater than some specified value, it is advantageous to make a number of assumptions regarding the nature of the excitation process. Basic assumptions are that the process is stationary, Gaussian and with a zero mean. If this process is denoted by $x(t)$, then the time derivative of the process, $\dot{x}(t)$, is also stationary, Gaussian, has a zero mean and is independent of $x(t)$. The joint probability density function and $x(t)$ and $\dot{x}(t)$ is

$$p_{x\dot{x}}(x,\dot{x}) = \frac{1}{2\pi\sigma_x\sigma_{\dot{x}}} \exp\left(-\frac{x^2}{2\sigma_x^2} - \frac{\dot{x}^2}{2\sigma_{\dot{x}}^2}\right) \quad . \tag{4.2}$$

The parameters σ_x and $\sigma_{\dot{x}}$ in the above equation are the root mean square values of $x(t)$ and $\dot{x}(t)$ respectively. These can be evaluated from the power spectrum of $\Phi_{xx}(\omega)$ by the formula of Eq. (4.1):

$$\sigma_x^2 = \int_{-\infty}^{\infty} \Phi_{xx}(\omega)\, d\omega \quad ,$$

$$\sigma_{\dot{x}}^2 = \int_{-\infty}^{\infty} \omega^2 \Phi_{xx}(\omega)\, d\omega \quad . \tag{4.3}$$

A second assumption is that large values of $x(t)$ arrive independently of one another. (Ref. 31 shows that this assumption is quite conservative for narrow band processes.) This assumption leads to a Poisson probability function for the number of times, n, that a

large magnitude, U, is exceeded in time interval, t,

$$P_U(n,t) = \frac{\lambda t}{n!} \exp(-\lambda t) \quad . \qquad (4.4)$$

The λt term is the expected number of times the load will be exceeded in time interval t. Figure 4.1 helps in explaining this and in bringing out a further point.

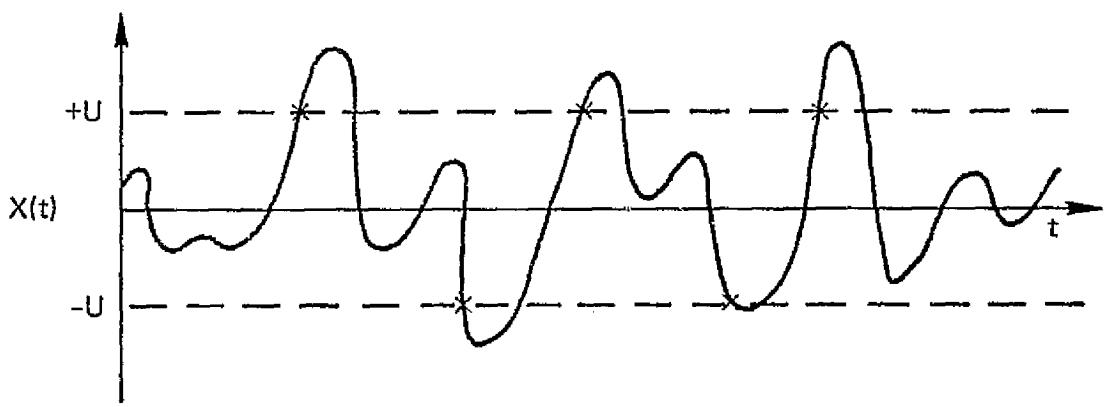

FIG. 4.1--Exceedances of U.

In the diagram, an exceedance occurs when $x(t)$ crosses through U with a positive slope or through $-U$ with a negative slope. Including the negative exceedances can be justified by the physical argument that the examples presented later deal with bending stresses in structures that are symmetric about their neutral axis. Therefore, a compressive stress of magnitude U is accompanied by a tension stress

of magnitude U on the opposite surface. Note that since the process has a zero mean, the number of negative exceedances can be assumed equal to the number of positive exceedances.

With this formulation, Eqs. (4.2) and (4.4) provide the basis for determining the expected time to the first arrival of value U. The λ term of Eq. (4.4) is twice the expected number of positive exceedances of U per unit time. After placing $x(t) = U$ into Eq. (4.2), the expected number of exceedances can be determined by use of the formula for expected value:

$$\lambda = E(N_U) = 2 \int_0^\infty \frac{\dot{x}}{2\pi\sigma_x\sigma_{\dot{x}}} \exp\left(- U^2/2\sigma_x^2 - \dot{x}^2/2\sigma_{\dot{x}}^2\right) d\dot{x}$$

$$= \frac{1}{\pi} \frac{\sigma_{\dot{x}}}{\sigma_x} \exp\left(- U^2/2\sigma_x^2\right) \quad . \tag{4.5}$$

With the use of Eq. (4.4), the probability of failure in time interval t is simply one minus the probability of no failure:

$$p_F(t) = 1 - e^{-\lambda t} \quad . \tag{4.6}$$

The probability of failure <u>at</u> time t is found by differentiating Eq. (4.6) with respect to t . The expected time to failure is then found by multiplying this probability density function times t and

integrating it over times ranging from zero to infinity:

$$E(T) = \int_0^\infty t\lambda\, e^{-\lambda t}\, dt \quad . \tag{4.7}$$

Integrating by parts yields

$$E(T) = 1/\lambda \quad . \tag{4.8}$$

Equation (4.8) can now be coupled with Eq. (4.5) to provide the means for determining the constraint on the life of the structure due to first excursion failure. If it is specified that the stress in the structure cannot exceed some specified value U_S in the time period L_S, the constraint can be written in the form:

$$g_1 = 1 - L_S \pi \frac{\sigma_{\dot{S}}}{\sigma_S} \exp\left(-U_S^2/2\sigma_S^2\right) \geq 0 \quad . \tag{4.9}$$

Here σ_S and $\sigma_{\dot{S}}$ are the root mean square values of the stress and the stress rate.

This constraint is applied independently to each element in the structure. It should be mentioned that the concept of fleet or lot size has been ignored here. Frequently, first excursion failure is defined as the time to failure of just one member of a larger sample. If the arrival times of the loads are independent from one sample member to another, the expected time to first failure of one structure in

a sample size of n is simply $1/n\lambda$. This would impose a more severe constraint on the individual structure, but, as was mentioned, this concept was arbitrarily disregarded.

2. Fatigue Failure

An evaluation of the fatigue life can be made using some of the results from the previous section, but it also requires further concepts. An assumption that makes the fatigue life calculation analytically straightforward is one that has come to be known as the Palmgren-Miner Theory (Ref. 45). This "theory" is based on the physically observable fact that a tension specimen that is loaded cyclically at a constant amplitude of stress, S , fails in fatigue after approximately N_S cycles. It is postulated that a structure that is loaded at this same stress level for η_S cycles $(\eta_S < N_S)$ has been damaged to the extent that it is at the $\eta_S/N_S{}^{th}$ fraction of being failed. It is recognized that experimental results do not always support this theory, but it provides a simple general rule adaptable to analyses of the type presented here.

This theory is applied to a continuous random process by determining the rate at which peaks of a given magnitude occur. The rate of damage is then computed using the formula

$$DR = \int_0^\infty \frac{\eta(S)\, dS}{N(S)} \quad , \tag{4.10}$$

where

$\eta(S)$ = number of stress peaks of magnitude S occurring per unit time ,

$N(S)$ = number of cycles to failure at stress magnitude S .

For the purposes of this work, it is assumed that the damage done in a time interval T is simply $DR \times T$.

The parameter $N(S)$ in Eq. (4.10) can be obtained from curves that show the number of cycles to failure as a function of the stress amplitude, commonly referred to as S-N diagrams. A convenient analytical expression that is used in this work to represent this relationship, and one that is partially supported by data, is the familiar relation

$$N(S)\, S^b = c \quad . \tag{4.11}$$

S is the stress amplitude and b and c are positive constants that must be determined empirically. This clearly gives $N(S) = c/S^b$.

The remaining factor needed for Eq. (4.10) is $\eta(S)$. Powell (Ref. 43) presents an analysis that can be used to readily evaluate $\eta(S)$. This analysis starts by modifying Eq. (4.5) to obtain the expected number of times a stress exceeds a specified positive value

S per unit time:

$$E[N^{+}(S)] = \frac{1}{2\pi} \frac{\sigma_{\dot{S}}}{\sigma_S} \exp\left(-S^2/2\sigma_S^2\right) \quad . \qquad (4.5a)$$

The derivative of this expression with respect to S can be considered a measure of the number of peaks occurring at the level S per unit time:

$$\eta(S) = -\frac{\partial E[N^{+}(S)]}{\partial S} = \frac{S}{2\pi} \frac{\sigma_{\dot{S}}}{\sigma_S^3} \exp\left(-S^2/2\sigma_S^2\right) \quad . \qquad (4.12)$$

A point that must be considered here is that it is very difficult to specify what a cycle is for a random process. Equation (4.12) counts only the net number of peaks at level S with the "troughs" of magnitude S subtracted from the peaks. Figure 4.2 presents the reasoning behind this argument.

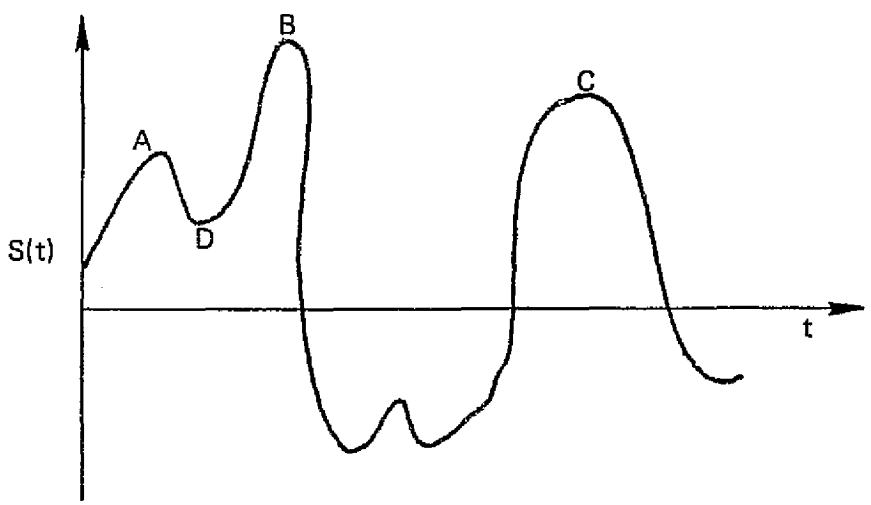

FIG. 4.2--Peaks in a Record of Random Noise.

There are three peaks in this diagram at points A , B , and C , plus one trough at D . Powell's method says that the damage done by this patch of noise is equivalent to the damage done by cycles with the magnitude of A , B , and C minus the damage resulting for a cycle of magnitude D . Without belaboring the point, on physical grounds this seems to be a better method of counting cycles than one that uses the gross number of peaks. Lin (Ref. 42) arrives at the same conclusion as that given below by assuming that the process is narrow band. For such a process, "troughs" with a positive magnitude are not likely to occur so that the problem of net versus gross number of peaks is of no importance. Finally, Yang (Ref. 46) derives an expression based on the magnitude of the excursion rather than the peak magnitude; this is clearly an improvement, but was discovered too late to be included in the present work.

The final step in the derivation is the substitution of the expressions for $N(S)$ and $\eta(S)$ into Eq. (4.10):

$$DR = \int_0^\infty \frac{S^{b+1}\sigma_{\dot{S}} \exp\left(-S^2/2\sigma_S^2\right) dS}{2c\pi\sigma_S^3} \quad . \qquad (4.13)$$

The integral is evaluated by making the transformation $S^2/2\sigma_S^2 = v$, leading to

$$DR = \frac{\sigma_{\dot{S}}}{c\sigma_S\pi} \int_0^\infty (2\sigma_S^2 v)^{b/2} e^{-v} dv \quad .$$

This integral can be evaluated by the use of Eq. (3.381.4) of Ref. 42

$$DR = \frac{\sigma_{\dot{S}}}{2\pi c \sigma_S} (2\sigma_S^2)^{b/2} \Gamma\left(\frac{b+2}{2}\right) \quad ,$$

where Γ is the gamma function.

To put this in constraint form, it is specified that the structure have a fatigue life greater than L_f . The constraint is then written as

$$g_2 = 1 - DR \times L_f \geq 0 \quad . \tag{4.15}$$

This completes the description of the constraints used for the randomly loaded structure. It is seen that the structural response quantities that are required in order to evaluate the constraints are the root mean square values of the stress and the stress rate. The next section details how these can be obtained and also develops methods for obtaining the derivative quantities that are needed for the optimization process.

C. RESPONSE TO WHITE NOISE

A finite element representation of the response problem can be given by

$$[M]\{\ddot{w}\} + [K]\{w\} = F\{E\} \quad . \tag{4.16}$$

The right-hand side indicates that the equivalent forcing function is a scalar multiplying a vector that discretizes the uniform load. The scalar F has a white noise power spectrum:

$$\Phi_{FF}(\omega) = N_w \qquad -\infty \leq \omega \leq \infty \quad . \tag{4.17}$$

Given this representation, the problem is to find the mean square values of the stresses, which are in turn a matrix function of the displacement for the examples dealt with here:

$$\{S\} = [T]\{w\} \quad . \tag{4.18}$$

The exact form of $[T]$ depends on the structure being studied, but it is always independent of the excitation frequency and the design variables for the present study.

In order to make the problem meaningful, it is necessary to assume that the system has damping. Otherwise, the white noise excitation would result in unbounded resonances and an infinite mean square response. This was done by assuming that the structure has damping which is manifested by a complex shear modulus or Young's modulus. This, in turn, means that the stiffness matrix can be represented by:

$$[K] = (1 + i\alpha)[K_0] \quad . \tag{4.19}$$

$[K_0]$ is a real matrix that is developed in the Appendix and $1 + i\alpha$ is a complex scalar with α representing the damping factor which is much less than unity. This same representation was used in Chapter III and, again, Ref. 36 contains a good discussion of it.

The response is determined by modal superposition. The modes used are the first mn modes of the system:

$$\{w\} = \sum_{i=1}^{mn} a_i \{p_i\} = [P]\{a\} \quad , \tag{4.20}$$

where the $\{p_i\}$'s are the mode shapes and the a_i's are the modal participation factors. The mode shapes are independent of the excitation while the a_i's are not, so the next step is to determine power spectra of the a_i's .

At a given excitation frequency, ω_e , Eq. (4.16) becomes:

$$(-\omega_e^2 [M] + [K])\ [P]\{a\} = F\{E\} \quad . \tag{4.21}$$

By premultiplying Eq. (4.21) by $[P]^T$, the equation for $\{a\}$ can be determined as a function of the generalized forces, masses and stiffnesses:

$$(-\omega_e^2 [\mathbb{M}] + [\mathbb{K}])\ \{a\} = F[P]^T \{E\} \quad . \tag{4.22}$$

The eigenvectors are normalized so that the generalized masses are unity:

$$[\mathbb{M}] = [P]^T[M][P] = [\,I\,] \quad ,$$

$$[\mathbb{K}] = [P]^T[K][P] = (1 + i\alpha)\,[\,\lambda\,] \quad . \qquad (4.23)$$

$[\,\lambda\,]$ is a diagonal matrix containing the eigenvalues of the system.

This is a system of mn uncoupled equations that can be solved independently for the modal participation factors:

$$[-\omega_e^2 + \omega_i^2(1 + i\alpha)]\, a_i = F\{p_i\}^T\{E\} \Longrightarrow a_i$$

$$= F\{p_i\}^T[E]/[-\omega_e^2 + \omega_i^2(1 + i\alpha)] \quad . \qquad (4.24)$$

The term multiplying F is the transfer function $H_{a_iF}(j\omega)$ that relates a_i to F. This makes it possible to form the power spectra for the a's :

$$\Phi_{a_ia_j}(\omega) = H_{a_iF}(j\omega)\, N_w\, \overline{H_{a_jF}(j\omega)} \quad . \qquad (4.25)$$

The bar signifies the complex conjugate.

The most direct route to attaining the variances of the stress and stress rates is to express them in terms of the covariances of the

a_i's . For computational purposes, this report distinguishes four separate covariance integrals:

$$I_1 = \sigma^2_{a_i a_i} = \int_{-\infty}^{\infty} \Phi_{a_i a_i} \, d\omega \quad ,$$

$$I_2 = \mathrm{Re}\ \sigma^2_{a_i a_j} = \mathrm{Re} \int_{-\infty}^{\infty} \Phi_{a_i a_j} \, d\omega \quad ,$$

$$I_3 = \sigma^2_{\dot{a}_i a_i} = \int_{-\infty}^{\infty} \omega^2 \, \Phi_{a_i a_i}(\omega) \, d\omega \quad ,$$

$$I_4 = \mathrm{Re}\ \sigma^2_{\dot{a}_i a_j} = \mathrm{Re} \int_{-\infty}^{\infty} \omega^2 \, \Phi_{a_i a_j}(\omega) \, d\omega \quad , \qquad (4.26)$$

where Re designates that only the real part is of interest.

The integrals can be evaluated by making a contour integration around the upper half plane. Combining terms from Eqs. (4.17), (4.24) and (4.25) into (4.26) gives:

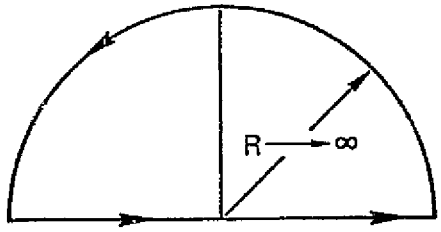

$$I_1 = N_w \left(\{p_i\}^T \{E\}\right)^2 \oint_C \frac{d\omega}{[\omega^2 - \omega_i^2(1 + i\alpha)][\omega^2 - \omega_i^2(1 - i\alpha)]} \quad . \qquad (4.27)$$

For convenience and clarity, set $\beta = \omega_i$.

The integrand has no zeroes and four poles:

$$\begin{aligned} z_1 &= \beta(1 + i\alpha)^{\frac{1}{2}} \quad , \\ z_2 &= -z_1 \quad , \\ z_3 &= \beta(1 - i\alpha)^{\frac{1}{2}} = \bar{z}_1 \quad , \\ z_4 &= -z_3 = -\bar{z}_1 \quad . \end{aligned} \tag{4.28}$$

Only poles z_1 and z_4 are inside the contour. The relationships between the roots given by Eq. (4.28) and standard contour integration give

$$I_1 = C_1 2\pi i \left[\frac{1}{(z_1 - z_2)(z_1 - z_3)(z_1 - z_4)} + \frac{1}{(z_4 - z_1)(z_4 - z_2)(z_4 - z_3)} \right] ,$$

where $C_1 \equiv N_w(\{p_i\}^T\{E\})^2$. Continuing:

$$I_1 = 2\pi i C_1 \left[\frac{1}{2z_1 2\,\mathrm{Re}\, z_1 2i\,\mathrm{Im}\, z_1} + \frac{1}{2\,\mathrm{Re}\, z_1 2i\,\mathrm{Im}\, z_1 2\bar{z}_1} \right]$$

$$= \frac{\pi C_1}{2\,\mathrm{Im}\, z_1 |z_1|^2} \quad . \tag{4.29}$$

The magnitude of z_1 is calculated directly:

$$|z_1|^2 = \beta^2(1 + \alpha^2)^{\frac{1}{2}} \quad . \tag{4.30}$$

The $\mathcal{I}m(z_1)$ calculation is a bit more difficult;

$$z_1 = \mathcal{R}e(z_1) + i\,\mathcal{I}m(z_1) = \beta(1 + i\alpha)^{\frac{1}{2}} \quad .$$

By equating the real and imaginary parts of z_1^2, two equations that can be used to solve for $\mathcal{I}m(z_1)$ are formed:

$$2\,\mathcal{I}m(z_1)\,\mathcal{R}e(z_1) = \beta^2\alpha \Longrightarrow$$

$$\mathcal{R}e(z_1) = \beta^2\alpha/[2\,\mathcal{I}m(z_1)] \tag{4.31}$$

$$[\mathcal{R}e(z_1)]^2 - [\mathcal{I}m(z_1)]^2 = \beta^2 = \frac{\beta^4\alpha^2}{4[\mathcal{I}m(z_1)]^2} - [\mathcal{I}m(z_1)]^2 \quad . \tag{4.32}$$

This results in a quadratic equation in $\mathcal{I}m(z_1)$ that has the solution

$$[\mathcal{I}m(z_1)]^2 = -\frac{\beta^2 \pm \sqrt{\beta^4 + \beta^4\alpha^2}}{2} \quad . \tag{4.33}$$

Since $\mathfrak{Im}(z_1)$ is real, the minus sign can be rejected and

$$\mathfrak{Im}(z_1) = \frac{\sqrt{2}}{2}\beta[(1+\alpha^2)^{\frac{1}{2}} - 1)]^{\frac{1}{2}} \quad . \tag{4.34}$$

By substitution of Eqs. (4.34) and (4.30) into the final result of Eq. (4.29)

$$I_1 = \frac{C_1\pi}{\sqrt{2}\beta[(1+\alpha^2)^{\frac{1}{2}} - 1]^{\frac{1}{2}}\beta^2(1+\alpha^2)^{\frac{1}{2}}} \quad . \tag{4.35}$$

Since $\alpha < 0.1$, it is appropriate to make the approximation that

$$\sqrt{1+\alpha^2} = 1 + \frac{\alpha^2}{2} + O(\alpha^4) \quad . \tag{4.36}$$

The substitution of the first two terms of Eq. (4.36) into Eq. (4.35) gives:

$$I_1 = \frac{C_1\pi}{\beta^3\alpha[1 + (\alpha^2/2)]} \tag{4.35a}$$

It is now possible to neglect the $\alpha^2/2$ term compared with unity to get the final result:

$$\boxed{I_1 = N_w\,(\{p_i\}^T\{E\})^2\,\pi/\omega_i^3\alpha} \quad . \tag{4.37}$$

The remaining integrals are evaluated in a similar fashion. Since the calculations are lengthy, but straightforward, only the final results are presented:

$$I_2 = \frac{N_w\{p_i\}^T\{E\}\{E\}^T\{p_j\}\ \pi\alpha\ (\omega_i + \omega_j)}{2\omega_i\omega_j[(\omega_i - \omega_j)^2 + (\alpha^2/4)(\omega_i + \omega_j)^2]} \quad , \qquad (4.38)$$

$$I_3 = N_w(\{p_i\}^T\{E\})^2\ \pi/\omega_i\alpha \quad , \qquad (4.39)$$

$$I_4 = \frac{N_w\{p_i\}^T\{E\}\{E\}^T\{p_i\}\ \pi\alpha\ (\omega_i + \omega_j)}{2[(\omega_i - \omega_j)^2 + (\omega_i + \omega_j)^2(\alpha^2/4)]} \quad . \qquad (4.40)$$

The variances of the stresses are obtained by a linear combination of the covariances that have just been calculated. The examples in the sections to follow use the explicit relationships between the stress and the displacement. The general form of Eq. (4.18) is adequate for the present derivation:

$$\{S\} = [T]\{w\} = [T][P]\{a\} \quad .$$

The power spectra of the stresses are, therefore, related to the power spectra of the modal participation factors by the simple relation:

$$[\Phi_{SS}(\omega)] = [T][P][\Phi_{aa}(\omega)][P]^T[\bar{T}]^T \quad . \qquad (4.41)$$

The complex conjugate is included in the above equation because the [T] matrix contains a complex structural parameter. Since neither [T] nor [P] are functions of the excitation frequency, the stress variances are found by replacing $\Phi_{aa}(\omega)$ with the covariance matrix for the a's in Eq. (4.41),

$$[X_{SS}] = [T][P][X_{aa}][P]^T[\bar{T}]^T \quad . \qquad (4.42)$$

Similarly,

$$[X_{\dot{S}\dot{S}}] = [T][P][X_{\dot{a}\dot{a}}][P]^T[\bar{T}]^T \quad .$$

The square roots of the diagonal elements of $[X_{SS}]$ and $[X_{\dot{S}\dot{S}}]$ are the rms values of the stresses and stress rates needed in order to evaluate Eqs. (4.9) and (4.15).

It is readily shown that these diagonal elements are real and that they involve only the real parts of the $[X_{aa}]$ matrix. To prove this, some preliminary notations must be defined.

Express [T] as $(1 + i\alpha)[T_0]$, where $[T_0]$ is real.

Define tp_{ij} as the i,j^{th} element of $[T_0][P]$, and pt_{ij} as the i,j^{th} element of $[P]^T[T_0]^T$.

Note that $tp_{ij} = pt_{ji}$ and that $X_{a_i a_j} = X_{a_j a_i}$.

The diagonal elements of the stress covariance matrix can therefore be explicitly expressed by:

$$
\begin{aligned}
X_{S_i S_i} &= (1+\alpha^2) \sum_{j=1}^{mn} tp_{ij} \sum_{k=1}^{mn} X_{a_j a_k} pt_{ki} \\
&= (1+\alpha^2) \sum_{j=i}^{mn} \Bigg[(tp_{ij})^2 X_{a_j a_j} \\
&\qquad + \sum_{\substack{k=1 \\ k\neq j}}^{mn} tp_{ij} tp_{ik} X_{a_j a_k} \Bigg] \\
&= (1+\alpha^2) \Bigg[\sum_{j=1}^{mn} (tp_{ij})^2 X_{a_j a_j} \\
&\qquad + 2 \sum_{k=j+1}^{mn} tp_{ij} tp_{ik} \, \mathrm{Re}\, X_{a_j a_k} \Bigg] \qquad . \qquad (4.43)
\end{aligned}
$$

All the elements in the equation above are real and, as was to be proved, only the real parts of the $[X_{aa}]$ matrix are included. This explains why only the real parts of the integrals I_2 and I_4 of Eq. (4.26) were required.

This concludes the derivation of the terms needed for the constraint evaluation. A remaining task is the calculation of the derivatives needed for the gradient in the optimization algorithm.

1. Derivative Calculations

The design variables for these problems, the structural thicknesses, are manifested in the mass and stiffness matrices. The gradient technique of the optimization algorithm requires that the derivative of the constraints be calculated. This in turn requires that the derivatives be calculated for all the quantities used to compute the constraints and that are a function of the design variables.

The first step is the calculation of the derivatives of the eigenvalues and eigenvectors of the system. Fox and Kapoor (Ref. 15) presented a straightforward method for calculating these quantities, and this method is summarized below.

Consider the unforced system with a given eigenvalue and eigenvector:

$$(-\lambda_i [M] + [K])\{p_i\} = \{0\} \quad . \tag{4.44}$$

For ease of notation, set $[F_i] \equiv -\lambda_i [M] + [K]$.

The derivative of Eq. (4.44) with respect to the design variable t_j is

$$\left(-\lambda_i \frac{\partial [M]}{\partial t_j} + \frac{\partial [K]}{\partial t_j} - \frac{\partial \lambda_i}{\partial t_j}[M]\right)\{p_i\} + [F_i]\left\{\frac{\partial p_i}{\partial t_j}\right\} = 0 \quad . \tag{4.45}$$

The system given by Eq. (4.44) is self-adjoint so that if Eq. (4.45) is premultiplied by $\{p_i\}^T$, the last term drops out, leaving

$$\frac{\partial \lambda_i}{\partial t_j} \{p_i\}^T [M] \{p_i\} = \{p_i\}^T \left[\frac{\partial [K]}{\partial t_j} - \lambda_i \frac{\partial [M]}{\partial t_j} \right] \{p_i\} \quad . \quad (4.46)$$

Since the eigenvectors have been normalized to make the generalized masses equal to unity, the eigenvalue derivative can be expressed as:

$$\frac{\partial \lambda_i}{\partial t_j} = \{p_i\}^T \left[\frac{\partial [K]}{\partial t_j} - \lambda_i \frac{\partial [M]}{\partial t_j} \right] \{p_i\} \quad . \quad (4.46a)$$

From Eq. (4.44), with the eigenvalue derivative calculated, the eigenvector derivative can be solved for:

$$[F_i] \left\{ \frac{\partial p_i}{\partial t_j} \right\} = - \frac{\partial [F_i]}{\partial t_j} \{p_i\} \quad . \quad (4.47)$$

But since $[F_i]$ is singular, another equation is needed to specify the magnitude of $\{\partial p_i / \partial t_j\}$. This equation comes from differentiating the generalized mass:

$$\frac{\partial}{\partial t_j} \{p_i\}^T [M] \{p_i\} = 0 = 2\{p_i\}^T [M] \left\{ \frac{\partial p_i}{\partial t_j} \right\} + \{p_i\}^T \frac{\partial [M]}{\partial t_j} \{p_i\} \quad . \quad (4.48)$$

Equations (4.47) and (4.48) can be combined to give:

$$\begin{bmatrix} [F_i] \\ 2\{p_i\}^T[M] \end{bmatrix} \left\{ \frac{\partial p_i}{\partial t_j} \right\} = - \begin{bmatrix} \partial[F_i]/\partial t_j \\ \{p_i\}^T \, (\partial[M]/\partial t_j) \end{bmatrix} \{p_i\} \quad . \quad (4.49)$$

In order to obtain a square, non-singular matrix, both sides of Eq. (4.49) are premultiplied by $[F_i \, , 2[M]\{p_i\}]$ to obtain

$$\left[[F_i]^2 + 4[M]\{p_i\}\{p_i\}^T[M] \right] \left\{ \frac{\partial p_i}{\partial t_j} \right\} = \left[- [F_i] \, \frac{\partial [F_i]}{\partial t_j} \right.$$

$$\left. - 2[M]\{p_i\}\{p_i\}^T \, \frac{\partial [M]}{\partial t_j} \right] \{p_i\} \quad . \quad (4.50)$$

This is a matrix equation that can be used to solve for the eigenvector derivatives $\{\partial p_i/\partial t_j\}$. Note that since the matrix multiplying the eigenvector derivative is not a function of the design variable, it is necessary to decompose this matrix only once to solve for the n design variable derivatives. A further note is that experience with this method has indicated that it is frequently helpful to multiply Eq. (4.48) by λ_i as a scaling procedure.

The remaining steps in the derivative calculation are much less complicated. The derivatives of modal covariances I_1 and I_2 are given below as an example, but it seems of little purpose to show the

entire analysis here. A few terms must be derived first:

$$\omega_i^2 = \lambda_i \rightarrow \frac{\partial \omega_i}{\partial t_j} = \frac{1}{2\omega_i} \frac{\partial \lambda_i}{\partial t_j} \quad ,$$

$$\frac{\partial(\{p_i\}^T\{E\})}{\partial t_j} = \frac{\partial\{p_i\}^T}{\partial t_j}\{E\} \quad . \qquad (4.51)$$

Then:

$$\frac{\partial I_1}{\partial t_j} = I_1 \left[-\frac{3}{\omega_i} \frac{\partial \omega_i}{\partial t_j} + \frac{2}{\{p_i\}^T\{E\}} \frac{\partial\{p_i\}\{E\}}{\partial t_j} \right] \quad . \qquad (4.52)$$

Designate:

$$\gamma \equiv \left[(\omega_i - \omega_k)^2 + \frac{\alpha^2}{4} (\omega_i + \omega_k)^2 \right] \quad .$$

Then:

$$\frac{\partial I_2}{\partial t_j} = I_2 \left\{ \frac{1}{\{p_i\}^T\{E\}} \frac{\partial\{p_i\}^T\{E\}}{\partial t_j} + \frac{1}{\{p_k\}^T\{E\}} \frac{\partial\{p_k\}^T\{E\}}{\partial t_j} \right.$$

$$\left. - \frac{\omega_k}{\omega_i(\omega_i + \omega_k)} \frac{\partial \omega_i}{\partial t_j} - \frac{\omega_i}{\omega_k(\omega_i + \omega_k)} \frac{\partial \omega_k}{\partial t_j} \right\}$$

$$- \frac{1}{\gamma} \left[\left(2(\omega_i - \omega_k) + \frac{\alpha^2}{2} (\omega_i + \omega_k) \right) \frac{\partial \omega_i}{\partial t_j} \right. \qquad \text{(Cont'd)}$$

$$+ \left(- 2(\omega_i - \omega_k) + \frac{\alpha^2}{2} (\omega_i + \omega_k) \right) \frac{\partial \omega_k}{\partial t_j} \Bigg] \quad . \qquad (4.53)$$

This should indicate that the remaining derivative calculations are tedious, but uncomplicated. It is mostly a matter of the continuous application of the chain rule until the final derivatives that are required are reached. These are the derivatives of the constraints, the first of which is given in Eq. (4.9);

$$g_1 = 1 - L_S \frac{\sigma_{\dot{S}}}{\sigma_S} e^{-U_S^2/2\sigma_S^2} \geq 0 \quad .$$

The derivative is:

$$\frac{\partial g_1}{\partial t_j} = (g_1 - 1) \left[\frac{1}{\sigma_S} \left(\frac{U_S^2}{2\sigma_S^2} - 1 \right) \frac{\partial \sigma_S}{\partial t_j} + \frac{1}{\sigma_{\dot{S}}} \frac{\partial \sigma_{\dot{S}}}{\partial t_j} \right] \quad . \qquad (4.54)$$

Similarly for g_2 , from Eq. (4.15)

$$g_2 = 1 - L_F \frac{\sigma_{\dot{S}}}{2\pi c \sigma_S} (2\sigma_S^2)^{b/2} \Gamma \left(\frac{b+2}{2} \right) \quad .$$

And the derivative is

$$\frac{\partial g_2}{\partial t_j} = (g_2 - 1) \left(\frac{1}{\sigma_{\dot{S}}} \frac{\partial \sigma_{\dot{S}}}{\partial t_j} + \frac{(b-1)}{\sigma_S} \frac{\partial \sigma_S}{\partial t_j} \right) \quad . \qquad (4.55)$$

D. EXAMPLES

As in the previous chapter, cantilevered rods and beam examples were optimized. Figure 4.3(a) shows the power spectrum of the white noise excitation while Fig. 4.3(b) is a qualitative depiction of a response quantity. The peaks on the latter figure represent structural resonances which are the main contributors to the mean values of the response.

It is perhaps necessary to justify the use of a finite number of modes to represent the response of a structure excited by loads with a white noise spectrum. As mentioned in the introduction to this chapter, Bogdanoff and Goldberg (Ref. 40) show that the mean square values of the stress and displacement in an Euler-Bernoulli beam are finite when the beam is excited by the noise. They do this while taking into account an infinite number of modes and by assuming constant viscous damping. A further indication that a finite number of modes suffice is given by Eqs. (4.24) and (4.25) which show that the peaks of the spectra for the modal participation factors are inversely proportional to ω_i^4 . This indicates that the contributions to the rms responses from the separate modes die off quickly as the mode number and, therefore the natural frequency increases. Finally an empirical justification for using a finite number of modes is given by the results below which show that solutions found using four modes differ only marginally from solutions using two modes.

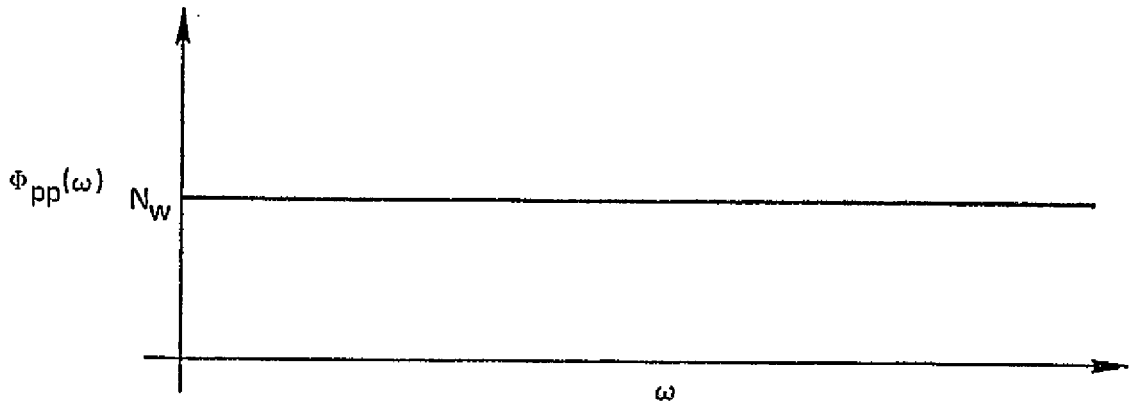

(a) White Noise Excitation

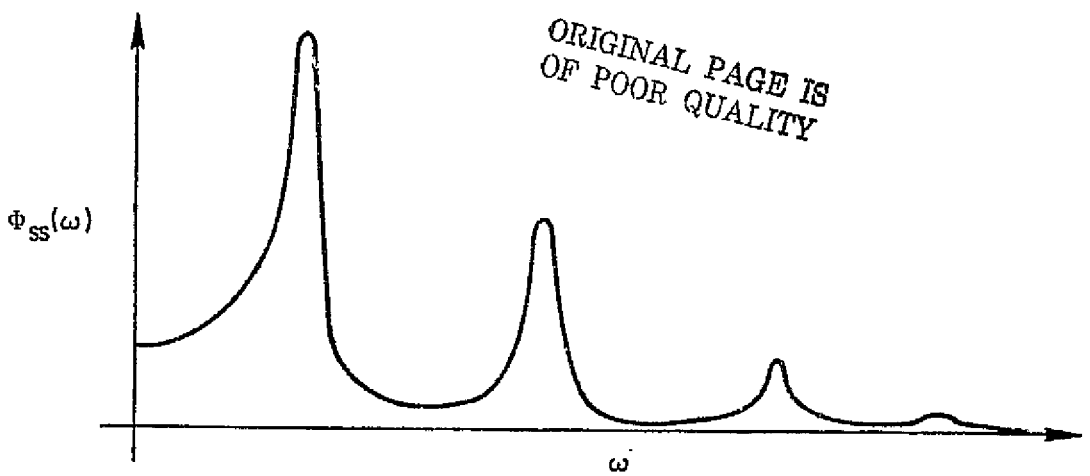

(b) Representative Response

FIG. 4.3--Representative Power Spectral Density Shapes for a Structural System with a White Noise Input.

1. Torsion Rod

The thin walled rod of Section III.D.1 is used again in this section, except that a white noise excitation is now present. The following list of parameters repeats some of the previous values and adds new ones for the special requirements of this problem.

$G = 3.75 \times 10^6$ psi

$R = 6$ inches

$L = 120$ inches

$J_O = 2\pi R^3 = 1352$ in^3

$N_w = 1240$ (lb)^2/rad/sec

$\rho_s = 0.1$ lbm/in^3

$I_{\alpha O} = 4.2$ slugs

$\alpha = 0.05$

$b = 8$

$c = 10^{41}$

$U_S = 40{,}000$ psi

The parameters b and c are from the equation $NS^b = c$ and were obtained by fitting an S-N curve for aluminum given in Crandall and Dahl (Ref. 46, Sec. 5-13). The value chosen for α is rather high and it is recognized that an important part of an actual design process using the methods described here would be to obtain more accurate and justifiable values for the α, b and c parameters.

The constraint placed on the fatigue life was that it be no less than one year, and the expected time to stress value U_S was set to be no less than one-half year.

The results of the optimization algorithm are presented in Figs. 4.4 and 4.5. Figure 4.4 compares the optimal thickness distributions when two, three and eight elements are used to represent the structure. It is seen that as more elements are used, the total weight remains nearly constant while there is some qualitative difference in the distributions. For the eight element structure, more mass tends to be concentrated near the tip. More will be said about this later.

All the results presented in Fig. 4.4 used two structural modes in their solution. Figure 4.5 compares results of analyses using two modes and four modes. It is seen that there are some minor differences at the tip, but they have to be considered negligible. Table 4.1 gives numerical results for the two cases.

Element Number	Thickness		Fatigue Constraint	
	2 Modes	4 Modes	2 Modes	4 Modes
1	1.694	1.698	$9.5 \cdot 10^{-3}$	$5.93 \cdot 10^{-4}$
2	1.582	1.577	$1.8 \cdot 10^{-3}$	$3.90 \cdot 10^{-4}$
3	1.382	1.392	$4.0 \cdot 10^{-3}$	$1.04 \cdot 10^{-3}$
4	1.128	1.129	$9.1 \cdot 10^{-3}$	$2.78 \cdot 10^{-3}$
5	0.8592	0.8754	$4.8 \cdot 10^{-3}$	$9.37 \cdot 10^{-3}$
6	0.6111	0.6170	$5.0 \cdot 10^{-4}$	$1.46 \cdot 10^{-2}$
7	0.5262	0.5230	0.925	0.874
8	0.5618	0.5868	1.000	1.000

TABLE 4.1--Comparison of Two and Four Mode Solutions.

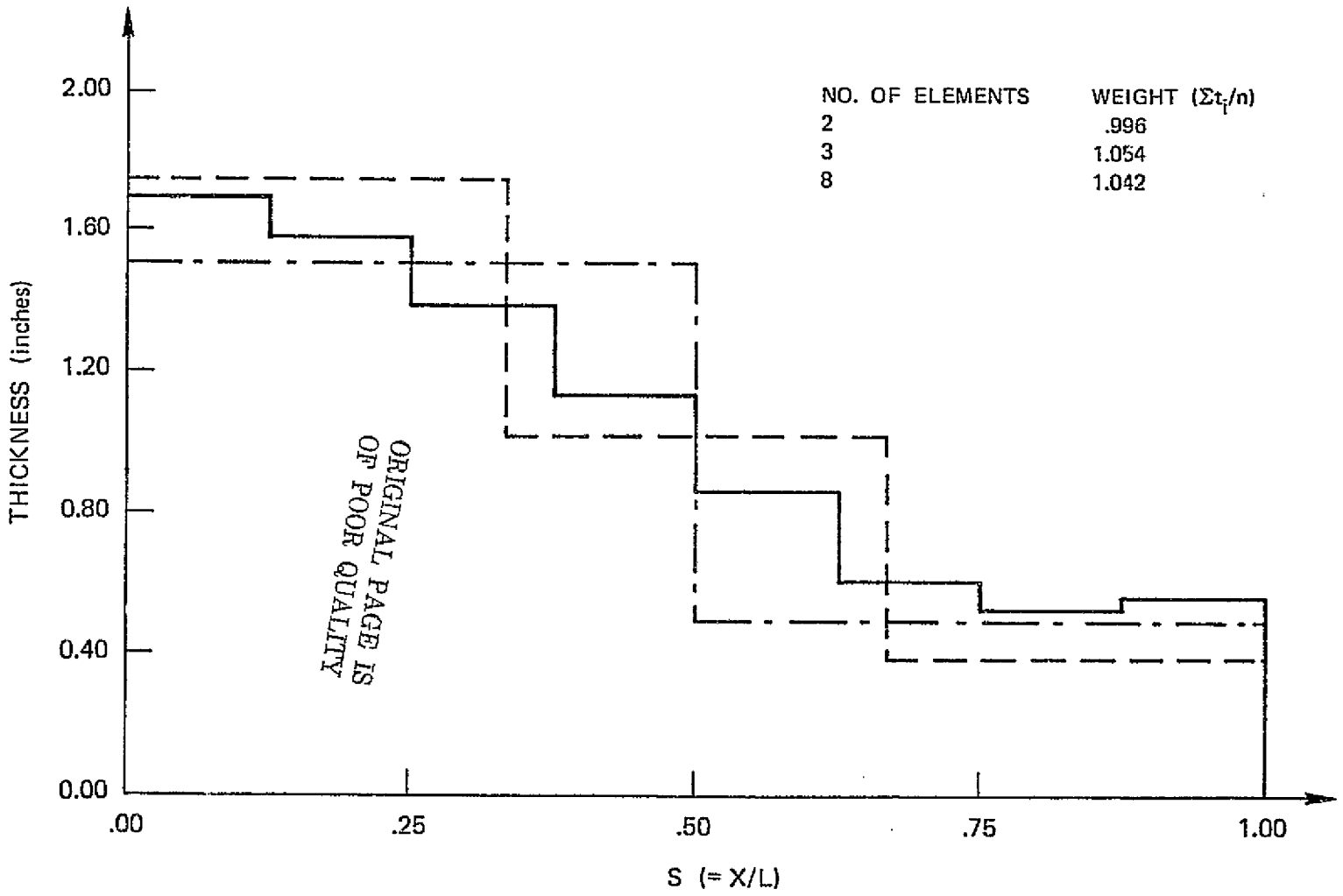

FIG. 4.4--Optimal Thickness Distributions for a Cantilevered Rod Excited by a Uniformly Distributed White Noise Torque.

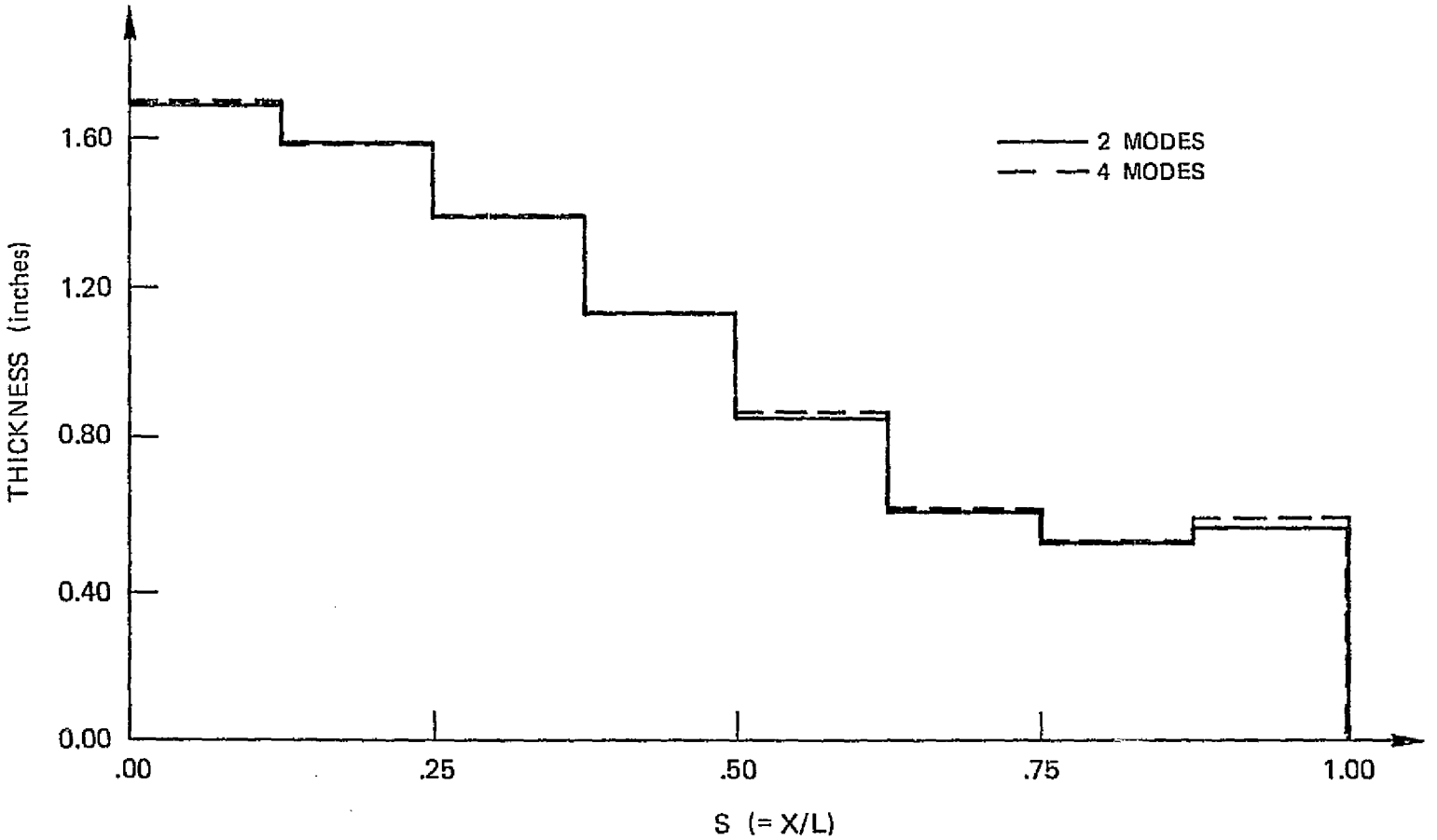

FIG. 4.5--Optimal Thickness Distribution for a Cantilevered Rod Excited by a Uniformly Distributed White Noise Torque — Comparison of Solutions Using Two and Four Natural Modes.

This shows that although the four mode solution took 50% more computer time to converge, it did not appreciably change the results. The fatigue constraint values are presented to show that the optimization proceeded to the same level in determining the active constraints. The values given are those computed using Eq. (4.15); therefore, the numbers near zero indicate that the constraint is almost exactly satisfied (i.e., it is active).

The optimization seems to have found that placing some weight at the tip provides an inertial load that relieves the inboard stress. Since this phenomenon is exhibited in the beam results as well, it is appropriate to consider this in somewhat more detail.

2. Effect of a Tip Mass

This section presents some findings of a brief study that was made to justify the optimal solutions that included a large finite thickness at the tip. In particular, the study sought to determine what effect a concentrated mass at the tip would have on the maximum stress in a cantilevered beam. The hypothesis was that the effect would be to reduce the stress. Obviously, this would not be the case for a static loading or for a low frequency harmonic excitation, but the results of the optimization indicated that something different was happening for the white noise excitation.

The model studied was a uniform cantilevered beam with a point mass at the tip. The excitation was assumed to be uniform across the span

and random in time with a white noise power spectral density. The mass of the beam was kept constant while the tip mass was varied as the only independent parameter.

The problem could be solved by a differential equation approach coupled with modal superposition as was done in Ref. 40. However, since a computer program that analyzed this type of problem using finite elements already existed, it was more expedient to use it. The next section presents the structural parameters and the excitation spectrum used for the analysis. The thickness distribution was held fixed for all elements at a value of one. A nonstructural point mass was added to the last element and was varied through a range of values.

Figures 4.6 and 4.7 present the results for the rms stress and stress rate, respectively, for four values of the concentrated mass, nondimensionalized by the mass of the beam. It is seen that the mass has the effect of reducing the maximum rms stress, which always occurs at the root. The effect on the rms stress rate is to increase its peak value, but since the stress is of far more importance in the evaluation of fatigue life than the stress rate, this increase is relatively unimportant. It is interesting to note that the higher modes are obviously present in the stress rate distribution but that the first two modes seem to dominate the stress distribution.

The main finding is that the addition of mass at the tip can improve the fatigue life. In hindsight it is clear what has happened:

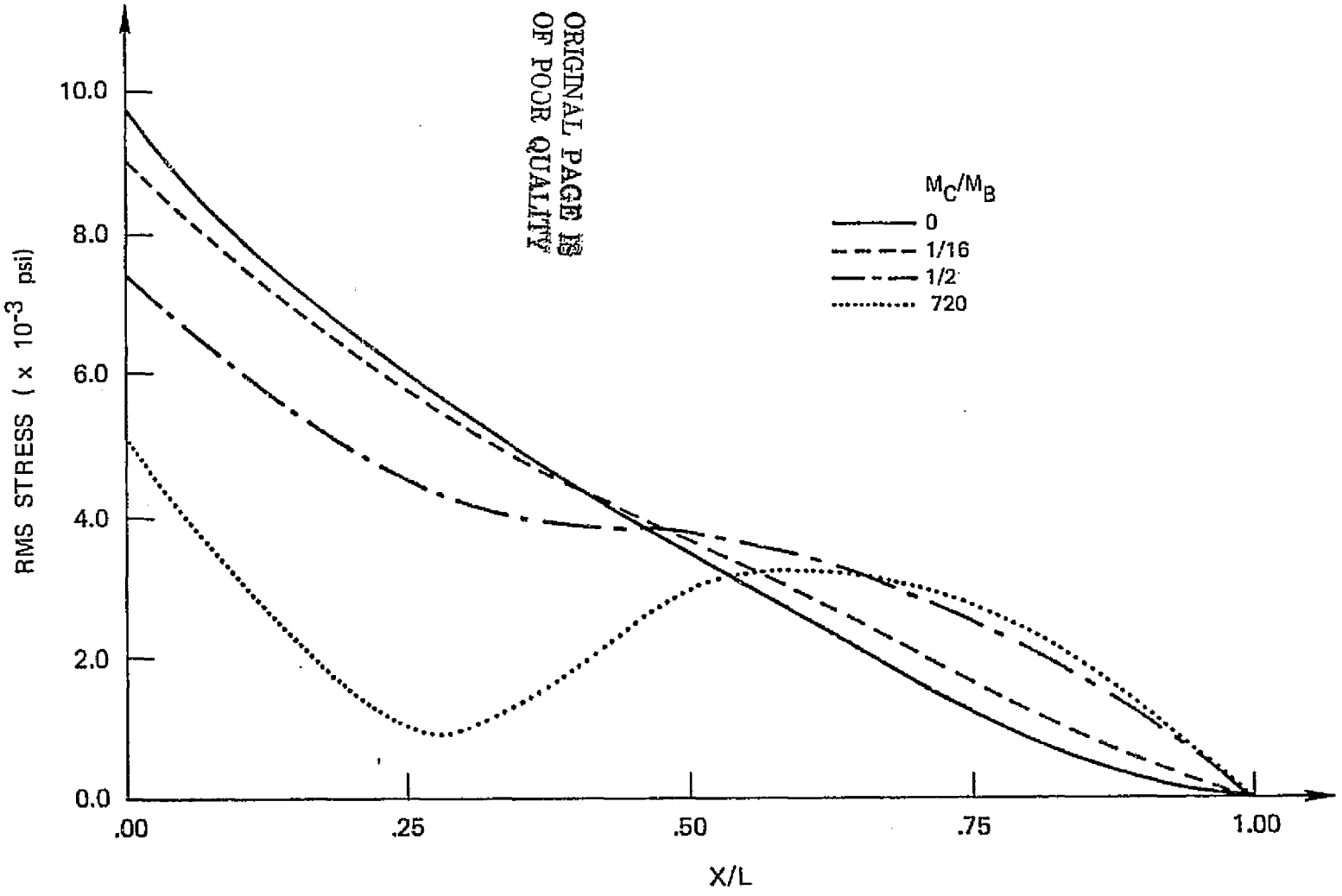

FIG. 4.6--Root Mean Square Stress in a Uniform Cantilevered Beam with a Concentrated Tip Mass Excited by Uniformly Distributed White Noise.

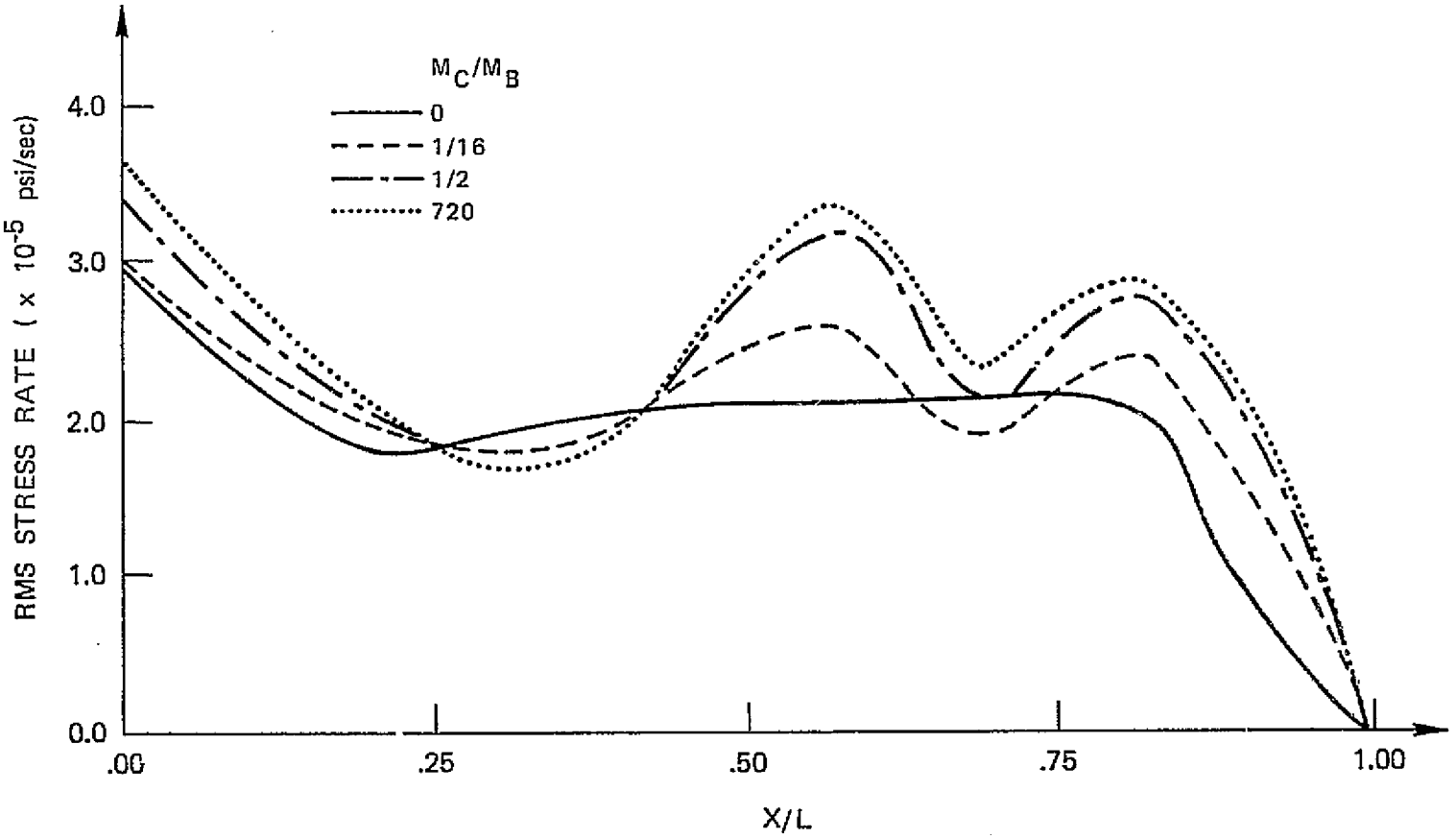

FIG. 4.7--Root Mean Square Stress Rate of the Beam of Fig. 4.6.

the added mass acts as an inertial force that resists the excitation and, in the limit as the mass becomes very large, acts as a simply supported boundary.

For the cantilevered rod, a similar effect takes place in that a mass would act to restrain the tip rotation and in the limit act as a fixed boundary.

This is an interesting and unanticipated result. A further study that could be done is a two design variable optimization study using the concentrated mass and the uniform thickness as the variables. Constraints could be placed on the rms stress or on the fatigue life. The above analysis shows that the optimal concentrated mass would not be zero.

3. Cantilevered Beam

A beam example was optimized to see if it had any new, interesting characteristics. The methods of Section IV.B are directly applicable to the beam example so that the only changes necessary are the inclusion of the proper forms for the finite element representation of the beam structure. Since the Appendix and Chapter III are quite thorough in these aspects, they are not repeated here.

The properties chosen for the beam and the load are

Length	= 240 inches	E	$= 10.5 \times 10^6$ psi
Width	= 30 inches	ρ_s	$= 0.1$ lbm/in^3
Depth	= 3.0 inches	α	$= 0.05$

$b = 8$ $\qquad$ $c = 10^{41}$

$N_w = 0.01\ (lb/in)^2/rad/sec$ $\qquad$ $U_S = 40{,}000$ psi

The large width to depth ratio was chosen because of a future anticipated application of the model to aeroelastic problems where it would represent a wing.

The constraints were continued at one year for the fatigue life and one-half year for the expected time to failure.

A comparison of the results obtained using two elements and eight elements is presented in Fig. 4.8, while Fig. 4.9 compares results obtained from an analysis that used four modes with one that used two. The concentration of mass near the tip is more pronounced for the problem, but the qualitative effects are the same as for the rod example.

Table 4.2 compares the four mode and the two mode solutions.

Element	Thickness		Fatigue Constraint		First Excursion Failure Constraint	
	2 Modes	4 Modes	2 Modes	4 Modes	2 Modes	4 Modes
1	0.1750	0.1751	0.042	0.034	0.990	0.990
2	0.1335	0.1352	0.049	0.043	0.961	0.977
3	0.1015	0.1033	0.055	0.064	0.941	0.968
4	0.0801	0.0809	0.069	0.070	0.940	0.994
5	0.0596	0.0602	0.113	0.096	0.999	0.999
6	0.0381	0.0387	0.165	0.249	1.00	1.00
7	0.0554	0.0590	1.00	1.00	1.00	1.00
8	0.644	0.0647	1.00	1.00	1.00	1.00
Total	0.7078	0.7171				

TABLE 4.2--Cantilevered Beam: Comparison of Two and Four Mode Solutions

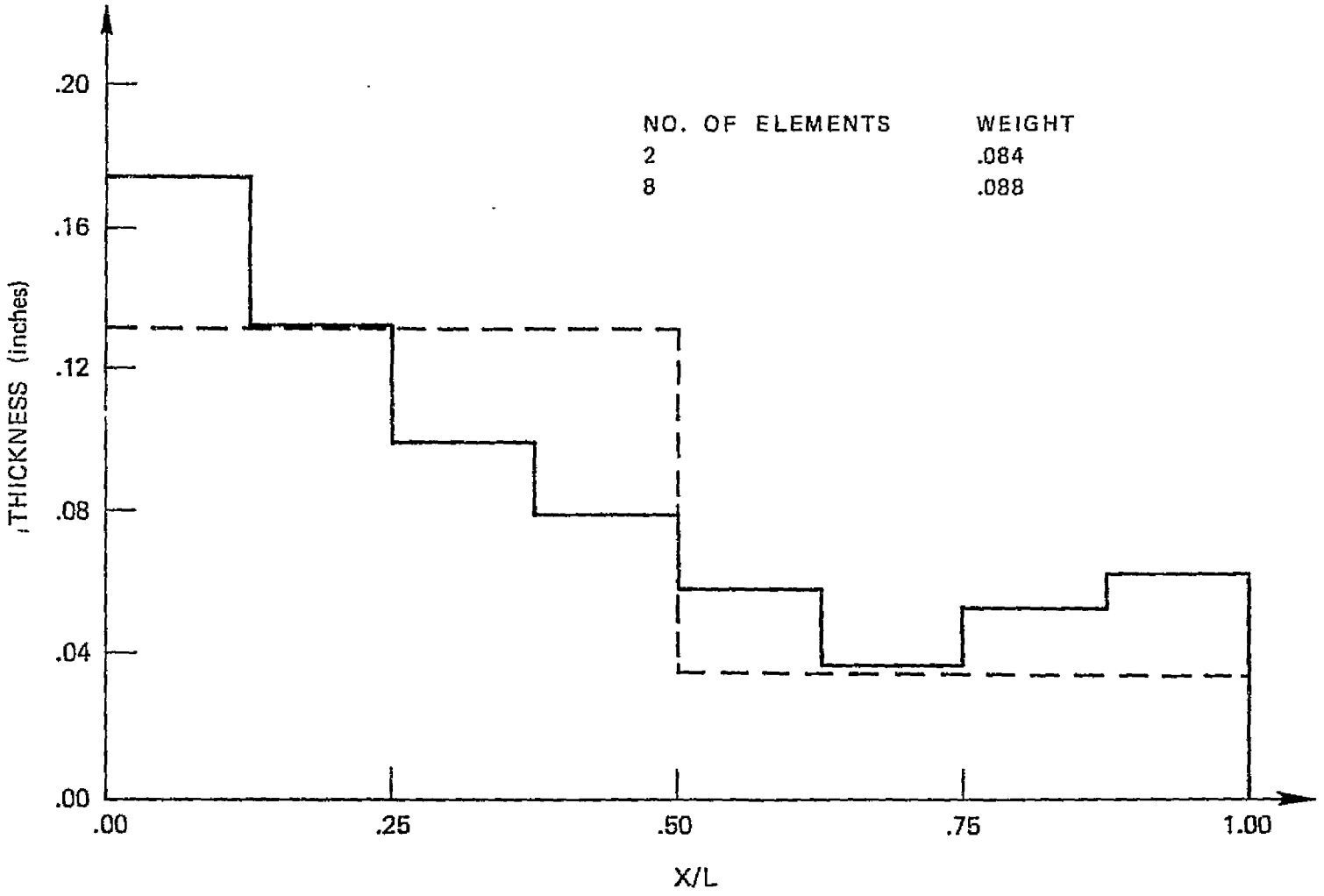

FIG. 4.8--Optimal Thickness Distribution of a Cantilevered Beam Excited by a Uniformly Distributed White Noise Transverse Load.

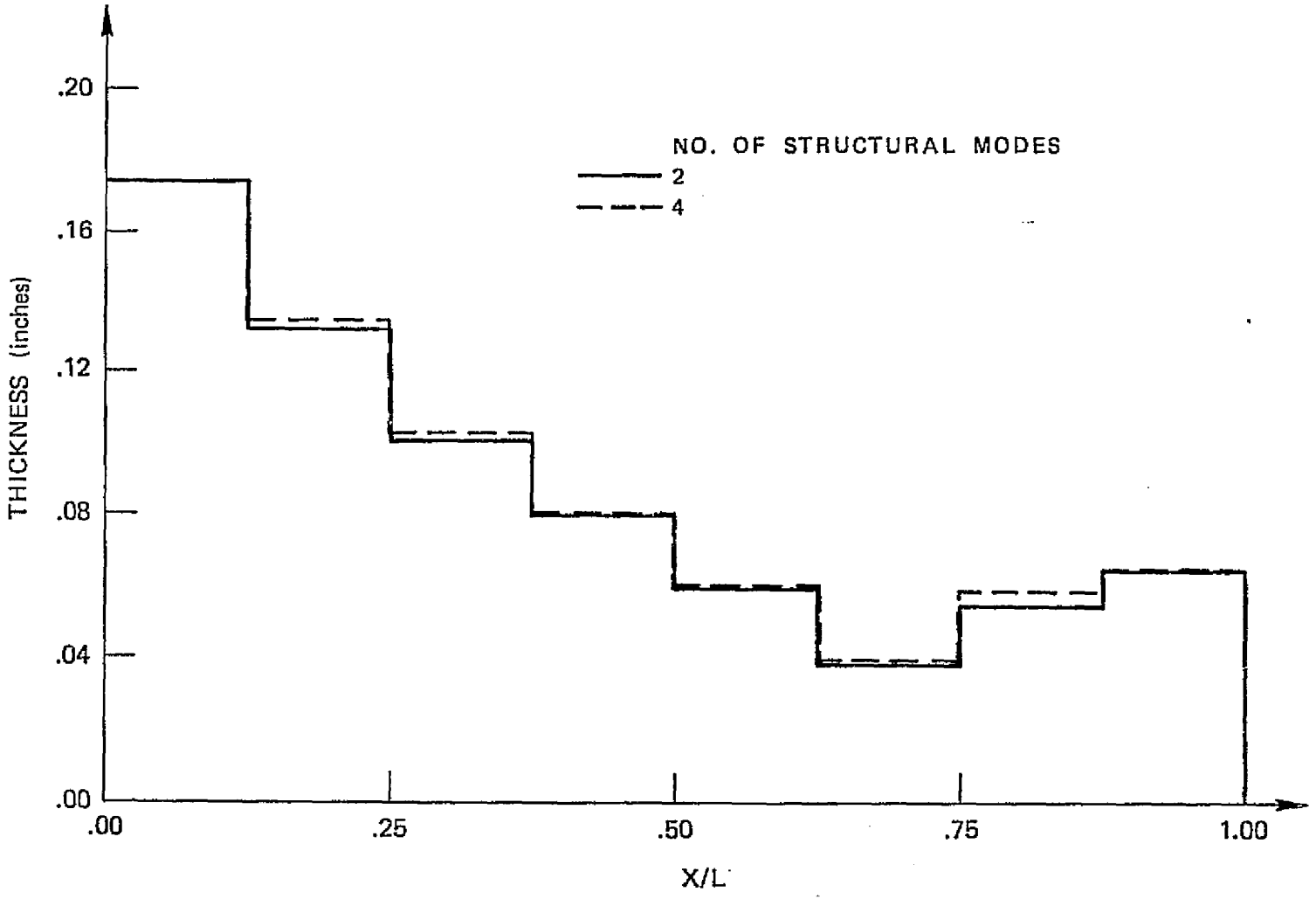

FIG. 4.9--Optimal Thickness Distribution for a Cantilevered Beam Excited by a Uniformly Distributed White Noise Transverse Load — Effect of the Number of Structural Modes.

The four mode solution is 1.3% heavier than the two mode solution; a disparity that is probably less than the percentage by which these solutions differ from the true optimum. It is possible that further iteration would make some of the constraints tighter, but it is felt that little information would be returned to justify the added computer time.

E. CONCLUDING COMMENTS

The results of the two examples tend to show that, as in some of the harmonically forced solutions of the previous chapter, there is a tendency for some of the mass to be concentrated near the tip. In fact, the solutions obtained for the white noise examples could perhaps be thought of as a superposition of the two solutions given for a single harmonic excitation, such as those of Fig. 3.6. It is not known whether this observation has any practical significance for the solution of this class of problems.

It is felt that a formulation of this type makes a useful contribution in that it presents new results and extends the methods of structural optimization into an almost unexplored field. Obviously, however, the examples studied in this chapter are mainly of theoretical interest. Methods of fracture mechanics combined with load spectra that are of great practical interest would aid greatly in the application of the techniques to more applied studies.

The next chapter does attempt to perform an optimization on a structure that is of more interest: an aircraft wing in the presence of atmospheric turbulence.

CHAPTER V

CONTINUOUS ATMOSPHERIC TURBULENCE

A. INTRODUCTION

Structural fatigue and failure resulting from stochastic loads are one of the most commonly occurring maintenance and safety problems for aircraft structures. The nature of these vehicles is such that there is a very high payoff in terms of performance and operating economy for savings made in the structural weight. These two facts combine to provide a powerful motivation for finding optimal structures under the condition of random aerodynamic excitation with fatigue life as one of their constraints. Specifically, this chapter deals with the minimization of the structural weight of an aircraft wing that is subjected to continuous atmospheric turbulence.

The formulation used in this study is, in keeping with the scope of the thesis, of a preliminary nature with a continual tradeoff made between physical realism and computational simplicity. The main objectives in the development of the mathematical models that are presented in the next section are to obtain a representation that is consistent in terms of level of sophistication and to retain the important elements of the problem. After the presentation of these models, it is necessary to develop the analytical tools needed for the constraint evaluation and then some results are presented.

B. COMPUTATIONAL MODELS

There are three distinct areas that have to be considered in the development of the mathematical representation of a wing excited by turbulence: (1) the structure of the wing, (2) the aerodynamic operators and (3) the disturbing gust forces. Before dealing with each of these separately, some general limitations on the analysis should be mentioned here.

The motion of the wing was constrained to consist of rigid body plunging motion plus transverse bending. A more general formulation would include at least rotational deformation and perhaps rigid body rotations as well. While it would not be impossible to include these, it is felt that the present formulation is the logical place to start.

A similar decision was made to limit the constraints to those dealing with the life of the structure. It is realized that an actual design has to meet a myriad of criteria so that the results presented here represent only the specific designs obtained for a specifically posed problem.

1. Structural Model

Many of the mathematical aspects of the present problem were provided by Ref. 32. In selecting a structural model to use in this study it seemed natural, therefore, to choose a wing that is used extensively in the examples of that text. In particular, Example 10.6 of that text presents an analysis that parallels much of what is presented below. Figure 5.1 shows a planform of that wing with its important dimensions.

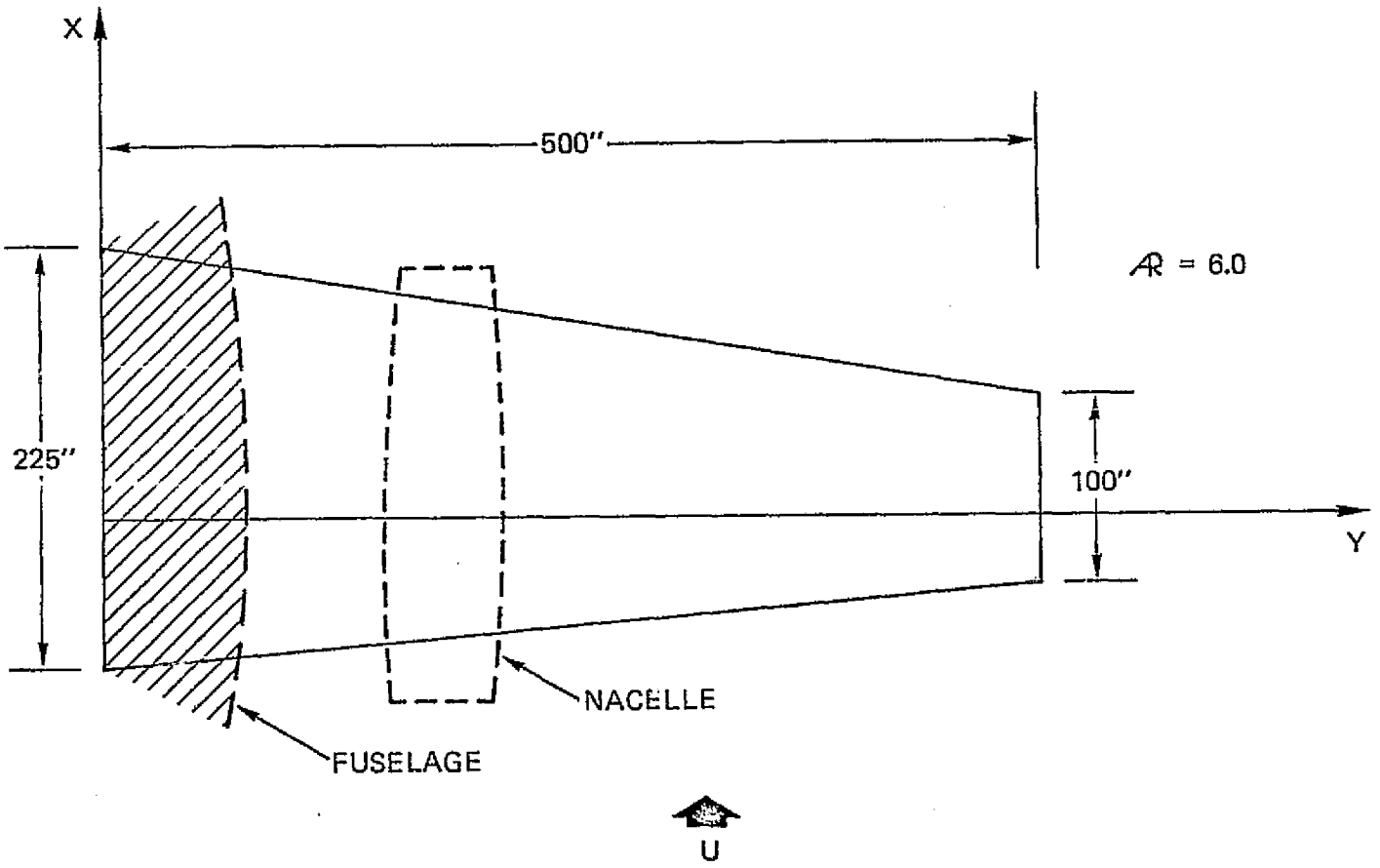

FIG. 5.1--Wing Planform.

As the figure shows, the structural model chosen includes a nacelle and fuselage. The masses of these two elements were held fixed during the optimization at the values of

$$m_{FUS} = 430.4 \text{ slugs} \quad ,$$

$$m_{NAC} = 163.0 \text{ slugs} \quad .$$

The assumption regarding linearity between the design variables and the structural inertia and mass was retained in this chapter. By fitting data given in Ref. 32, the following factors of proportionality were obtained:

$$m(y) = \text{mass/inch} = 2.2\ t(y) \text{ slugs/inch} \quad ,$$

$$EI = \text{stiffness} = 5.94 \cdot 10^{10}\ t(y) \text{ lbs-in.}^2 \quad .$$

The taper of the chord adds complexity to the numerical calculations that determine the mass and stiffness matrices. Section C of the Appendix details corrections that are made to the untapered results to account for this fact. In addition, the Appendix describes how the non-structural masses representing the nacelle and the fuselage are incorporated into the mass matrix.

2. Turbulence Model

The previous chapter dealt with the responses to a random excitation whose power spectrum was constant over all frequencies. Numerous studies have shown that this white noise assumption is inadequate as a model for atmospheric turbulence. Chapter 13 of Ref. 47 and Ref. 48 contain excellent discussions of the procedures used and the approximations made in the development of alternative models. From these references it was decided that the analytical expression for the turbulence spectrum that is best suited for the present study is the one designated the von Karman model. The power spectrum of the vertical component of the atmospheric turbulence given by this model is

$$\Phi_{w_g}(\Omega) = \frac{\sigma_{w_g}^2}{\pi} \frac{L_T[1 + \frac{8}{3}(1.339\, L_T\Omega)^2]}{[1 + (1.339\, L_T\Omega)^2]^{11/6}} \quad . \tag{5.1}$$

The terms of this equation are defined in the list of symbols.

A number of crucial assumptions have to be made about the nature of the turbulence in order to arrive at this form (e.g., that the turbulence is homogeneous and that it has a Gaussian distribution). The adequacy of these assumptions are evaluated quite well in Ref. 48 and will not be discussed here.

Values for the turbulence scale and the mean square value of the turbulence had to be selected. From Ref. 48, values were chosen that

were typical for severe thunderstorm conditions. These were

$$L_T = 5000 \text{ ft.} \quad ,$$

$$\sigma_{w_g} = 14 \text{ ft./sec.} \quad .$$

The scale length (which is a measure of the turbulence wavelength) is considerably greater than the 83 ft. span of the wing used for this study. This large difference in scale reinforces the approximation that the turbulence is one-dimensional with a uniform value across the span at any instant.

Figure 5.2 compares the von Karman spectrum used in the present study with the spectrum used in Example 10.6 of Ref. 32. It is necessary to present the comparison here because a later figure compares two bending moment spectra that were obtained using the two different excitation spectra. It is seen that the von Karman spectrum has a considerably higher proportion of its energy in the lower frequencies.

3. Aerodynamic Operators

The most important difference in the nature of the present problem compared to those of the previous chapters is in the manner in which the loading is exerted on the structure. In the previous chapter, the random disturbance was assumed to be transferred directly to the structure in some unspecified manner. In the present example, the aerodynamic loads that result from the unsteady gust differ in phase and magnitude from the gusts themselves. This is due to the fact that

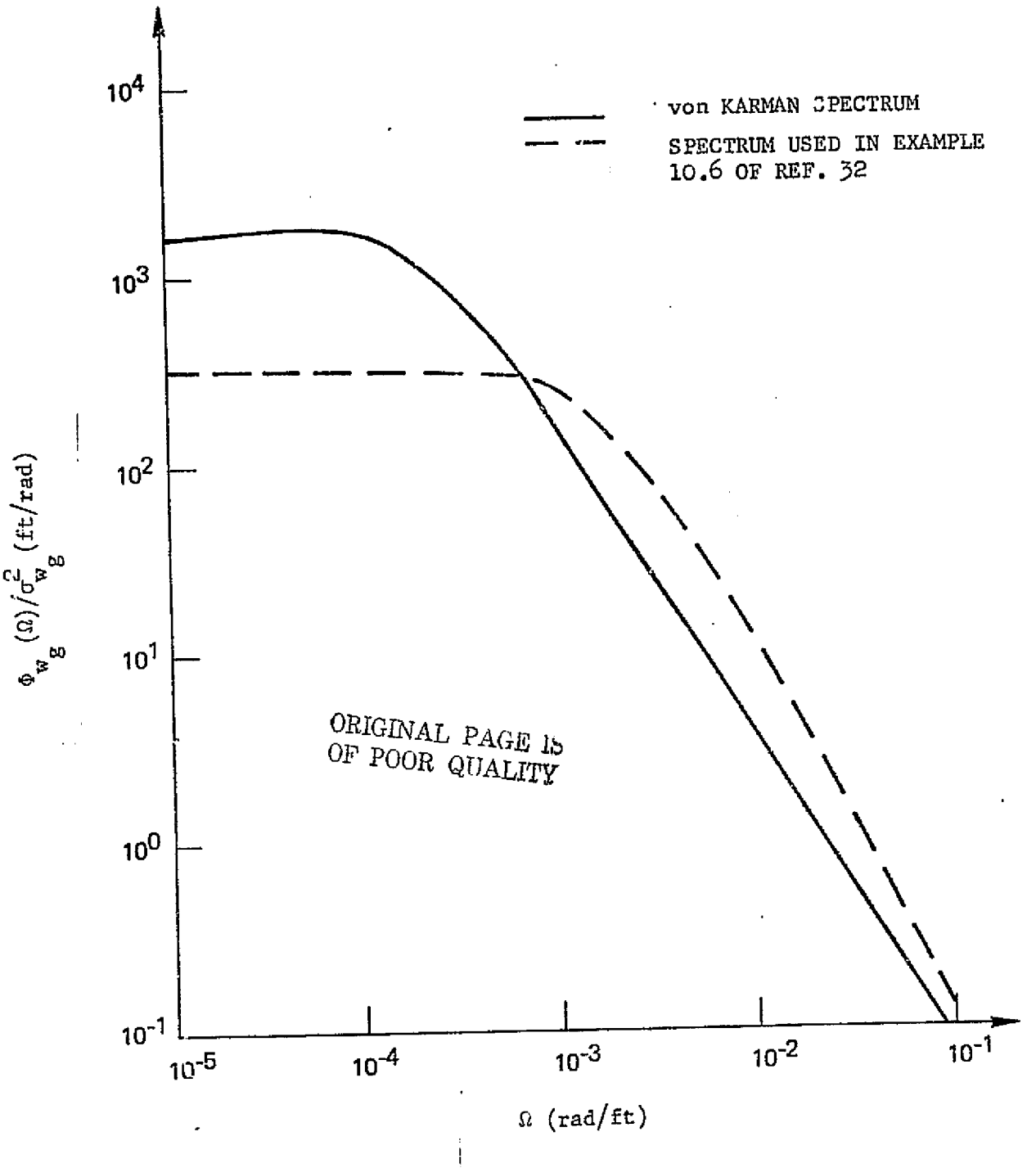

FIG. 5.2--Comparison of Excitation Spectra.

the loads on the structure, which are a function of the circulation, do not respond instantaneously to the gust. A further complication is the fact that the motion of the wing moving in response to the gust's excitation gives rise to additional forces.

This study is restricted to vertical motions only; therefore, the relevant load acting on the wing is the lift. As the previous paragraph indicates, this load can be separated into two components:

$$P = L_m + L_g \quad . \tag{5.2}$$

L_g is the direct lift associated with the impingement of the gust while L_m is the added lift resulting from the wing's motion. Values for these two components are developed in Chap. 5 of Ref. 32 for a two-dimensional airfoil in incompressible flow that is encountering a sinusoidal gust. These values are given by

$$\frac{L_g}{w_g} = 2\pi\rho_a U_b \left\{ C(k)[J_0(k) - iJ_1(k)] + iJ_1(k) \right\} , \tag{5.3}$$

$$L_m = \pi\rho_a b^2 [k^2 - 2ik\, C(k)]h \quad , \tag{5.4}$$

where:

h = vertical displacement ,

$C(k)$ = Theodorsen's function ,

J_0 and J_1 = Bessel functions of the first kind .

Theodorsen's function is a complex function of the reduced frequency and is an analytical representation of the change in amplitude and phase of the circulatory lift due to a vertical oscillation. It can be expressed explicitly in terms of Hankel functions, but for the low magnitudes of k of interest to this study, it was deemed adequate to use an approximation that is given by Fung in Section 6.9 of Ref. 49:

$$C(k) = 1.0 - \frac{0.165}{[1.0 - (0.0455i/k)]} - \frac{0.335}{[1.0 - (0.3i/k)]} \quad . \quad (3.5)$$

Perhaps it is in order to point out here that the complex nature of the aerodynamics makes it unnecessary to include structural damping. This damping was required in the previous chapter in order to obtain finite response, but the out of phase component of the aerodynamics acts as a damping mechanism that limits the structural response to finite values regardless of the excitation frequency.

In order to apply these results to the problem at hand, a number of additional assumptions must be made. These are mainly the approximations that are used in aerodynamic strip theory:

(1) The incompressible results are valid for the analysis. (The example considered has a free stream Mach number of 0.62 so that compressibility effects could be constructively considered.)

(2) The reduced frequency is computed using a reference chord, as opposed to the local chord, resulting in a k that is constant

across the span. While this is not strictly necessary, it greatly simplifies the calculation. The range of actual reduced frequency values across the span is small enough so that the error introduced by this assumption is not large.

(3) The loads on the three-dimensional wing are the same as would occur at that wing station in a two-dimensional flow (except for the disparity in k values mentioned in the previous assumption).

It would be interesting, and not too difficult, to determine what effect these assumptions have on the final results. However, these were considered to be secondary matters that did not require evaluation for the present study.

Once these aerodynamic loads have been evaluated, it is necessary to put them into a form consistent with the finite element models developed for the mass and stiffness matrices. Again, the Appendix provides the details of how this is done.

Finally, values of the parameters necessary for calculating the aerodynamic loads are:

$$U = 696.8 \text{ ft/sec} \quad ,$$

$$\rho_a = 2.378 \times 10^{-3} \text{ slugs/ft}^3 \quad ,$$

$$b_{ref} = 6.771 \text{ ft} \quad .$$

C. RESPONSE QUANTITIES AND GRADIENT EVALUATION

The end result of the development of the models in the previous section is the construction of an equation of motion in the form:

$$(-\omega_e^2 [M] + [K] - [A]) \{w\} = \{G\} \quad . \qquad (5.6)$$

Some new terms have been added to the formulation used to study white noise. These are

$\{G\}$ = Vector representing the load due to a unit sinusoidal gust of frequency ω_e .

$[A]$ = Matrix relating the loads on the aircraft due to the aircraft's oscillation at frequency ω_e .

The general method used in the previous chapter can be repeated here to find the root mean square response values for the stresses and the stress rates. However, the new elements of the problem necessitate going through a brief description of these methods. While it is not explicitly emphasized, it must be remembered that the analysis presented below is in terms of a unit gust excitation.

Modal superposition can again be used to obtain the response of the wing at a specified frequency:

$$\{w\} = \sum_{i=1}^{mn} \{p_i\} a_i = [P] \{a\} \quad . \qquad (5.7)$$

The $\{p_i\}$ vectors are the eigenvectors of the system $(-\lambda_i[M] + [K])\{p_i\} = 0.0$ and the a_i's are the modal participation factors that are to be determined for the forced response. The next step is to premultiply Eq. (5.6) by $[P]^T$:

$$(-\omega_e^2 [\,I\,] + [\,\lambda\,] - [GA])\{a\} = \{GG\} \quad . \quad (5.8)$$

The mode shapes have been normalized so that the generalized masses are unity. The new terms of Eq. (5.8) are clearly

$$[GA] = [P]^T[A][P] \quad ,$$
$$\{GG\} = [P]^T\{G\} \quad .$$

In the previous chapter, multiplying the equation of motion by the transposed eigenvector matrix uncoupled the equations in the a_i's by diagonalizing the mass and stiffness matrices. The generalized aerodynamic matrix is not diagonal, however, so the system of equations for the $\{a\}$ vector have to be treated simultaneously.

Also, since $[GA]$ and $\{GG\}$ vary in a complex fashion with the reduced frequency, it is necessary to evaluate Eq. (5.8) at a number of discrete reduced frequency values.

Once the modal participation factors have been found for a large enough number of reduced frequency values to represent the complete range of interest, it is possible to move on to the calculation of

the stresses. Once again, the methods of the previous chapter are inadequate for this problem. The difficulty now is that since the model permits rigid body motions, the bending moments cannot be calculated from a derivative of the displacement vector. Instead, external and inertial loads are summed and the bending moment is found from these forces and from the fact that the shear force and bending moment at the wing's tip are zero. The force acting is given by

$$F = L_g + L_m + m\omega_e^2 w \quad .$$

Or in matrix notation:

$$\{F\} = ([A] + \omega_e^2 [M]) \{w\} + \{G\} \quad . \qquad (5.9)$$

The $\{F\}$ vector represents concentrated forces and moments acting at the node points. From this vector, it is possible to calculate the bending moment acting at any specified location on the wing. For the purposes of this analysis, the bending moments were computed at the center of each element plus an additional calculation at the wing's root.

Performing the moment summations at these points gives:

$$BM_i = \sum_{j=i}^{n} \left[F_{2j+1} + \frac{L}{2n} F_{2j} \, [2(j - 1) + 1] \right] \qquad \text{(Cont'd)}$$

and

$$BM_{Root} = \sum_{j=1}^{n} \left(F_{2j+1} + F_{2j} \frac{jL}{n} \right) \quad . \qquad (5.10)$$

This can be summarized by a matrix equation: $\{BM\} = [T]\{F\}$.

The vector of bending moments calculated in this way can be thought of as the admittance functions for the structure. The factor that is of prime interest is the mean square bending stress. Given the bending moment, the remainder of the calculation is quite straightforward. First, the admittance of the bending stress is calculated using the standard $S = Mc/I$ formula. Proper account has to be made of the tapered property of the wing in this calculation as it enters into both the c and I terms in the stress equation. With the bending stress admittance calculated at a number of frequencies, the mean square response is calculated from:

$$\sigma_{SS}^2 = \int_0^\infty |S|^2 \Phi_{w_g}(\omega) \, d\omega \quad . \qquad (5.11)$$

The mean square stress rate is computed in a similar fashion:

$$\sigma_{\dot{S}\dot{S}}^2 = \int_0^\infty \omega^2 |S|^2 \Phi_{w_g}(\omega) \, d\omega \quad . \qquad (5.12)$$

Simpson's rule was used in performing the numerical integrations.

Once these two parameters have been determined, the analysis of Section IV.B can be used to determine the fatigue life and time to first excursion failure at the wing stations of interest. This analysis will not be repeated here.

The changes in formulation described above also create some differences in the way the gradients are calculated. Again, only the new details are described in this section, since the previous chapter is available to provide added detail.

The eigenvalue and eigenvector derivatives are found in the same manner as previously except that the rigid body mode allows certain simplifications. Specifically, since the rigid body frequency is zero, the derivatives of this frequency are trivally zero:

$$\frac{\partial \lambda_1}{\partial t_j} = 0 \qquad j = 1,2,\ldots,n \quad . \tag{5.13}$$

The rigid body mode shape is a vector given by relation:

$$\{p_1\}^T = \eta\{1,1,0,1,\ldots,1,0\} \equiv \eta\{U\}^T \quad , \tag{5.14}$$

where η is the normalizing factor used to obtain $\{p_1\}^T[M]\{p_1\} = 1.0 = \eta^2\{U\}^T[M]\{U\}$.

Since the mass matrix varies with the design variables, the rigid body mode does have a derivative with respect to the design

variables that can be evaluated by the use of the relationship just obtained:

$$2\eta\{U\}^T[M]\{U\}\ \frac{\partial\eta}{\partial t_j} = -\eta^2\{U\}^T\ \frac{\partial[M]}{\partial t_j}\ \{U\} \quad ,$$

$$\therefore\ \frac{\partial\eta}{\partial t_j} = -\eta^3\{U\}^T\ \frac{\partial[M]}{\partial t_j}\ \{U\}/2 \quad . \qquad (5.15)$$

The matrix triple product $\{U\}^T\ (\partial[M]/\partial t_j)\ \{U\}$ can be shown to be equal to the structural mass of the j^{th} element, m_j, divided by the design variable t_j. The derivative expression for the mode shape then becomes:

$$\frac{\partial\{p_1\}}{\partial t_j} = \frac{\partial\eta}{\partial t_j}\{U\} = -\frac{\eta^3}{2}\ \frac{m_j}{t_j}\{U\} \quad .$$

The next step is the determination of the derivative of the modal participation factors. Recall Eq. (5.8):

$$(-\omega_e^2\ [\ I\ ] + [\ \lambda\ ] - [GA])\ \{a\} = \{GG\} \quad .$$

Taking the derivative with respect to the thickness of the j^{th} element gives:

$$(-\omega_e^2\ [\ I\ ] + [\ \lambda\ ] - [GA])\ \left\{\frac{\partial a}{\partial t_j}\right\} = \frac{\partial[P]^T}{\partial t_j}\{G\} - \quad \text{(Cont'd)}$$

$$\left(\frac{\partial}{\partial t_j} [\lambda] - 2[P]^T[A] \frac{\partial [P]}{\partial t_j} \right) \{a\} \quad . \qquad (5.16)$$

As in previous cases of this type, the matrices on the left-hand sides of Eqs. (5.8) and (5.16) are the same, regardless of which design vector is of interest. Therefore, the matrix decomposition of $(-\omega_e^2 [I] + [\lambda] - [GA])$ needs to be evaluated only once for the $n + 1$ systems of $2n + 1$ simultaneous equations.

Another note is that the derivative of the generalized aerodynamics matrix involves only the mode shapes since the aerodynamics matrix, $[A]$, is not a function of the design variable. This is different from flutter optimization problems, where the aerodynamics are indirectly a function of the design variable because the flutter frequency is contained in the matrix (Ref. 50).

Finally, note that even though matrix $[GA]$ is symmetric, the derivative $\partial[GA]/\partial t_j$ is not.

The remaining derivative calculations can now be evaluated:

$$\left\{ \frac{\partial w}{\partial t_j} \right\} = \frac{\partial [P]}{\partial t_j} \{a\} + [P] \left\{ \frac{\partial a}{\partial t_j} \right\} \quad ,$$

$$\left\{ \frac{\partial F}{\partial t_j} \right\} = \omega_e^2 \frac{\partial [M]}{\partial t_j} \{w\} + (\omega_e^2 [M] + [A]) \left\{ \frac{\partial w}{\partial t_j} \right\} \quad ,$$

$$\left\{ \frac{\partial BM}{\partial t_j} \right\} = [T] \left\{ \frac{\partial F}{\partial t_j} \right\} \quad . \qquad (5.17)$$

Another new derivative that must be evaluated is:

$$\frac{\partial |S_i|^2}{\partial t_j} = 2\bar{S} \frac{\partial S_i}{\partial t_j} \quad , \tag{5.18}$$

where the bar indicates the complex conjugate.

Since the bending stress is proportional to the bending moment and inversely proportional to the element thickness, ($S_i = cp_i BM_i / t_i$, where cp_i is the constant of proportionality), the bending stress derivative is given by

$$\frac{\partial S_i}{\partial t_j} = cp_i \frac{\partial BM_i}{\partial t_j} - \frac{cp_i}{t_j^2} BM_i \delta_{ij} \quad , \tag{5.19}$$

where δ_{ij} is the Kronecker delta.

Finally,

$$\frac{\partial}{\partial t_j} \sigma^2_{S_i S_i} = \int_0^\infty \phi_{w_g} \frac{\partial}{\partial t_j} |S|^2 \, d\omega \quad , \tag{5.20}$$

and similarly for the stress rate. The remaining derivatives for the constraints and the objective function are identical in form to those of the previous chapter and are not repeated here.

D. RESULTS

As the above descriptions have perhaps indicated, the function evaluation and gradient calculation require a considerable amount of computation. Consider an example that has N elements and a mesh of

NF discrete frequencies used in the response calculations. Further specify that MN natural modes are used for modal superposition. Then each function evaluation requires the solution of a $2N + 1$ eigenvalue problem. In addition, the MN linear simultaneous equations given by Eq. (5.8) must be solved NF separate times. If gradient information is desired, the MN simultaneous equations given by Eq. (5.15) must be solved $NF \times N$ times. An additional factor is that unless one is very clever or sacrifices programming speed and clarity, the arrays needed for the computation quickly fill the computer's available core. E.g., a reasonable way to dimension $\partial S/\partial t_j$ of Eq. (5.19) is DS(N+1,NF,N) signifying that each of the $N + 1$ stress values for each of the NF frequencies has derivatives with respect to N different design variables.

For these reasons, the examples done for the thesis were kept as simple as possible while retaining the capability of obtaining meaningful results.

The first example used three structural elements and retained the rigid body mode plus one bending mode. Twenty-nine reduced frequency values ranging, at equal intervals, from 0.0 to 0.28 were used. Although this first example was worked mainly as a check on the algorithm, the results are of sufficient interest to be presented here. The constraints were identical with those of the previous chapter in that the fatigue life was specified to be greater than one year while the time to first excursion failure was specified to be greater than one-half year.

The initial and optimal* thickness distributions for this example are

$$\{t\}_i = \begin{Bmatrix} 1.00 \\ 0.90 \\ 0.50 \end{Bmatrix} \qquad \{t\}_o = \begin{Bmatrix} 0.04965 \\ 0.02539 \\ 0.01146 \end{Bmatrix} .$$

A plot of the final thickness distribution is given in Fig. 5.3. The active constraints designated on the figure are all first excursion failure type constraints.

The marked reduction in weight is partially due to the fact that the initial configuration is extremely overdesigned with respect to the constraints considered here. The rms stress at the root for the initial design is approximately 600 psi; a value so far below the specified ultimate strength level of 40000 psi as to be insignificant. This should not be too surprising, since the textbook example from which the model was obtained was not intended to be near a critical value with respect to this particular constraint. It is surprising that the weight is reduced by a factor greater than twenty. This fact is discussed following the presentation of the second and last example.

The final example used five elements to represent the structure and retained two bending modes plus the rigid body mode. The same

---

*The cost function used for the wing examples was the sum of the design variables. Due to the taper of the wing, this is not exactly proportional to the structural weight; therefore, the final thickness distribution is not the minimum weight solution. This oversight was detected after the two examples were completed, and it did not seem a large enough error to require re-optimizations with their attendant computer costs.

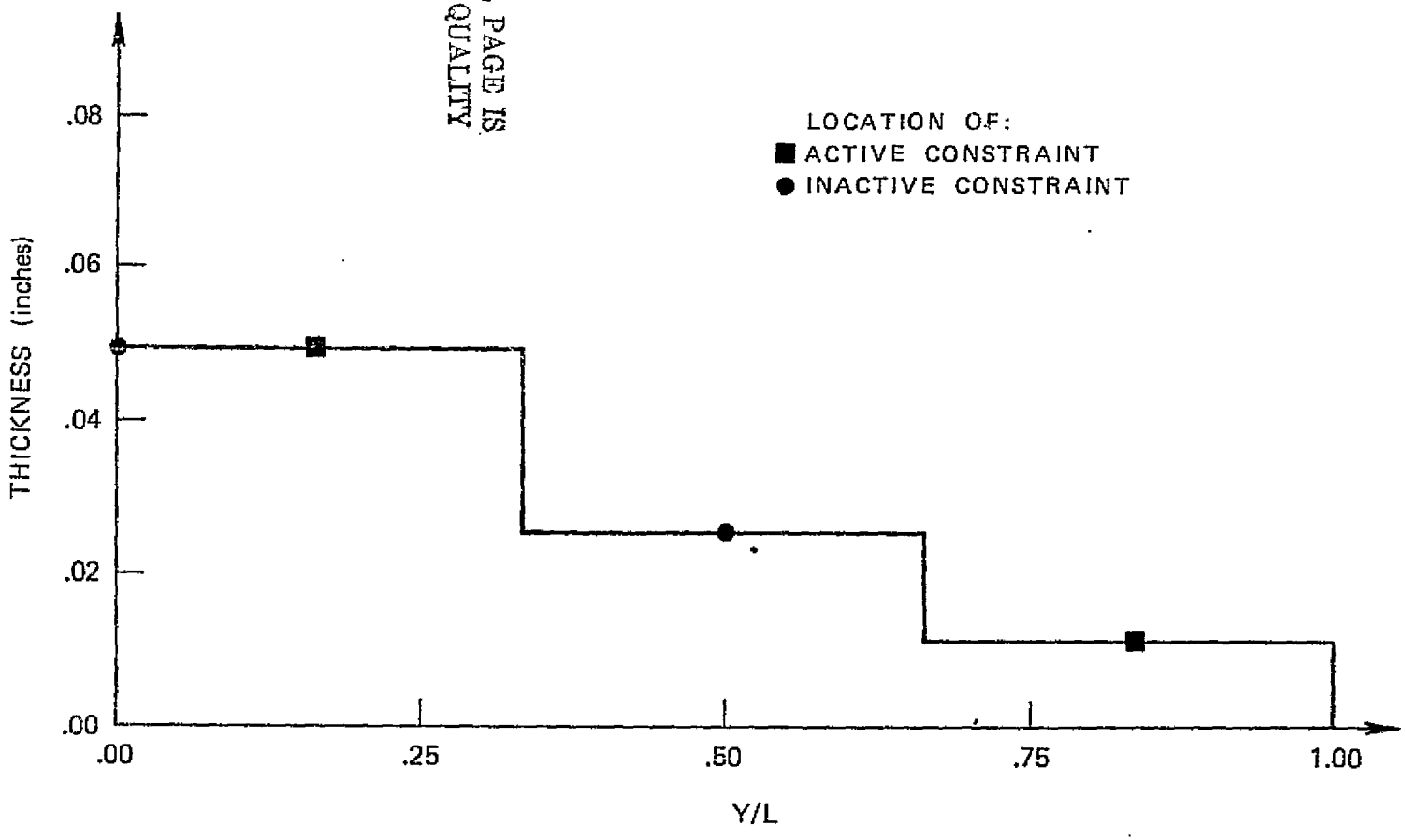

FIG. 5.3--Optimal Thickness Distribution for a Wing Excited by Continuous Atmospheric Turbulence (Three Finite Elements).

number of reduced frequencies were used. Since the previous example had permitted an optimal design that was unrealistically light, the constraint lives were multiplied by a factor of ten. The fatigue life was therefore constrained to be greater than ten years and the time to first excursion failure was required to be greater than five years. The remaining parameters were left unchanged.

Figure 5.4 compares the power spectral density of the root bending moment obtained from Example 10.6 of Ref. 32 with that obtained using the initial design and the models developed for the present study. The different turbulence spectra used for the two cases account for the majority of the discrepancy, while some differences in the modelling of the structure account for the shift in the location of the second peak. In the figure, the first peak is almost entirely due to the rigid body response while the second peak occurs very close to the natural frequency of the first bending mode. The second bending mode occurs at such a high frequency that it does not have an effect on the root bending moment. Of interest here is the fact that the two solutions are qualitatively the same, indicating that the computer analysis has been done correctly.

The initial and optimal thickness values, as well as the rms values of the stress and stress rate for the final design are given in Table 5.1.

Figure 5.5 plots the final thickness distribution and indicates where the constraints are active. In this example, all the active constraints were of the fatigue type.

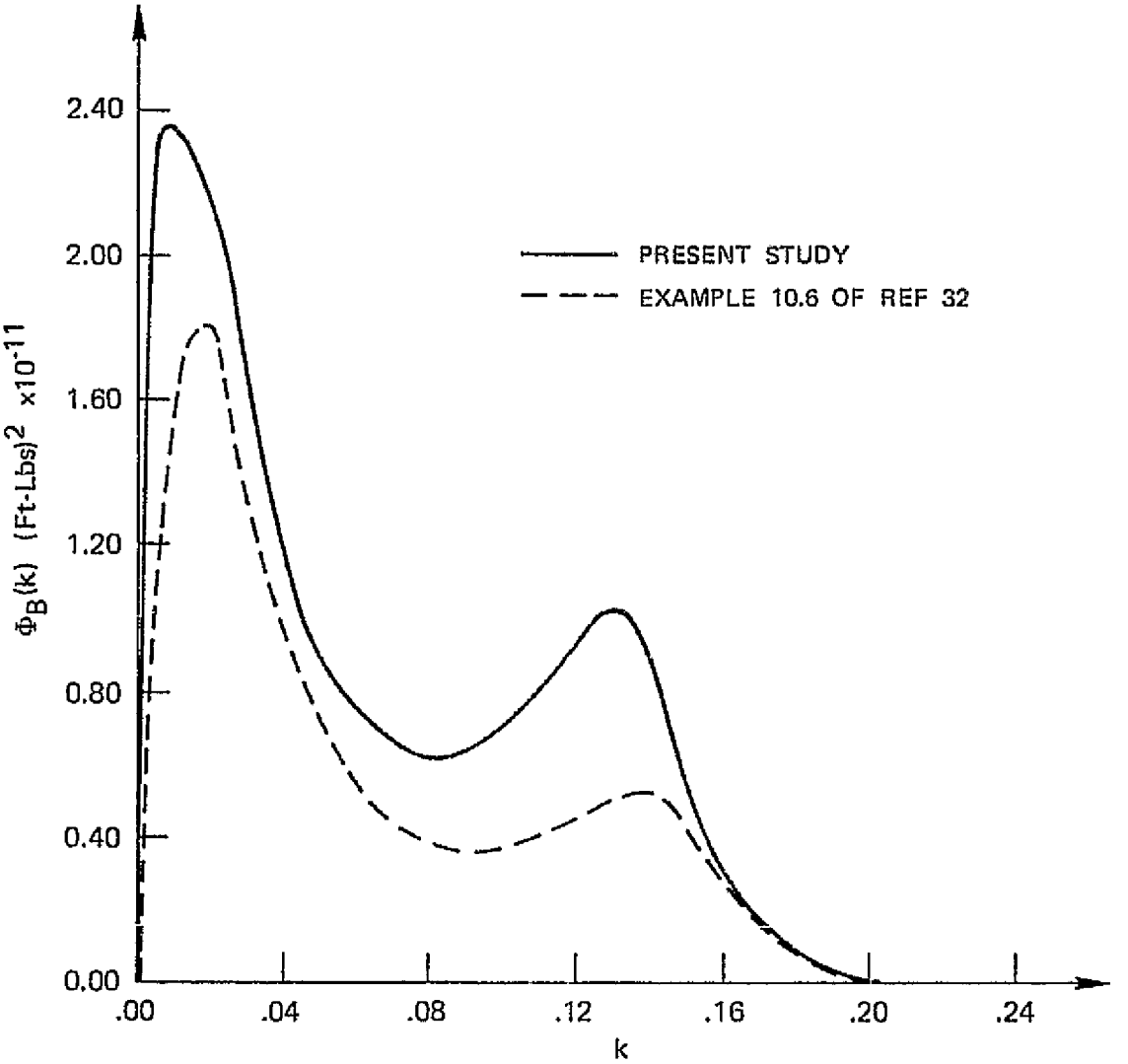

FIG. 5.4--Root Bending Moment Power Spectra of Initial Design.

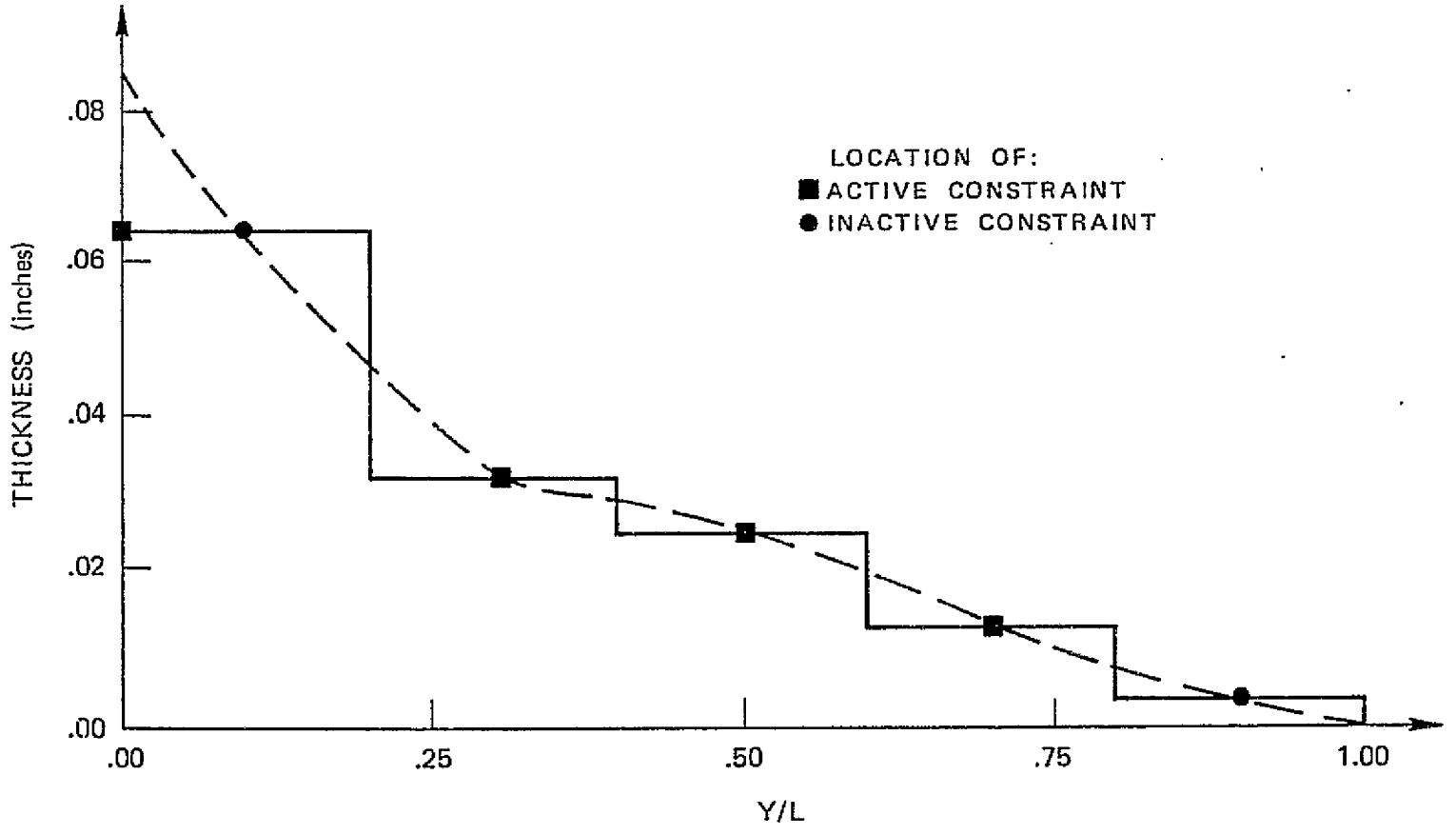

FIG. 5.5--Optimal Thickness Distribution for a Wing Excited by Continuous Atmospheric Turbulence.

Element	Thickness		Final Design	
	Initial	Optimal	RMS Stress	RMS Stress Rate
Root	--	--	4338 psi	25,706 psi/sec
1	1.00"	0.0628"	5965	18,562
2	0.955	0.0312	5521	31,506
3	0.915	0.0245	5733	24,971
4	0.810	0.0125	5394	34,877
5	0.380	0.0035	5157	32,590

TABLE 5.1--Wing in a Turbulent Atmosphere

The most striking fact that this solution exhibits is that, even with the constraint lives multiplied by ten from the previous example, there is a very large weight decrease from the initial to the final design. Part of the explanation for this behavior is indicated by Fig. 5.6. This figure shows the power spectral density of the root bending moment for the final design. A comparison of this figure with Fig. 5.4 points out two things: (1) The area under the power spectrum, and hence the rms bending moment, for the final design is substantially less than the area under the comparable curve for the original design and (2) the response to the first bending mode has disappeared in the optimal design. These two results are related to the fact that, as the weight is reduced, the inertial loads become increasingly less important compared to the aerodynamic loads.

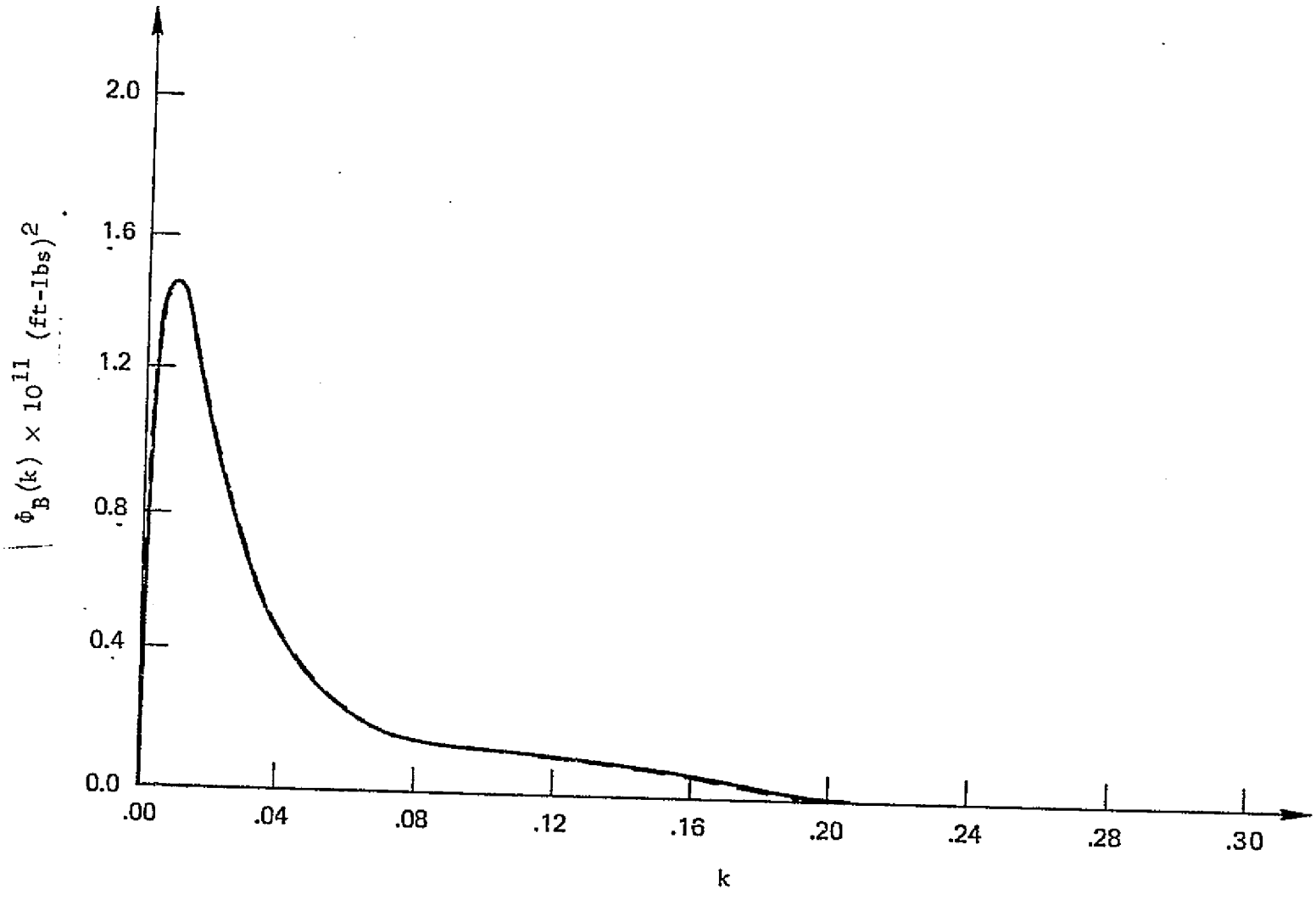

FIG. 5.6--Root Bending Moment Power Spectrum of the Optimal Design.

Of course the rms stresses are considerably greater for the final design since the stresses are inversely proportional to the design variables.

This example dramatically illustrates a tenet of structural optimization that is frequently ignored; viz., for the final result to be useful, all the design conditions that the structure will be required to meet must be considered simultaneously. Because this work was primarily interested in studying the effect of stochastic loads in the optimization process, other constraints that would have made the final design more meaningful were left out of the analysis. The following, concluding chapter offers some suggestions as to how the optimal design of a wing could include more complete design conditions.

CHAPTER VI

CONCLUSIONS AND RECOMMENDATIONS

A number of comments about the behavior and significance of the solutions have already been made. Sections II.D, III.E and IV.E are devoted to discussions of the material presented in their respective chapters. This final chapter reiterates and expands on these comments and lists areas that would benefit from further study.

A general conclusion is that despite the complications introduced by dynamic loadings, methods of mathematical programming can be applied to studies of this type. This is not a surprising, or even new, conclusion. Accordingly, the main contributions of this thesis must reside in the formulation of the analyses and in some of the interesting results obtained.

In particular, the discovery of disjoint feasible regions in Chapter III is of theoretical and perhaps practical interest. The two design variable example of Section III.A demonstrates the concepts of disjointness with a simplicity that makes it valuable as an instructive tool. The ease of the formulation, coupled with the large amount of information garnered, also reinforces the maxim that simple cases should be examined first. It is felt that some of the studies of optimization with dynamic loading have ignored this rule and have thereby suffered from a lack of understanding of the basic principles involved.

It is realized that the optimal structures shown in Chapter III with a first natural frequency that is less than the excitation frequency are impractical because of their inability to sustain even moderate static loads. However, when a design is influenced by a harmonic loading, it may be possible to obtain a more suitable structure by "loosening" it so that one or more natural frequencies are less than the forcing frequency rather than by stiffening it so that all natural frequencies are higher.

A design procedure that is related to this concept is that of "detuning". In this procedure, masses are added or moved on the structure in a manner that minimizes resonant responses. Another example is the "soft mounting" of nacelles. In the latter technique, the mounts minimize nacelle motion by giving the nacelle-mount combination a first natural frequency that is less than the predominant excitation frequency. Methods developed in this thesis can aid these design practices by performing them in a more systematic fashion.

The results of Chapter IV indicate that the optimal structure can differ markedly from intuitive designs that are based on static strength alone. Another conclusion is that the response to white noise can be adequately estimated by a very small number of modes. For the problems studied, the first two modes were of primary importance and further modes added little to the final results while increasing the computer time for solution significantly.

The results of the preceding chapter, dealing with a wing in atmospheric turbulence, make it clear that care must be taken to adequately

formulate problems of this nature. The example chosen had an initial design that was much too stiff to make a comparison between the initial and final designs meaningful. Also a number of features should be added to the model studied. Among these are additional loading and constraint conditions to insure that the optimal structure has adequate strength to withstand normal flight loads and landing impacts. The torsional modes are probably also of importance and should be included in further investigations. When other factors, such as fracture toughness, flaw growth, realistic aircraft structures and improved aerodynamics are added to this list, the analysis is clearly one that is beyond the scope of this developmental work. Hopefully, it has provided some of the techniques that a more ambitious research group could build upon.

One aspect of most papers on structural optimization which is absent from the present study is the presentation of the amount of computer time necessary for a problem's solution. Since the time to solution was not considered to be an important factor in the problems worked here, no attempt was made to minimize it. An indication of the magnitude of the computation time required is given by the fact that each design iteration for the problem of Chapter V required approximately a minute of CPU time on Stanford's IBM 360/67 in the "Quick" partition. By using a more efficient compiler and by using approximate techniques for the analysis, it seems quite conceivable that this figure could be reduced by roughly a factor of ten. For problems with a larger number of design

variables, these efficiencies are clearly needed in order to make the optimizations manageable from a computer resources standpoint.

Aside from the above comments on problem formulation and computational efficiency, further investigations could be conducted in a number of areas. Some of these that the author finds intriguing and of importance to gaining an understanding of the principles of structural optimization with dynamic loading include the following:

(1) Further work on the function space solutions of Chapter III. The most desirable goal would be analytical solutions for a range of constraint and loading conditions. Unfortunately, analytical results to date have been minimal despite considerable efforts made in a search for such results.

(2) Solving the two point boundary value problems of Section III.C by numerical methods could also be a worthwhile activity. Pierson (Ref. 10) describes an excellent algorithm that can be used to iteratively solve these types of problems.

(3) Design of optimal two-dimensional structures, such as plates and shells, with a harmonic or other dynamic excitation. To the author's knowledge, this is uncharted territory and should provide a wealth of problems and new results. It is anticipated that the disjoint feasible regions will continue to be a complicating factor in the search for optimal solutions for the harmonically loaded structures.

(4) For problems with stochastic excitation, this work uses relatively simple failure criteria. The discipline of fracture mechanics

has recently developed more sophisticated methods for predicting a structure's damage due to random loads. These methods should have application to the optimization problems.

(5) The problems of Chapter IV should be solved for a range of such parameters as structural damping, load magnitude, and constraints. This would show the qualitative effects that these parameters have on the solutions and might even point out some new properties of stochastic optimization problems.

These are suggestions that relate directly to the investigations of this thesis. There are, of course, many other problems involving optimization of structures under dynamic excitation that are of interest and importance. It is the author's view that the most critical current task for the optimizer is that of acquainting the designer with the techniques of optimization so that they can jointly determine where the methods are of most value. It is felt that this work has broadened the application of optimization methods and has therefore enhanced their attractiveness and usefulness. Hopefully, this promise will be furthered and fulfilled.

REFERENCES

1. Sheu, C. Y., and Prager, W., "Recent Developments in Optimal Structural Design," Applied Mechanics Reviews, Vol. 21, No. 10, Oct. 1968, pp. 985-992.
2. Fox, R. L., Optimization Methods for Engineering Design, Addison Wesley, Reading, Massachusetts, 1971.
3. Gellatly, R. A., Editor, Structural Optimization, AGARD Lecture Series No. 70, Hampton, Virginia, October 1974.
4. Schmit, L. A., Jr., Editor, Structural Optimization Symposium, American Society of Mechanical Engineers, New York, Nov. 1974.
5. Pierson, B. L., "A Survey of Optimal Structural Design Under Dynamic Constraints," International Journal for Numerical Methods in Engineering, Vol. 4, No. 4, July-Aug. 1972, pp. 491-499.
6. Ashley, H., and McIntosh, S. C., Jr., "Application of Aeroelastic Constraints in Structural Optimization," Proceedings of the Twelfth International Congress of Applied Mechanics, Springer, Berlin, 1969.
7. Weisshaar, T. A., "An Application of Control Theory Methods to the Optimization of Structures Having Dynamic or Aeroelastic Constraints," SUDAAR 412, Stanford University, Department of Aeronautics and Astronautics, October 1970.

8. Armand, J., and Vitte, W. J., "Foundations of Aeroelastic Optimization and Some Applications to Continuous Systems," SUDAAR No. 390, Stanford University, Department of Aeronautics and Astronautics, January 1970.

9. Turner, M. J., "Design of Minimum Mass Structures with Specified Natural Frequencies," AIAA Journal, Vol. 5, No. 3, March 1967, pp. 406-412.

10. Pierson, B. L., "Application of a Gradient Projection Optimal Control Method to a Class of Panel Flutter Optimization Problems," ISU-ERI-AMES 73186, Iowa State University, Ames, Iowa, 1973.

11. Iceman, L. J., "Optimal Structural Design for Given Dynamic Deflection," International Journal of Solids and Structures, Vol. 5, No. 5, May 1969, pp. 473-490.

12. Brach, R. M., "Optimum Design of Beams for Sudden Loadings," Proceedings of the ASCE Journal of the Eng. Mechanics Division, Vol. 94, No. EM6, Dec. 1968, pp. 1395-1407.

13. Brach, R. M., "Minimum Dynamic Response for a Class of Simply Supported Beam Shapes," International Journal of Mechanical Sciences, Vol. 10, No. 5, May 1968, pp. 429-439.

14. Fox, R. J., and Kapoor, M. P., "Structural Optimization in the Dynamic Response Regime: A Computational Approach," AIAA Structural Dynamics and Aeroelasticity Specialist Conference, New Orleans, Louisiana, April 1969, pp. 15-22.

15. Fox, R. J., and Kapoor, M. P., "Rates of Change of Eigenvalues and Eigenvectors," AIAA Journal, Vol. 6, No. 12, Dec. 1968, pp. 2426-2429.

16. Levy, H. J., Minimum Weight Design Under Dynamic Loading, Ph.D. Thesis, New York University, 1972.

17. Levy, H. J., and Wolf, B. M., "Fully Stressed Dynamically Loaded Structures," ASME Publication 74-WA/DE-19, ASME Winter Annual Meeting, Nov. 1974.

18. Venkayya, V. B., Khot, N. S., and Berke, L., "Application of Optimality Criteria Approaches to Automated Design of Large Practical Structures," Second Symposium on Structural Optimization, AGARD Conference Proceedings No. 123, Milan, Italy, April 1973.

19. Venkayya, V. B., and Khot, N. S., "Design of Optimum Structures to Impulse Type Loading," AIAA/ASME/SAE 15th Structures, Structural Dynamics and Materials Conference, Las Vegas, Nevada, April 1974. (Preprint AIAA Paper No. 74-345).

20. Solnes, J., and Holst, O. L., "Optimization of Framed Structures Under Earthquake Loads," 5th World Conference on Earthquake Engineering, Rome, June 1973, (Preprint Paper 376).

21. Nigam, N. C., and Narayanan, S., "Structural Optimization in Aseismic Design," 5th World Conference on Earthquake Engineering, Rome, June 1973, (Preprint Paper 374).

22. Nigam, N. C., "Structural Optimization in Random Vibration Environment," AIAA Journal, Vol. 10, No. 4, April 1972, pp. 551-553.

23. Kato, B., Nakamura, V., and Anraku, H., "Optimum Earthquake Design of Shear Buildings," ASCE Proceedings, Journal of the Engineering Mechanics Division, Vol. 98, No. EM4, Aug. 1972, pp. 891-910.

24. Cassis, J. H., "Optimum Design of Structures Subjected to Dynamic Loads," UCLA-ENG-7451, UCLA, School of Engineering and Applied Science, June 1974.

25. Plaut, R. H., "Optimal Structural Design for Given Deflection Under Periodic Loading," Quarterly of Applied Mathematics, Vol. 29, No. 2, July 1971, pp. 315-318.

26. Mroz, Z., "Optimal Design of Elastic Structures Subjected to Dynamic, Harmonically Varying Loads, Zeitschrift fur Angewandte Mathematik und Mechanik, Vol 50, No. 5, May 1970, pp. 303-309.

27. Hilton, H. H., and Feigen, M., "Minimum Weight Analy is of Structures Based on Structural Reliability," Journal of the Aerospace Sciences, Vol. 27, No. 9, Sept. 1960, pp. 641-652.

28. Kalaba, R., "Design of Minimal Weight Structures for Given Reliability and Cost," Journal of the Aerospace Sciences, Vol. 29, No. 3, March 1962, pp. 355-356.

29. Moses, F., and Kinser, D. E., "Optimum Structural Design With Failure Probability Constraints," AIAA Journal, Vol. 5, No. 6, June 1967, pp. 1152-1158.

30. Araslanov, A. M., "Calculation of Minimum Weight Beams Under Random Loading," The Journal of the Astronautical Sciences, Vol. XIX, No. 2, Sept.-Oct. 1971, pp. 150-158.

31. Lin, Y. K., Probabilistic Theory of Structural Dynamics, McGraw-Hill Book Co., New York, 1967.

32. Bisplinghoff, R. L., Ashley, H., and Halfman, R. L., Aeroelasticity, Addison-Wesley, Reading, Massachusetts, 1955.

33. Fletcher, R., and Powell, M. J. D., "A Rapidly Convergent Descent Method for Minimization," Computer Journal, Vol. 6, No. 2, 1963, pp. 163-168.

34. Vanderplaats, G. N., and Moses, F., "Structural Optimization by Methods of Feasible Directions," Computers and Structures, Vol. 3, No. 4, July 1973, pp. 739-755.

35. Segenreich, S., and Rizzi, P., "Some Properties of Axial or Free Vibration Frequencies of Rods," AIAA Journal, (to appear).

36. Scanlan, R. H., and Rosenbaum, R., Aircraft Vibration and Flutter, Dover Publications, Inc., New York, 1968.

37. Bryson, A. E., and Ho, Y., Applied Optical Control, Blaisdell Publishing Company, Waltham, Massachusetts, 1969.

38. Murphy, G. M., Ordinary Differential Equations and Their Solutions, Van Nostrand Reinhold Co., New York, 1960.

39. Weaver, W., Computer Programs for Structural Analysis, Van Nostrand Reinhold Company, New York, 1967.

40. Bogdanoff, J. L., and Goldberg, J. E., "On the Euler Bernoulli Beam Theory With Random Excitation," Journal of the Aero/Space Sciences, Vol. 27, No. 5, May 1960, pp. 371-376.

41. Yang, J-N, and Trapp, W. J., "Reliability Analysis of Aircraft Structures Under Random Loading and Periodic Inspection," AIAA Journal, Vol. 12, No. 12, Dec. 1974, pp. 1623-1630.

42. Gradshteyn, I. S., and Ryzhik, I. M., Table of Integrals, Series, and Products, Academic Press, New York and London, 1965.

43. Powell, A., "On the Fatigue Failure of Structures Due to Vibrations Excited by Random Pressure Fields," The Journal of the Acoustical Society of America, Vol. 30, No. 12, December 1958, pp. 1130-1135.

44. Papoulis, A., Probability, Random Variables and Stochastic Processes, McGraw-Hill Book Company, New York, 1965.

45. Miner, M. A., "Cumulative Damage in Fatigue," Journal of Applied Mechanics, Vol. 12, Sept. 1945, pp. 159-164.

46. Crandall, S. H., and Dahl, N. C., Editors, An Introduction to the Mechanics of Solids, McGraw-Hill Book Company, New York, 1959.

47. Etkin, B., Dynamics of Atmospheric Flight, John Wiley & Sons, Inc., New York, 1972.

48. Houbolt, J. C., Steiner, R., and Pratt, K. G., "Dynamics Response of Airplanes to Atmospheric Turbulence Including Flight Data on Input and Response," NASA TR-R-199, 1964.

49. Fung, V. C., The Theory of Aeroelasticity, Dover Publications, Inc., New York, 1969.

50. Gwin, L. B., Optimal Sizing of Complex Structural Systems for Flutter Requirements, Ph.D. Thesis, Stanford University, May 1973.

51. Przemieniecki, J. S., Theory of Matrix Structural Analysis, McGraw-Hill Book Company, New York, 1968.

APPENDIX: FINITE ELEMENT MODELS

The finite element formulations used in the thesis are presented in this appendix. The first two sections deal with the representation of rod and beam elements with constant cross sections. A standard text on finite elements (e.g., Ref. 51) contains most of the results shown in these sections; they are included here for completeness and to demonstrate the notation used. A third section deals with the representation of the tapered wing used in the fifth chapter of the thesis. It is necessary to go into added detail in order to indicate the adjustments that the tapered elements require. Lastly, the aerodynamic matrices needed in Cahpter V are formulated.

Throughout the Appendix, a distinction is made between matrices that represent a single element and those that represent an assembled structure. The former are denoted by a subscript that defines the element being considered (e.g., $[K]_i$) while the latter have no subscript (e.g., $[K]$).

A. TORSION ROD

Figure A.1 shows the rod and the degrees of freedom used. For a single element, the mass and stiffness matrices are represented by:

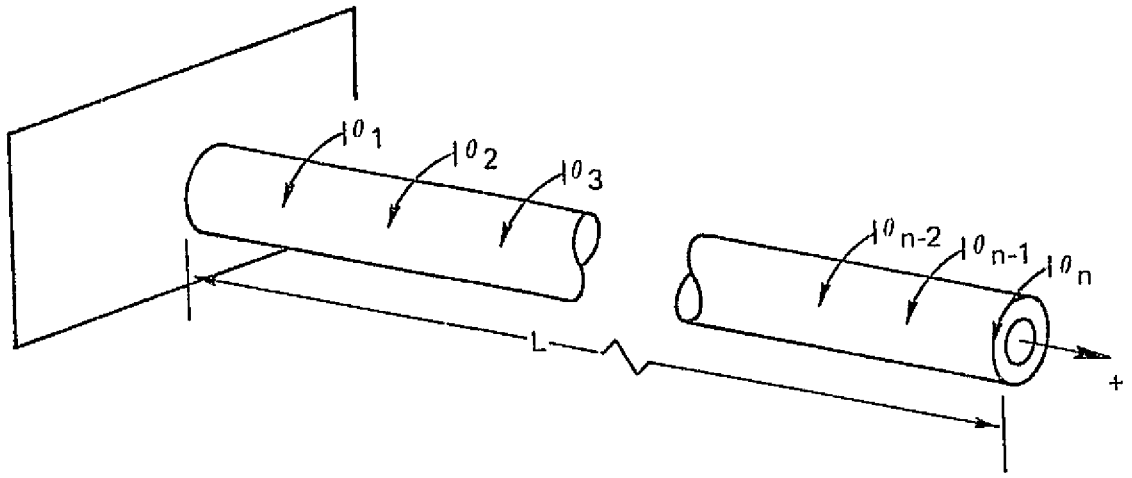

(a) Representation Using n Elements

ORIGINAL PAGE IS
OF POOR QUALITY

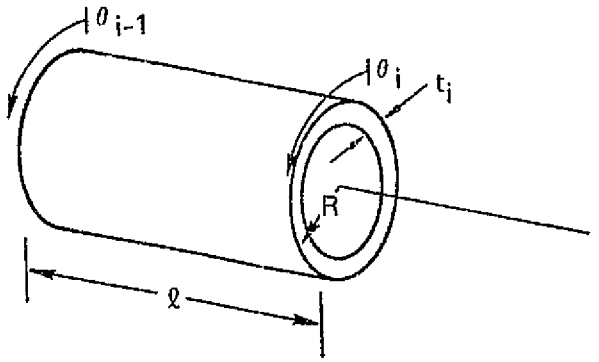

(b) Individual Rod Element

FIG. A.1--Cantilevered Rod.

$$[K]_i = \left(\frac{GJ}{\ell}\right)_i \begin{bmatrix} 1 & -1 \\ -1 & 1 \end{bmatrix} ,$$

$$[M]_i = \left(\frac{I_\alpha \ell}{6}\right)_i \begin{bmatrix} 2 & 1 \\ 1 & 2 \end{bmatrix} . \qquad (A.1)$$

From these elements matrices, the final matrices are readily assembled. Some assumptions made when this is done are:

(1) The one-dimensional structure is divided into n elements of equal length: $\ell = L/n$.

(2) The rod is a thin walled tube with structural properties that are proportional to the thickness:

$$(GJ)_i = GJ_0 t_i ,$$

$$(I_\alpha)_i = I_{\alpha 0} t_i . \qquad (A.2)$$

GJ_0 and $I_{\alpha 0}$ are constants for the structure.

(3) The cantilevered boundary condition is accounted for by deleting the degree of freedom associated with the root station.

The matrix is then assembled by adding the contributions of the individual elements at the node points. The assembled [M] and [K] matrices have dimensions $n \times n$.

The equivalent force vectors are needed to represent a uniform load across the rod. They are found by using the formula

$$\{P_{eq}\}_i = p_x \ell \int_0^1 \{a\}\, ds \quad . \tag{A.3}$$

Here $\{a\}$ gives the relation between the discrete displacement representation and the continuous actual displacement. For rod elements, $\{a\}^T$ is given by

$$\{a\}^T \quad \{1.0 - s\,,\, s\} \quad . \tag{A.4}$$

Then

$$\{P_{eq}\}_i = p_x \ell \begin{Bmatrix} \frac{1}{2} \\ \frac{1}{2} \end{Bmatrix} \quad . \tag{A.5}$$

The assembled equivalent force vector is

$$\{P\} = p_x \ell \begin{Bmatrix} 1 \\ 1 \\ 1 \\ 1 \\ \vdots \\ 1 \\ \frac{1}{2} \end{Bmatrix} \quad . \tag{A.6}$$

Another finite element matrix needed is one for determining the stresses. The relation between the stress and the displacement is found using:

$$S_i = G\{b\}^T\{\theta\} \quad , \tag{A.7}$$

where

$$\{b\}^T = \frac{R}{\ell}\frac{d\{a\}^T}{ds} = \frac{R}{\ell}\{-1\ ,\ 1\} \quad . \tag{A.8}$$

Therefore,

$$S_1 = \frac{GR}{\ell}\theta_1$$

and

$$S_i = \frac{GR}{\ell}(\theta_i - \theta_{i-1}) \quad . \tag{A.9}$$

B. CANTILEVERED BEAM IN BENDING

Figure A.2 shows the beam and the degrees of freedom used in this thesis. Note that a slope as well as a vertical deflection are used at each node. The mass and stiffness matrices for a single element

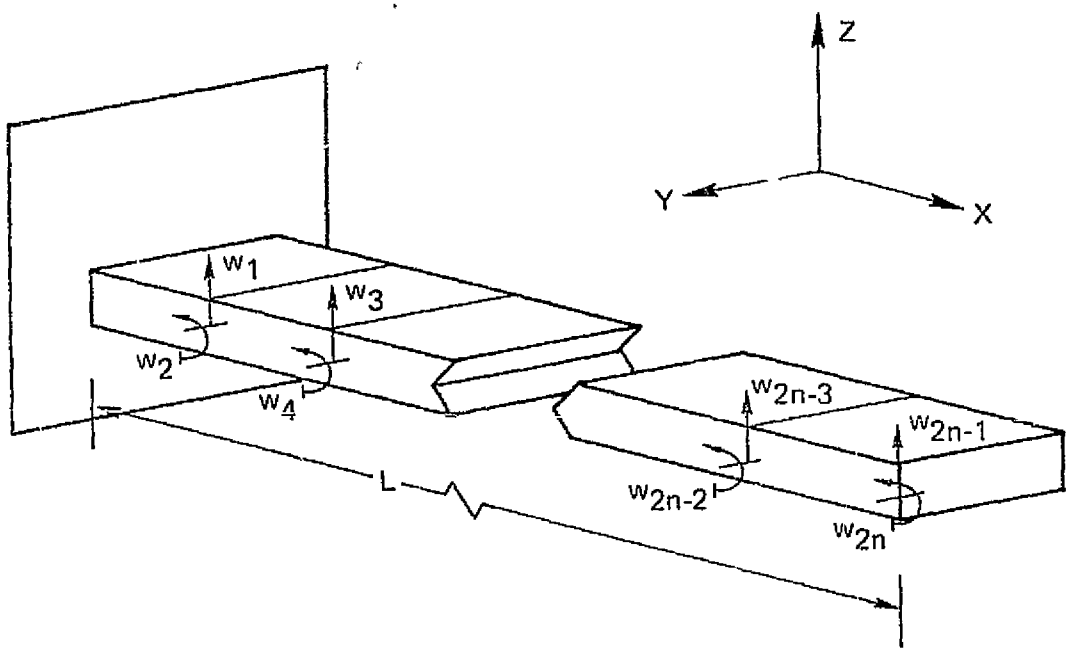

(a) Representation Using n Elements

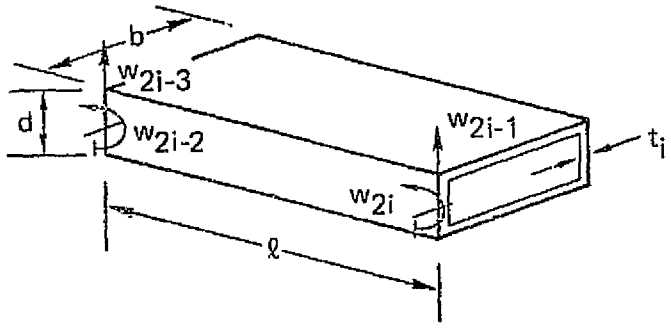

(b) Individual Beam Element

FIG. A.2--Cantilevered Beam.

are given by (Ref. 51)

$$[K]_i = \left(\frac{EI}{\ell^3}\right)_i [KO] \quad ,$$

$$[M]_i = \left(\frac{\rho_s A \ell}{420}\right)_i [MO] \quad , \qquad \text{(A.10)}$$

where

$$[KO] = \begin{bmatrix} 12 & 6\ell & -12 & 6\ell \\ & 4\ell^2 & -6\ell & 2\ell^2 \\ & & 12 & -6\ell \\ \text{Symmetric} & & & 4\ell^2 \end{bmatrix}$$

$$[MO] = \begin{bmatrix} 156 & 22\ell & 54 & -13\ell \\ & 4\ell^2 & 13\ell & -3\ell^3 \\ & & 156 & -22\ell \\ \text{Symmetric} & & & 4\ell^2 \end{bmatrix} \quad . \qquad \text{(A.11)}$$

As in the previous section, the structure is divided into n equal elements of length $\ell = L/N$. The inertia and cross sectional

areas are expressed as linear functions of the element thickness:

$$(EI)_i = EI_o t_i \quad ,$$

$$(\rho A)_i = \rho A_o t_i \quad . \tag{A.12}$$

The cantilevered boundary condition requires that the degrees of freedom corresponding to the root displacement and slope be eliminated. The assembled mass and stiffness matrices can again be formed by adding contributions from the individual elements at the nodes. The assembled matrices have dimensions $2n \times 2n$.

The equivalent force vector and the stress vector are found in the same way as in the previous section with the $\{a\}^T$ and $\{b\}^T$ vectors replaced by

$$\{a\}^T = \{1 - 3s^2 + 2s^3 \ , \ (s - 2s^2 + s^3)\ell \ , \ 3s^2 - 2s^3 \ , \ (-s^2 + s^3)\ell\}^T \quad , \tag{A.13}$$

$$\{b\}^T = \frac{d}{2\ell^2} \left\{\frac{d^2 a}{ds^2}\right\}^T \quad , \tag{A.14}$$

where d is the depth of the beam.

Using Eq. (A.3), the equivalent force vector is

$$\{p_{eq}\}_i = p_x \ell \begin{Bmatrix} 1 \\ \ell/12 \\ 1 \\ -\ell/12 \end{Bmatrix} \quad . \tag{A.15}$$

The assembled vector has the form:

$$\{P\} = p_x \ell \begin{Bmatrix} 1 \\ 0 \\ 1 \\ 0 \\ \cdot \\ \cdot \\ \cdot \\ 0 \\ 1 \\ -\ell/12 \end{Bmatrix} \quad . \qquad \text{(A.16)}$$

The stress vector is found using:

$$S_i = E\{b\}^T\{w\} = \frac{Ed}{2\ell^2}\{-6+12s\ ,\ (-4+6s)\ell\ ,\ 6-12s\ ,\ (-12+6s)\ell\}^T \begin{Bmatrix} w_{2i-3} \\ w_{2i-2} \\ w_{2i-1} \\ w_{2i} \end{Bmatrix}$$

(A.17)

If the stresses are calculated at $s = \frac{1}{2}$, the above relation is greatly simplified in that the first and third elements of $\{b\}^T$ are zero. This was done for this thesis giving an assembled stress vector of the form

$$\{S\} = \frac{Ed}{2\ell} \begin{bmatrix} 0 & 1 & 0 & 0 & 0 & - & - & - & - & 0 & 0 \\ 0 & -1 & 0 & 1 & 0 & 0 & - & - & - & 0 & 0 \\ 0 & 0 & 0 & -1 & 0 & 1 & - & - & - & 0 & 0 \\ - & - & - & - & & & & & & & \\ - & - & - & - & & & & & & & \\ 0 & 0 & 0 & - & - & - & -1 & 0 & 1 & 0 & 0 \\ 0 & 0 & 0 & - & - & - & 0 & 0 & -1 & 0 & 1 \end{bmatrix} \begin{Bmatrix} w_1 \\ w_2 \\ w_3 \\ - \\ - \\ w_{2n-1} \\ w_{2n} \end{Bmatrix}$$

(A.18)

C. TAPERED WING

This section develops the matrices needed for Eq. (5.6):

$$(-\omega_e^2 [M] + [K] - [A]) \{w\} = \{G\} \quad . \qquad (5.6)$$

The wing used for this analysis is shown in Fig. 5.1. The linear taper of the chord adds complexity to the analyses of the previous sections and these complications are outlined in this section.

The first step is to represent the nondimensional semi-chord length as

$$a(y) = b/b_{ref} = \frac{b_{root}}{b_{ref}} (1.0 - y/t_f) \quad . \qquad (A.19)$$

For the wing used, the numerical values of the parameters are given by

$$b_{root} = 112.5" \quad , \quad t_f = 900" \quad , \quad b_{ref} = 81.24" \quad .$$

It is assumed that the thickness to chord ratio remains constant across the span so that the aerodynamic thickness is also linearly tapered. In order to avoid further complications of doubtful utility, the structural thickness is held constant across the length of an element. The consequences of these two assumptions are that the mass varies as $(1.0 - y/t_f)$ while the inertia varies as $(1.0 - y/t_f)^3$.

As in the previous section, submatrices that deal with a single element are the building blocks that make up the final assembled matrices. It is therefore necessary to have structural properties expressed in terms of each element. As an example, the dimensional chord length for the i^{th} element can be expressed as:

$$C_i(s) = C_{root}\,\alpha_i(1 - s/\delta_i) \qquad 0 \le s \le 1 \quad . \tag{A.20}$$

By the use of Eq. (A.19), it can be shown that

$$\alpha_i = 1 - L(i-1)/nt_f \quad ,$$

$$\delta_i = \frac{nt_f}{L} + 1 - i = \frac{nt_f}{L}\,\alpha_i \quad . \tag{A.21}$$

1. Mass and Stiffness Matrices

The mass matrix for an element is found by evaluating the integral:

$$[M]_i = t_i \rho_s A_{root} \frac{L}{n} \int_0^1 \alpha_i \left(1 - \frac{s}{\delta_i}\right) \{\eta\}\,\{\eta\}^T\,ds \quad , \tag{A.22}$$

where $\{\eta\}^T$ is identical to $\{a\}^T$ given in Eq. (A.1). The integration gives

$$[M]_i = \frac{t_i \rho_s A_{root} L \alpha_i}{n} \left([M0] - \frac{[M1]}{2\delta_i}\right) \quad . \tag{A.23}$$

[MO] is given in Eq. (A.11) and

$$[M1] = \begin{bmatrix} 72 & 14\ell & 54 & -12\ell \\ & 3\ell^2 & 14\ell & -3\ell^2 \\ & & 240 & -30\ell \\ \text{Symmetric} & & & 5\ell^2 \end{bmatrix} \quad . \qquad (A.24)$$

Similarly, the stiffness matrix is evaluated using

$$[K]_i = E \left(\frac{n}{L}\right)^3 \int_0^1 I_i \{\beta\} \{\beta\}^T ds \quad , \qquad (A.25)$$

where

$$\{\beta\}^T = \left\{\frac{\partial^2 \eta}{\partial s^2}\right\}^T$$

and

$$I_i = \frac{1}{2} I_0 t_i \alpha_i^3 \left(1 - \frac{s}{\delta_i}\right)^3 \quad .$$

Since $s/\delta_i \ll 1$, it is reasonable to make the approximation

$$\left(1 - \frac{s}{\delta_i}\right)^3 \simeq 1 - \frac{3s}{\delta_i} \quad .$$

Then, Eq. (A.25) is evaluated to give

$$[K] = EI_0 \left(\frac{\alpha_i n}{L}\right)^3 \left([KO] - \frac{3[K1]}{\delta_i}\right) \quad . \qquad (A.26)$$

[KO] is given in Eq. (A.11) and

$$[K1] = \begin{bmatrix} 6 & 2\ell & -6 & 4\ell \\ & \ell^2 & -2\ell & \ell^2 \\ & & 6 & -4\ell \\ \text{Symmetric} & & & 3\ell^2 \end{bmatrix} \quad . \qquad (A.27)$$

Note that as t_f , and therefore δ_i , become large, the mass and stiffness matrices approach the untapered results of the previous section.

2. Aerodynamic Matrices

The aerodynamic matrix [A] results from the motion and can be formulated in a manner very similar to that used for the mass matrix. From Eq. (5.4), the distributed lift resulting from the motion is given by:

$$L_m(y) = \pi\rho_a U^2 \left[[a(y)k]^2 - 2ia(y)C(k)\right] h \qquad (5.4a)$$

The equivalent matrix for the finite element representation is found using

$$[A]_i = \pi\rho_a U^2 \ell \int_0^1 \left[(\alpha_i k)^2 \left(1 - \frac{s}{\delta_i}\right)^2 - 2ikC(k)\,\alpha_i \left(1 - \frac{s}{\delta_i}\right)\right]\{\eta\}\{\eta\}^T\,ds \quad . \qquad (A.28)$$

Using the approximation that $(1.0 - s/\delta_i)^2 \doteq 1.0 - 2s/\delta_i$:

$$[A]_i = \frac{\pi\rho_a U^2 \ell}{420} \left[\left(\alpha_i^2 k^2 - 2i\alpha_i kC(k)\right) [M0] - \frac{2(\alpha_i^2 k^2 - ikC(k)[M1]}{2\delta_i} \right] \quad . \qquad (A.29)$$

The [M0] and [M1] matrices are defined in Eqs. (A.11) and (A.24).

The distributed load resulting directly from the gust is given by Eq. (5.5):

$$\frac{L_g}{w_g} = 2\pi\rho_a U b_{ref} a(y) \left\{ C(k)\,[J_0(k) - iJ_1(k)] + iJ_1(k) \right\}$$

$$\equiv 2\pi\rho_a U b_{ref} a(y) K(k) \quad .$$

The equivalent force is determined from

$$\{G\}_i = 2\pi\rho_a Ub_{ref}\ell\, K(k) \int_0^1 \alpha_i \left(1 - \frac{s}{\delta_i}\right) \{\eta\}\, ds$$

$$= 2\pi\rho_a Ub_{ref}\ell\, K(k)\, \alpha_i \left[\{G0\} - \frac{\{G1\}}{\delta_i}\right] \quad , \qquad (A.30)$$

where:

$$\{G0\} = \begin{Bmatrix} 1/2 \\ \ell/12 \\ 1/2 \\ -\ell/12 \end{Bmatrix} \qquad \{G1\} = \frac{1}{60} \begin{Bmatrix} 9 \\ 2\ell \\ 21 \\ -3\ell \end{Bmatrix} .$$

Assembling the matrices is straightforward and is not performed here. The one boundary condition that enters in the assemblage procedure comes from the assumption that the deflections are symmetric about the fuselage. This requires that the slope of the displacement be zero at the root, which in turn requires that the degree of freedom associated with this boundary condition be eliminated.

A remaining task is the inclusion of the nonstructural masses of the fuselage and nacelle into the mass matrix. The fuselage is handled readily by approximating it as a point mass stationed at the root. This

mass is simply added to the single element in the mass matrix that deals with the root displacement.

The nacelle is slightly more complicated in that it is not positioned at a node point of the finite element structure. The procedure used is to determine which element contains the nacelle and to then add to the mass matrix of that element terms corresponding to the equivalent mass of the nacelle obtained using a formula similar to that of Eq. (A.22):

$$[M]_{NAC} = m_{NAC} \int_0^1 \delta(s - s_{NAC}) \{\eta\}\{\eta\}^T ds$$

$$= m_{NAC} \{\eta(s_{NAC})\} \{\eta(s_{NAC})\}^T \quad , \qquad (A.31)$$

where $\delta(\ )$ is the dirac delta. s_{NAC} is the nondimensionalized coordinate of the nacelle location.